

Dispersion Calculator³

User's Manual



Deutsches Zentrum
für Luft- und Raumfahrt
German Aerospace Center

Version 3.1
March 2025
Copyright © 2018-2025 DLR

Dr. Armin Huber

Center for Lightweight Production Technology (ZLP)
Institute of Structures and Design
German Aerospace Center (DLR)
86159 Augsburg
Germany

armin.huber@dlr.de





Preface

Many applications of ultrasonic guided waves exist, but, as the reader may confirm, getting the dispersion curves of guided waves is difficult. Although there are many researchers who are able to calculate dispersion diagrams with their own code, most people who deal with guided waves do not have such code, either because they don't know where to get it, or they don't have the money to buy Disperse. Clearly, writing such code is difficult, in particular in case of multilayered anisotropic laminates, and those who can do it keep the code like a treasure. When I started conducting air-coupled ultrasonic inspection of carbon composites using Lamb waves at DLR in Augsburg, Germany, in 2013, I had no code for calculating dispersion diagrams, too. Fortunately I got the budget in 2016 for buying Disperse. With this software, I am able to write and validate DC to this day. I found soon that it would be worth to make DC open to the public because of the high demand and lack of free software, but also because I considered it a waste of resources spending years on the code, and then only I could use it. Therefore, I released DC in 2018, and many user feedback from many countries as well as publications citing DC prove that DC is widely used today. I may say that it is a great pleasure for me to see how my "baby" performs, and I draw much satisfaction and motivation from it to continue the work on it. It is my sincere hope that the scientific community will benefit from DC, and that it might help create connections between humans belonging to different cultures or countries, which tend to compete or even fight each other.

In that sense, I want to express my gratitude to the researchers who have supported me in my work:

- Prof. Dr. Michael Lowe, Imperial College London, London, UK
- Prof. Dr. Michel Castaings, University of Bordeaux, Bordeaux, France
- Prof. Dr. Stanislav Rokhlin, Ohio State University, Columbus, OH, USA
- Prof. Dr. Marc Deschamps, University of Bordeaux, Bordeaux, France
- Dr. Eric Ducasse, University of Bordeaux, Bordeaux, France
- Prof. Dr. Victor Giurgiutiu, University of South Carolina, Columbia, SC, USA
- Prof. Dr. Markus Sause, University of Augsburg, Augsburg, Germany

Armin Huber

Augsburg, Germany

April 2022

Contents

1	Introduction	1
2	The Dispersion Calculator	4
2.1	Overview	4
2.2	Limitations	5
2.3	Download and installation	6
2.4	Warnings	6
3	Getting started quickly	7
4	The graphical user interface	8
4.1	Menu bar	8
4.2	Isotropic	9
4.3	Anisotropic	24
4.4	Signal simulator	31
4.5	Polar diagrams	36
4.6	Bulk waves	38
4.7	Laminate stiffness	45
4.8	Material editor	46
4.9	Advanced	48
5	Examples	55
5.1	T800M913 single layer plate @ 45°	55
5.2	T800M913 [0/90] ₄ plate @ 45°	56
5.3	T800M913 [0/90] _{100s} plate @ 0°	57
5.4	CarbonEpoxy_Hernando_2015_Viscoelastic single layer plate @ 30°	59
5.5	AS4M3502 [0/90] _{2s} plate @ 45° in water	60
5.6	Aluminum alloy 1100 pipe filled with water	61
5.7	Aluminum alloy 1100 circumference	63
A	Group velocity and energy velocity of guided waves	65
B	Bulk wave velocities in elastic media	72
C	List of default materials	73
C.1	Isotropic	73
C.2	Cubic	75
C.3	Transversely isotropic	75
C.4	Orthotropic	76
	References	78

1 Introduction

The nondestructive inspection (NDI) of components by means of guided waves is an emerging technology in fields like aerospace or pipeline construction. The guided waves' capability of propagating many meters in a structure is utilized for swift inspection tasks as well as structural health monitoring and acoustical emission. The German Aerospace Center (DLR) uses Lamb waves excited by air-coupled ultrasound for the quality assurance of large-scale aerospace vehicle components made from carbon composites. However, the use of guided waves in NDI requires knowledge of the dispersion curves. Disperse [1, 2] (Imperial College London, London, UK) is the most renown software for the calculation of dispersion curves. It has been developed since the early 1990s by Lowe and Pavlakovic, and it is used for the validation of the Dispersion Calculator (DC). But there are also free tools other than DC. GUIGUW [3, 4] is a software package developed by Marzani and Bocchini and released in 2011. Since it is based on the *semi-analytical finite-element method* (SAFE), it has the advantage of being able to model waveguides of arbitrary cross sections. Another promising contender, the open source MATLAB-toolbox ElasticMatrix [5, 6], was released by Ramasawmy et al. in 2020. It is able to compute dispersion curves for multilayered media made of isotropic and transversely isotropic layers where the wave propagation occurs in a material plane of symmetry. However, this covers decoupled cases only, so far excluding the majority of composites where we have arbitrary fiber orientations and wave propagation directions. Nonetheless, it is a promising project meant to be extended in the future. Then, the MATLAB-based “The Dispersion Box” was released by Orta et al. in 2022 [7, 8]. This tool is able to compute dispersion and attenuation curves in multilayered, viscoelastic, orthotropic plates. Its special feature is that up to six different methods can be used simultaneously, namely the *global matrix method* (GMM), the *stiffness matrix method* (SMM), the *hybrid compliance-stiffness matrix method* (HCSMM), the SAFE method, the *Legendre polynomial method* (LPM), and the *fifth order shear deformation theory* (5-SDT). The latter was developed also by Orta et al. [9] as an improvement to the previous lower order plate theories. A not to be underestimated advantage is also that The Dispersion Box has an easy-to-use graphical user interface. In 2023, Liu et al. released SAFEDC [10, 11]. This software has a similar layout as DC, but uses SAFE for the modeling of waveguides with arbitrary cross sections and general anisotropy. Also in 2023, Kiefer released the open source “GEWtool” [12] for MATLAB. It uses the *spectral element method* (SEM), enabling extremely fast calculations.

The task that triggered the development of DC was the calculation of incidence angles for the excitation of Lamb waves for the air-coupled ultrasonic inspection of rocket booster pressure vessels of the future launcher Ariane 6. These vessels are made of carbon fiber reinforced plastics (CFRP) in order to make them lighter, and therefore enable the launcher to carry more payload. In some areas, such pressure vessels can consist of up to four hundred layers, which is a challenging task to calculate them. To facilitate the calculation, it is a common practice to group layers, but this is not possible here because the layups are very complicated and irregular in terms of the winding angle (fiber orientation) and layer thicknesses. Therefore, every single layer has to be

calculated, and SMM, which has been developed by Rokhlin and Wang [13–15] in 2002, has been implemented in MATLAB to perform these calculations. A very useful paper for the coding of SMM is that by Kamal and Giurgiutiu [16]. Tan in 2005 introduced an improvement in efficiency [17], and shortly thereafter he presented HCSMM [18], which solved the instability of SMM for very small frequency-thickness products. Other researchers who use SMM are Barks et al. [19–21] and Muc et al. [22]. However, initially, the excellent and highly instructive book by Nayfeh [23] featuring the *transfer matrix method* (TMM) served as the backbone for the programming of DC. TMM was developed by Thomson [24] in 1950, and a small correction was conducted by Haskell [25] in 1953. Nayfeh extended TMM to guided SH waves in multilayered anisotropic plates in 1989 [26] and to general guided wave propagation in 1991 [27]. However, SMM solved the well-known numerical instability which TMM suffers from. Moreover, SMM retains the concise form and efficiency of TMM, unlike other stable methods such as GMM, which is used by Disperse and ElasticMatrix. GMM was proposed by Knopoff [28] in 1964, and it is discussed in the famous paper by Lowe [29]. The SAFE method, introduced by Gavric [30] in 1995, and used by GUIGUW, The Dispersion Box, and SAFEDC is an alternative to root-finding methods. The SAFE method discretizes the waveguide's cross section into finite elements, allowing the modeling of guided waves in complex geometries. At the same time, the wave propagation direction is solved analytically, which makes this approach more efficient than full FEM modeling. It should be noted, however, that the SAFE method (similar as the *spectral collocation method* (SCM)) is an approximate method, i.e., the accuracy of the results depends on the number of discrete elements set through the thickness of the waveguide. The above-mentioned SCM was introduced by Adamou and Craster for guided wave modeling in elastic media in 2004 [31]. SCM is similar to SAFE in that it is using a one-dimensional mesh over the system's cross section, but SCM possesses a higher accuracy and speed of computation (whereas SEM seems to be even faster than SCM). Instead of solving a differential equation directly, SCM uses a spectral approximation, which satisfies the differential equation and boundary conditions. Hernando-Quintanilla et al. have provided comprehensive studies of guided wave modeling in generally anisotropic media by means of SCM [32–35]. According to the authors, SCM is easier to code than root-finding methods, it is faster, and most importantly, it does not miss modal solutions. More recently, the method has been used to model also leaky waves [36–38]. SCM is currently implemented in Disperse. Probably, SCM/SEM are the best discretizing methods and SMM is the best root-finding method.

The theoretical work on guided wave modeling and the implementation into DC is reported in detail in Refs. [39–41]. Starting in DC v3.0 and completed in DC v3.1, TMM can be used in situations where it is stable. Dispersion curves for isotropic plates are obtained most efficiently by applying the Rayleigh-Lamb equations [42,43], and the excellent book by Rose [44] served well for the coding. The advanced model for the group/energy velocity of guided waves in anisotropic specimen, introduced in DC v1.11, has been developed with help of the highly recommended book by Giurgiutiu [45]. The coding of the characteristic equations used for fluid-loaded cases, introduced in DC v2.0, was done with help of the excellent book by Rokhlin *et al.* [15]. The modeling of axial guided waves in isotropic cylinders, introduced in DC v3.0, was programmed with the

help of several publications. For isotropic rods, the dispersion equations for flexural, longitudinal, and torsional modes were published in 1964 by Meeker and Meitzler [46]. A more efficient equation for flexural modes with circumferential order $n = 1$ is given in the 1960 paper by Pao and Mindlin [47]. The dispersion equation for flexural waves in isotropic hollow cylinders (pipes) was introduced by Gazis in 1959 [48]. However, the equations in his paper contain an error (see the discussion and correction in the Disperse manual), and also the way he derived the equations is harder to follow and more unwieldy than the equations presented by Kumar in 1971 [49] (who made no error). Furthermore, Kumar's paper added the fluid-filling (the outer fluid-loading can be added by another equation with a Hankel function for the leaky waves, see Ref. [44]). In fact, Kumar's 1971 paper is everything needed, as the equations for longitudinal and torsional modes in pipes as well as flexural, longitudinal, and torsional modes in rods are naturally contained in his equations (for the rod, remove the equations at the inner radius and also remove the outgoing bulk wave terms; for longitudinal and torsional waves, set $n = 0$ and separate the L- and SV bulk waves terms from the SH terms). Nonetheless, the 1972 paper by Kumar [50], presenting the equations for longitudinal modes, should be mentioned. The dispersion equations for Lamb-type circumferential waves in a pipe are taken from Refs. [51, 52] and those for shear horizontal circumferential waves from Ref. [53].

2 The Dispersion Calculator

2.1 Overview

DC is an interactive and fully validated stand-alone software for the computation of dispersion curves (phase velocity, energy velocity, attenuation, etc. vs frequency) and mode shapes (displacement, stress, strain, etc.) of guided waves in isotropic plates, rods and pipes (axial and circumferential waves) as well as in multilayered anisotropic plates. The material(s) can be perfectly elastic or viscoelastic, and the waveguide can be surrounded by and, in case of a pipe, be filled with inviscid fluids. DC can handle laminates consisting of several hundreds of layers, and it is able to distinguish the different mode families, like symmetric, anti-symmetric, and non-symmetric (leaky) Lamb, shear horizontal, and Scholte waves, depending on the symmetry and coupling properties of a given layup. DC features a highly efficient and robust dispersion curve tracing algorithm. The initial release of DC took place in November 2018.

DC offers an easy-to-use graphical user interface (GUI) (see for example the **Anisotropic** tab in Fig. 1). Basically, it provides only the parameter setting interfaces like editable fields and buttons as well as some output windows displaying data and other information. All plots like dispersion diagrams or mode shapes are plotted in extra windows, which open when the user presses the corresponding button. This basic arrangement aims to improve user-friendliness by avoiding options in multi-leveled submenus where they are out of sight of the user initially. Instead, DC provides all options that are related to one task in just one tab. For example, in the “Isotropic” tab, the user can set up the specimen, define the computational parameters, calculate the dispersion curves, through-thickness profiles, and mode shapes, adjust the plot layout, and manage the export of data and plots. DC has eight tabs, of which six cover the main tasks, one allows to enter material parameters, and the last one contains advanced options. The tabs are listed below:

1. **Isotropic:** Calculation of dispersion diagrams and mode shapes for single layer isotropic plates, rods, and pipes (axial and circumferential waves)(fast computation by using the Rayleigh-Lamb equations, respectively, those specific to isotropic cylinders).
2. **Anisotropic** Calculation of dispersion diagrams and mode shapes for multilayered anisotropic plates (using SMM and TMM).
3. **Signal simulator:** Simulation of the signal of single and multiple guided wave modes (for plates only).
4. **Polar diagrams:** Calculation of polar dispersion diagrams for multilayered anisotropic plates.
5. **Bulk waves:** Calculation of the bulk waves’ phase and group velocities, slow-nesses, and polarization, propagating in anisotropic media as well as their scattering on solid-fluid interfaces.

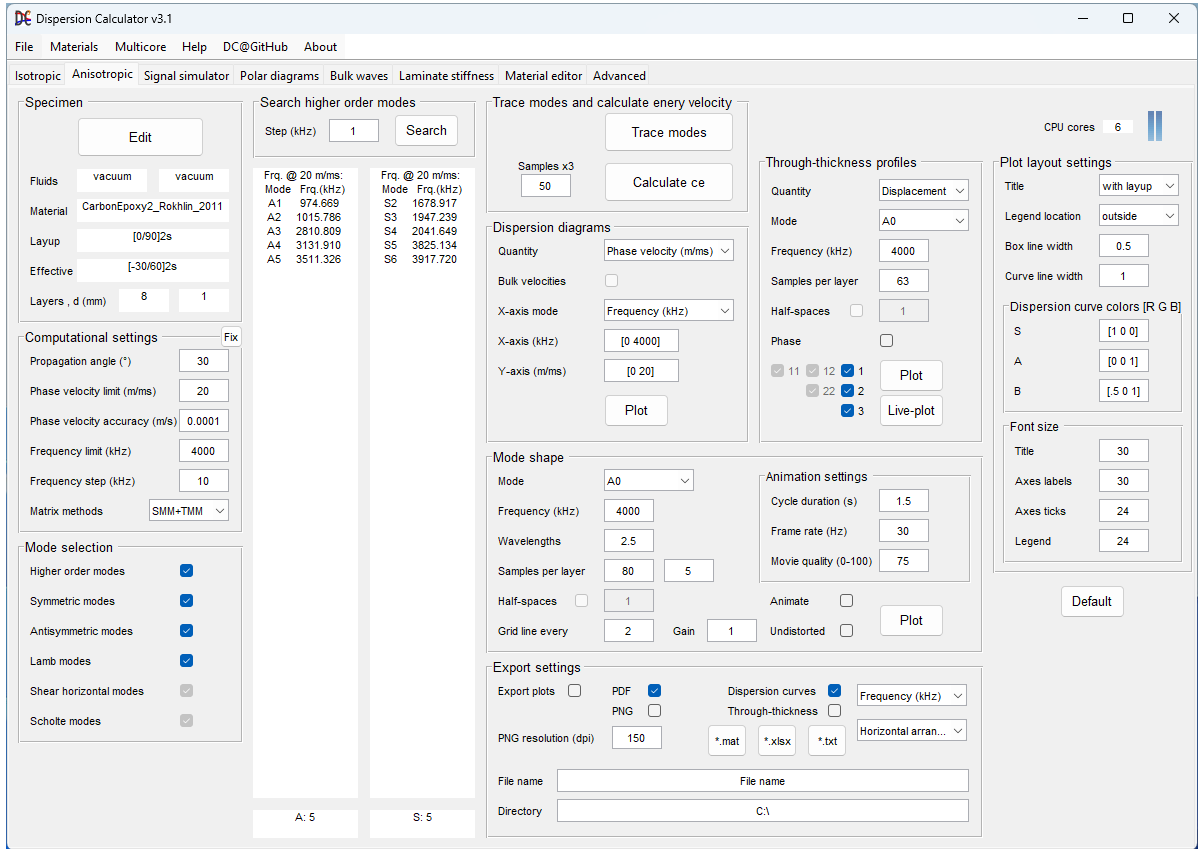


FIG. 1. The screenshot shows the **Anisotropic** tab for the calculation of dispersion diagrams and mode shapes of guided waves in multilayered composites.

6. **Laminate stiffness:** Calculation of the homogenized stiffness tensor of laminates.
7. **Material editor:** To enter engineering constants or stiffnesses of orthotropic, transversely isotropic, cubic, and isotropic materials as well as fluids.
8. **Advanced:** Contains the advanced options for the dispersion curve tracing algorithm.

2.2 Limitations

- DC computes only modal solutions with purely real or complex wavenumbers. Purely imaginary wavenumbers are not covered.
- DC computes backward propagating modes (phase and energy velocity point in opposite directions) only in nonattenuated systems. They are missed if there is attenuation involved.
- Piezoelectric effects are not supported.

- The half-spaces surrounding a waveguide can only be filled with fluids, not with solids.
- Viscosity in fluids is not supported.
- If the waveguide is immersed in a fluid, the power normalization of the mode shapes is no strict because the components in the half-spaces are ignored in the integration.
- Wave propagation in rods and pipes (axial and circumferential waves) is limited to isotropic single layers. Multilayered, anisotropic layups are not possible.
- In case of circumferential waves in a pipe, no fluid-loading can be applied and viscoelastic damping is ignored.

2.3 Download and installation

DC is available on GitHub [54]. One can download the stand-alone installer, for which no MATLAB is required, and one can download the MATLAB code (notice that the Curve Fitting Toolbox is required also). When running the standalone installer, the required MATLAB runtime will be downloaded and installed automatically. In case the MATLAB runtime is not downloaded and installed automatically, download it from

<https://www.mathworks.com/products/compiler/matlab-runtime.html>

and install it manually. The required runtime version number can be found in the change log file. For more information, see the README on GitHub [54].

2.4 Warnings

The numerical model for obtaining dispersion diagrams in DC has been fully validated against Disperse. In some cases, however, DC disagrees with Disperse. In some of these cases, validation was made against published data to ensure that DC computes correctly. However, this does not mean that DC is without errors. No software is without them. There are two main sources for erroneous calculations in DC. The first source is the possibility that a dispersion equation is incorrect. I consider this problem rather unlikely in DC. The second source is the dispersion curve tracing algorithm. Dispersion curve tracing is notoriously difficult, in particular when damping is involved in the system. It is impossible to write a tracing routine which works perfectly robust for an infinite number of thinkable combinations of wave guide geometries, material parameters, layups, fluid-loading, etc.. Hence, dispersion curves can be incomplete, sudden jumps can appear, and some modes may be missing completely. Please contact me in case you encounter a bug or if you need help.

3 Getting started quickly

1. Go to the **Material editor**.
2. In the **Anisotropic materials** panel, enter the engineering constants or stiffness components of your material.
3. Enter a **New material's name** and press **Save material**.
4. Go to the **Anisotropic** tab.
5. Press **Edit**, select your material, and enter your layup.
6. Press **Calculate** to calculate the dispersion diagram.
7. Press **Plot** in the **Dispersion diagrams** panel.
8. Click on a dispersion curve to display values. Press the Shift key to place multiple data tips.
9. Press **Plot** in the **Through-thickness profiles** panel to display the displacement components of the A_0/B_0 Lamb wave at the highest frequency covered by the dispersion diagram.
10. Activate the **Animate** check box in the **Animation settings** panel and press **Plot** below to animate the displacement pattern of the A_0/B_0 Lamb wave at the above frequency.

4 The graphical user interface

4.1 Menu bar

In the **File** menu, a new project can be generated by pressing **New project**. This closes the current DC instance and opens a new one. An existing project file can be loaded via the **Open project** button. By pressing **Save project**, the current project can be saved. Pressing **Quit** closes DC. The **Materials** menu allows to export material lists from DC or to import them from local. Upon pressing **Export**, you are asked to select a directory to which the material lists are exported. Five separate txt-files containing orthotropic, transversely isotropic, cubic, and isotropic materials as well as fluids will be exported to the selected directory. You can rename the material lists. Export material lists when you want to install a new DC version and transfer your custom materials to it. To import material lists, press **Import** and select one or multiple material lists. The names of the imported lists do not matter. DC automatically assigns the material lists to the respective material symmetry class. Once you have imported all lists, you have to restart DC (**File → New project**) to make the materials available. You also can open the directory holding the material lists by pressing **Open directory**.

Important note:

To add, edit, and delete materials, use the Material editor (see Sec. 4.8). Do not edit the material lists directly.

In the **Multicore** menu, you can **Enable** parallel computing. The two bars in the upper right corner of the GUI turn blue. The number shown in the **CPU cores** field is the number of CPU cores available for parallel computing. If multi-core computing is enabled, DC uses all CPU cores on your machine for dispersion curve tracing in the **Isotropic** and **Anisotropic** tabs. Each mode family is calculated on one core. If more mode families are scheduled than cores are available, the first idle core takes over the next waiting mode family. This is particularly useful when many mode families are scheduled like many higher circumferential mode orders of axial waves in pipes and rods, thereby reducing computation time drastically compared to sequential computing (multi-core computing is off). In the **Polar diagrams** tab, the dispersion curve tracing is performed on two cores. The energy velocity calculation in the **Isotropic**, **Anisotropic**, and **Polar diagrams** tabs is performed on all cores. During parallel computation, the two bars turn green, and turn back to blue when the computation is completed. By pressing **Disable**, multi-core computing can be turned off. The two blue bars turn gray. By default, multi-core computing is off. In this case, the mode families are calculated sequentially, and polar dispersion curves are calculated on a single core. The energy velocity calculation is performed on one core as well. Press **Help** to read DC User's manual. Press **DC@GitHub** to visit the DC repository on GitHub [54], which is the official download platform.

4.2 Isotropic

The **Isotropic** tab consists of several panels. Start by defining the **Specimen (1)** (see Fig. 2). At first, choose the waveguide **Geometry**. You can select from **Plate**, **Rod**, **Pipe**, and **Circumferential**. Table 1 lists the guided wave mode families propagating in the various waveguide geometries. If you select **Plate**, symmetric and anti-symmetric Lamb waves S_p , A_p and shear horizontal waves S_p^{SH} , A_p^{SH} can be distinguished (p is the normal mode order with $p = 0, 1, 2, \dots, \infty$). If you add fluid-loading (see further below), Scholte modes appear in addition. If the same fluid is on both sides, there are symmetric and anti-symmetric Scholte waves $S_p^{Scholte}$, $A_p^{Scholte}$. However, if there are different fluids on each side or if only one side is covered with a fluid, non-symmetric Scholte modes $B_p^{Scholte}$ occur. In this case, the leaky waves S_p , A_p become non-symmetric B_p , while S_p^{SH} , A_p^{SH} retain their symmetric because they do not couple to inviscid fluids (DC does not support viscosity in fluids). If you select **Rod** or **Pipe**, torsional, longitudinal, and flexural modes $T(0,p)$, $L(0,p)$, $F(n,p)$ are modeled. If you add fluid-loading the corresponding Scholte modes $L(0,p)^{Scholte}$, $F(n,p)_p^{Scholte}$ occur in addition. All of these modes propagate in the axial direction of the waveguide. In the nomenclature, n is the circumferential order. For T- and L modes, n is zero, but for the flexural modes, n can take any integer number $n = 1, 2, 3, \dots, \infty$, and each mode family n has its own set

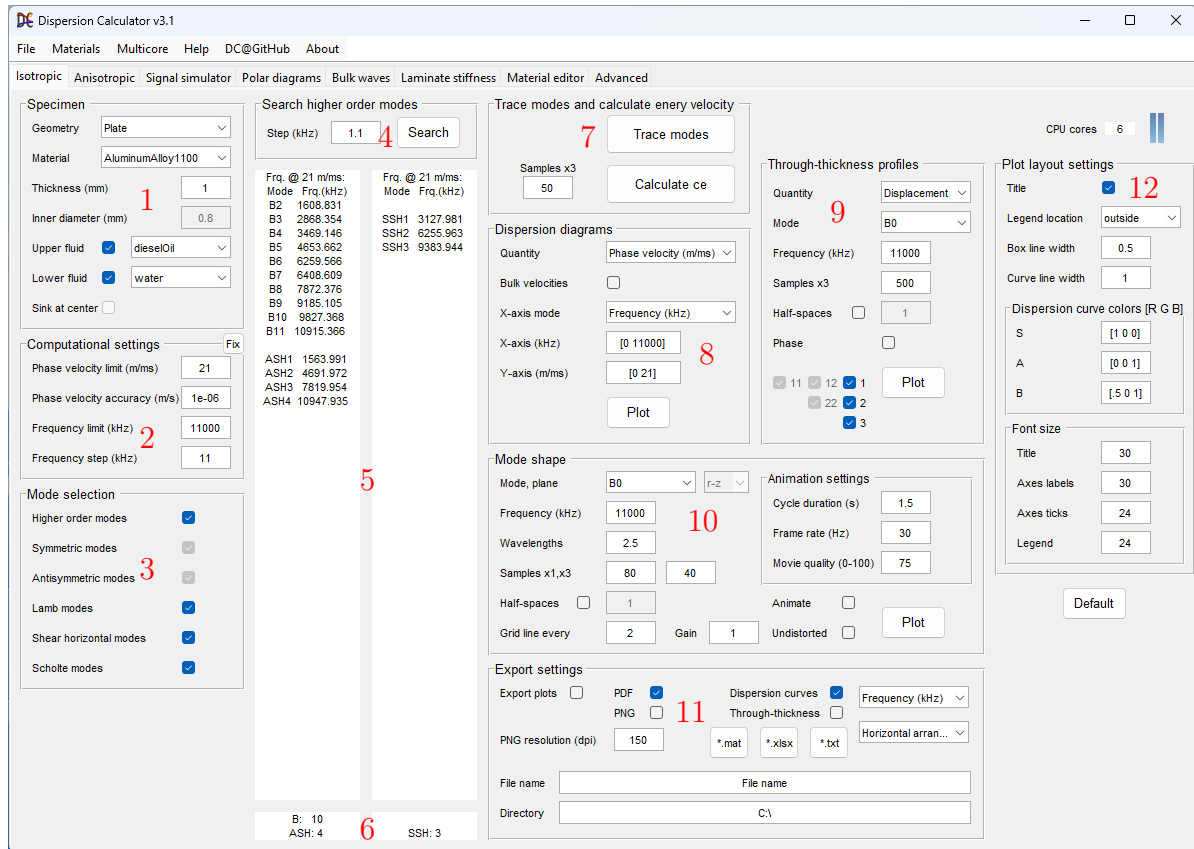


FIG. 2. The tab for the calculation of isotropic specimens.

TABLE 1. Guided wave mode families propagating in the various waveguide geometries (p : normal mode order; n circumferential mode order).

Geometry	Mode families
Plate	$S_p, A_p, B_p^a, S_p^{SH}, A_p^{SH}, S_p^{Scholte b}, A_p^{Scholte b}, B_p^{Scholte a}$
Rod, Pipe	$T(0,p), L(0,p), F(n,p), L(0,p)_p^{Scholte}, F(n,p)_p^{Scholte}$
Circumferential	C_p, C_p^{SH}

^a In case of non-symmetric fluid-loading

^b In case of symmetric fluid-loading

of normal mode orders $p = 1, 2, 3, \dots, \infty$. If you select **Circumferential**, the guided waves propagating in the circumferential direction of a pipe are calculated. In analogy to the modes in a plate, there exist Lamb-type modes and SH-type modes C_p, C_p^{SH} . In fact, when the inner radius to outer radius ratio approaches unity, the dispersion curves closely resemble those of a flat plate (DC issues a recommendation to calculate the plate in such cases). DC supports no fluid-loading in the circumferential case, and material damping is ignored.

Next, select a **Material**. Then set the dimension(s) of the waveguide. If you have selected **Plate** as a **Geometry**, you can set its **Thickness**. For a **Rod**, this option is renamed to **Outer diameter**. If you have selected **Pipe** or **Circumferential**, the **Inner diameter** field becomes active. DC does not allow you to set **Inner diameter** larger than **Outer diameter**.

Then come the fluid-loading settings. In case of a **Plate**, you can fill the upper and lower half-spaces with fluids by checking the **Upper fluid** and **Lower fluid** check boxes, and then select the respective fluids from the drop-down menus. If you leave a check box empty, the corresponding half-space is a vacuum. In case of a **Rod**, only the **Outer fluid** option is available, but for a **Pipe**, there is also the **Inner fluid** option. If the pipe is filled with a fluid, the **Sink at center** check box can be used. If it is on, the bulk waves traveling from one side of the inner pipe wall through the fluid-filling to the other side are absorbed such that the (numerous) fluid modes are suppressed, and only the pipe modes are left (see example in Sec. 5.6). No fluid-loading options are available in case of **Circumferential** wave propagation.

When a half-space is filled with a fluid, energy leaks from the waveguide into the fluid such that the guided waves suffer attenuation as they propagate. Hence, the wavenumber is complex and the dispersion curve tracing is much more demanding compared to the case where the waveguide is surrounded by a vacuum. Without damping, the wavenumber is real, and DC performs only a one-dimensional search on the real wavenumber axis instead of a two-dimensional search in the complex wavenumber plane. Notice that a fluid-filling inside a pipe alone does not cause attenuation because the energy remains in the system. The dispersion curve tracing algorithms in the cases with and without fluid-loading are discussed in Sec. 4.9. Therefore, apply fluid-loading only if you are interested in the damping explicitly and if the fluid has a notable effect on the propagation

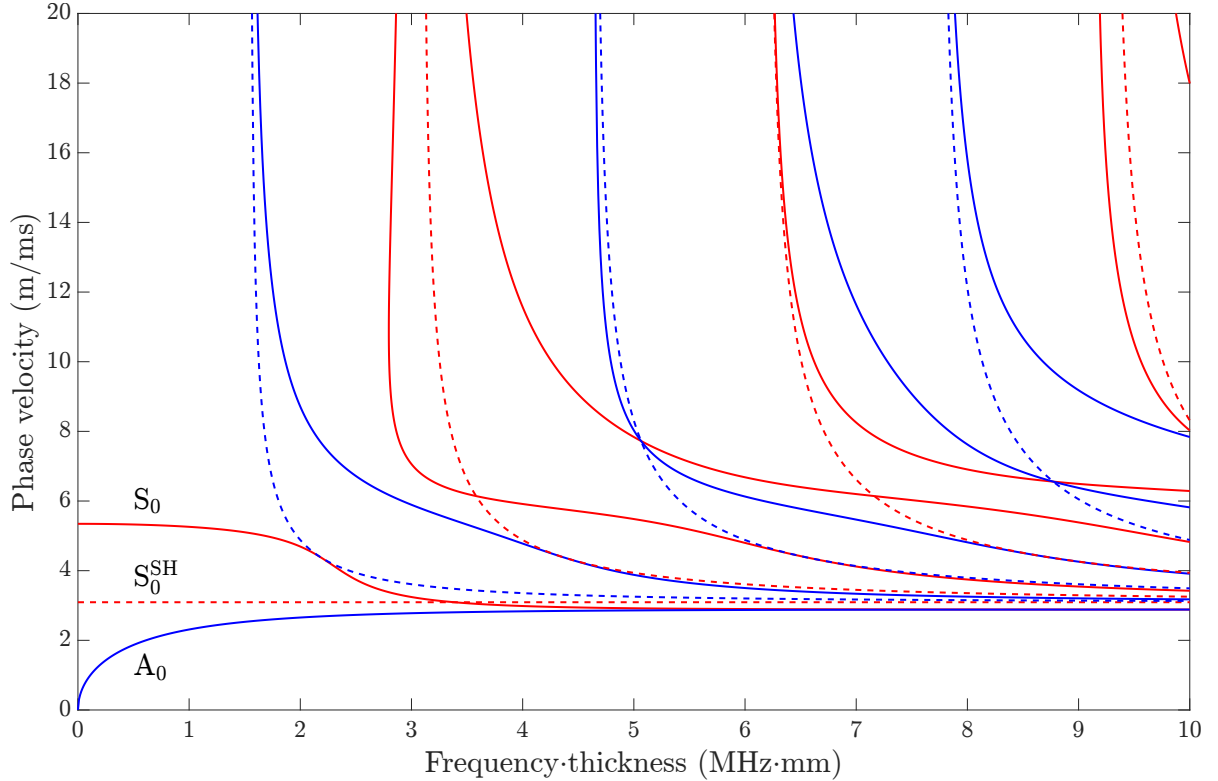


FIG. 3. Dispersion diagram for a free aluminum alloy 1100 plate. Solid lines indicate Lamb modes, dashed lines are shear horizontal modes. Red curves represent symmetric and blue ones anti-symmetric modes.

of the guided waves. The effect of the fluid becomes the more significant the “heavier” the fluid-loading is, i.e., the greater the mass density of the fluid is with respect to that of the plate. For instance, guided wave dispersion curves for a metal plate immersed in air will be hardly different from those for a free metal plate. Skip the fluid-loading in this case because the dispersion curve tracing is much faster and more robust. Figure 3 shows the dispersion diagram for a free (in vacuum) aluminum alloy 1100 plate. The opposite situation is present when you have water as a surrounding medium and a low-mass density material such as a (carbon fiber-reinforced) polymer. The guided waves will be strongly damped, and the dispersion curves will look completely different from the free case. Unfortunately, the greater the damping becomes the more difficult becomes the dispersion curve tracing. You will notice that the dispersion curves look more and more unusual in strongly damped cases, and it becomes more likely that the dispersion curve tracing fails. Figure 4 shows such a heavily damped case phase velocity dispersion diagram, namely that for an epoxy plate immersed in water. The corresponding attenuation is plotted in Fig. 5. Notice that Scholte and shear horizontal modes are not damped. For the latter, the reason is because they do not couple to the inviscid water. Both wave types are damped only in case the plate or the fluid is viscoelastic.

Viscoelasticity is the second physical phenomenon causing attenuation of elastic waves.

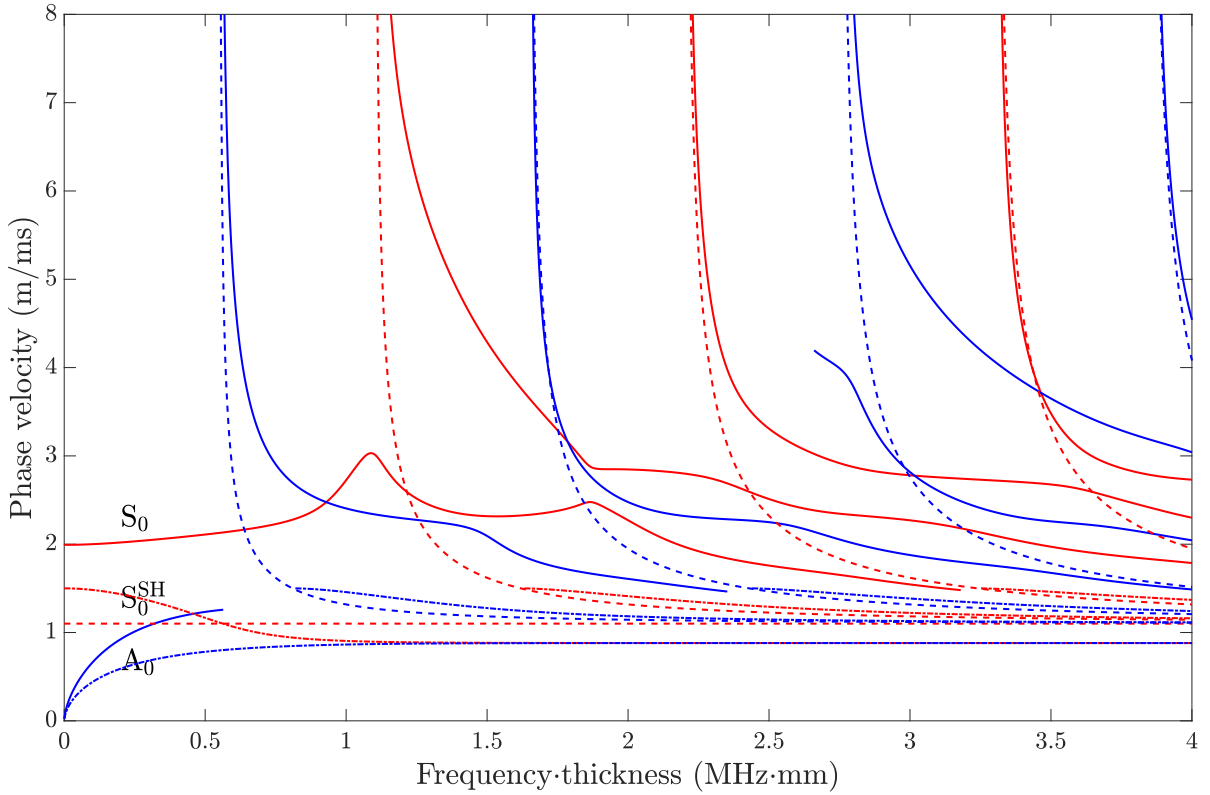


FIG. 4. Phase velocity dispersion diagram for an epoxy plate immersed in water. The dashed-dotted curves are the Scholte modes.

Viscoelasticity means that vibrational energy is dissipated as heat, thereby reducing the amplitude of the vibration with propagated distance. Its effect on attenuation is generally smaller than that caused by fluid-loading with water (but not necessarily with air). Technically, viscoelasticity is expressed by complex stiffness components, where the imaginary parts account for the damping. DC uses the hysteretic damping model where the damping loss increases linearly with frequency, i.e., the loss per wavelength is constant. Many viscoelastic default materials are available in DC, listed in Appendix C. To distinguish them from the perfectly elastic materials, they carry the suffix “_viscoelastic”. Of course, you can model viscoelastic waveguides which are also fluid-loaded.

You now can change the **Computational settings** (2). The **Phase velocity limit** determines up to which phase velocity the dispersion curves are calculated. The **Phase velocity accuracy** gives the accuracy of the modal solutions that has to be obtained. Bisections are performed until this value is reached (see Sec. 4.9). Notice that the through-thickness profiles and modes shapes, as well as the simulated signals will be the more accurate the smaller the value of the **Phase velocity accuracy** is. The **Frequency limit** determines up to which frequency the dispersion curves are calculated. The **Frequency step** sets the frequency increments in the dispersion curves. If the **Fix** button is switched off, **Phase velocity limit**, **Frequency limit**, and **Frequency step** are set automatically whenever you make changes in the **Specimen** (1) settings. Other-

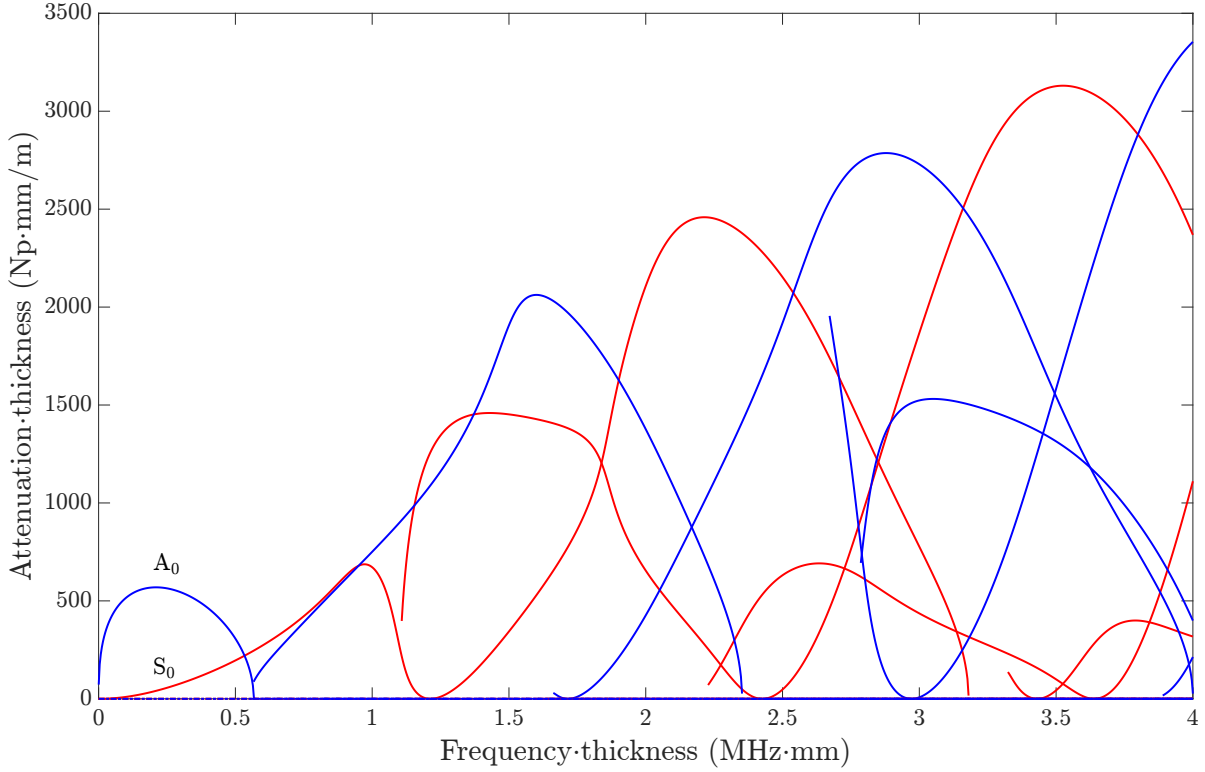
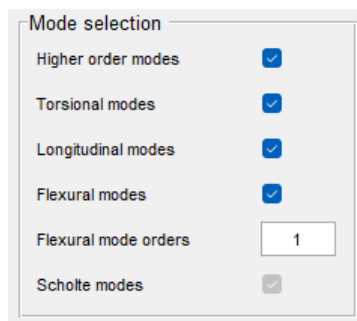


FIG. 5. Attenuation dispersion diagram for an epoxy plate immersed in water. Shear horizontal and Scholte modes are not damped.

wise, if the **Fix** button is switched on, the three settings are not changed automatically.

In the **Mode selection** (3) panel, you can select which mode families shall be calculated and whether the **Higher order modes** shall be calculated in addition to the fundamental modes. The mode family names shown in Fig. 2 appear when the **Geometry** is selected as **Plate** or **Circumferential**. When you select **Pipe** or **Rod**, the panel appearance changes according to Table 1, as shown on the left.



A specific option here is the **Flexural mode orders** field. In flexural modes $F(n,p)$, an infinite number $n = 1, 2, 3, \dots, \infty$ of circumferential wavenumbers can fit into the circumference of a pipe or rod (n is zero for torsional and longitudinal modes). Enter the maximum number of mode families n to be calculated. Some check boxes become disabled under certain conditions, e.g., **Scholte modes** if there is no fluid-loading involved and **Symmetric modes** and **Antisymmetric modes** in case of non-symmetric fluid-loading on a **Plate** or if **Geometry** is **Circumferential**.

If you want to calculate the **Higher order modes**, a frequency sweep at the **Phase velocity limit** is performed to find their cut-off frequencies. This can be done in the **Search higher order modes** (4) panel by pressing **Search**. Otherwise, it will be per-

formed automatically upon pressing **Trace Modes** in the **Trace modes and calculate ce** (7) panel. The **Step** determines the frequency increments in the sweep. The value is set automatically, but you can change it if you are not sure that you have detected all modes. Try a smaller **Step** in this case. It is essential for the dispersion curve tracing that you have detected *all* higher order modes. Notice that, even if you are considering a damped case, the frequency sweep is always performed for the nonattenuated case, i.e., without fluid-loading and viscoelasticity. The resulting cut-off frequencies will be the starting points for the search of the higher order modes also in the attenuated case. In this case, the dispersion curves start at more or less shifted cut-off frequencies, and some modes, which are present without attenuation, are not present or are not found otherwise.

The upper output windows (5) list the detected modes with their cut-off frequencies, and the lower output windows (6) summarize how many modes of each family have been found.

Now go to the **Trace modes and calculate ce** (7) panel and press **Trace modes** to compute the dispersion diagram. A window opens, showing the dispersion curve tracing. Meanwhile the **Trace modes** button turns into a **Stop trace** button. Hit it to cancel the dispersion curve tracing. When the dispersion curve tracing is complete, the window closes and a message informs you about the time elapsed. Directly after that, the energy velocity is calculated automatically. During this, the **Calculate ce** button turns into a **Stop calculate** button. Press it to cancel the energy velocity calculation. You can repeat the energy velocity calculation by pressing **Calculate ce**, for example if you want increase the accuracy by using a higher number of through-thickness **Samples x3**. As explained in Appendix A, the energy velocity calculation involves an integration of the mode shape through the thickness of the waveguide. Technically, DC uses trapezoidal numerical integration with respect to the number of through-thickness points defined in the **Samples x3** field. Notice that the accuracy of the energy velocity calculation decreases with an increasing frequency-thickness product because the mode shapes become more complex. Therefore, choose a sufficiently high number of samples. There are some exceptions where DC does not use the numerical integration method, but uses analytic equations (derived using Eq. (10)) for the energy velocity calculation instead. In the exceptions listed below, the prerequisite is that no damping is in the system:

- Lamb and SH waves in plates
- Torsional and longitudinal waves in rods
- Torsional waves in pipes

In case only these mode families are calculated, the **Samples x3** field becomes disabled. The advantage of using the analytic equations is that they compute very fast and that the result is accurate in the limit of the accuracy of the phase velocity dispersion curves.

Now you can go to the **Dispersion diagrams** (8) panel. Use the **Quantity** drop-down menu to choose between the **Phase velocity**, **Energy velocity**, **Propagation**

time, Coincidence angle, Wavelength, Wavenumber, and Attenuation. Notice that **Attenuation** is nonzero only in case of fluid-loading and/or viscoelasticity. The option below **Quantity** switches depending on what kind of **Quantity** you have selected. If you have selected **Phase velocity** or **Energy velocity**, you have a check box to choose whether the **Bulk velocities** should be displayed in the dispersion diagram or not. If you have selected **Propagation time**, you can enter the **Distance** for which the **Propagation time** shall be calculated. Finally, if you have chosen **Coincidence angle**, you have a drop-down menu that allows to choose the **Couplant** for which the coincidence angle shall be calculated. The **Coincidence angle** angle is given with respect to the normal to the plate. Use the **X-axis mode** drop-down menu to draw the dispersion curves as a function of the frequency in **kHz**, **MHz**, or frequency-thickness product in **MHz·mm**. Set the **X-axis**, e.g., [0 1000], and the **Y-axis** limits, e.g., [0 20]. Upon pressing **Plot**, the dispersion diagram is plotted in a new window. In the menu bar of the dispersion diagram, you can export the plot by going to **File → Save**, or **Save As**, or **Export Setup**. The **Show modes** menu allows you to show/hide dispersion curves easily. Use the **Analyze** menu to read values at constant frequency, phase velocity, wavelength, etc. Select the quantity which shall be kept constant from the drop-down menu and enter the value into the field on the right. A line will be drawn and all intersections with the dispersion curves are indicated with the corresponding coordinates.



Upon hovering the cursor over the plot, the axes toolbar becomes visible. It offers up to seven tools, depending on the plot type (see on the left). The first symbol opens a drop-down menu containing three more symbols. The floppy disk symbol allows to export tightly cropped png and pdf-images, a very useful tool if you want to insert the plots into publications. The other two symbols below copy the image to the clipboard as a pixel or as a vector graphic, respectively. If you want to remove data or replace them by NaN, toggle the **Brush/Select Data** tool and left-click on a data point or drag an rectangle over the data while pressing the left mouse button. Then right-click on the selected data and choose an action from the pop-up menu. Note that data are removed only from the plot, but not from the storage, i.e., your changes will be lost once you close the plot window.

Activate the **Data Tips** and click on a curve to display actual values. You can place multiple data tips by pressing the Shift key. Move the curves by using **Pan** and **Zoom In** and **Zoom Out**. Use **Restore View** to reset the plot.

Let's have a closer look at the dispersion diagram in Fig. 3, showing the phase velocity dispersion of Lamb and shear horizontal waves in a free aluminum alloy 1100 plate. Red curves indicate modes with a symmetric displacement pattern, blue curves are anti-symmetric modes. Solid lines indicate Lamb waves, dashed ones represent shear horizontal waves. The fundamental anti-symmetric Lamb mode A_0 starts at zero phase velocity while S_0 starts at the plate wave velocity of that material. Both fundamental modes tend toward the Rayleigh velocity for high frequencies. The fundamental shear horizontal wave S_0^{SH} is nondispersive at the transverse bulk velocity. The higher order modes start at their cut-off frequencies at high phase velocity and tend toward the transverse velocity. The higher order modes are labeled A_p , S_p for Lamb modes and A_p^{SH} ,

S_p^{SH} , $p = 1, 2, \dots$, for shear horizontal modes from left to right in the dispersion diagram. Figure 4 shows the dispersion diagram of an epoxy plate immersed in water. Because of the fluid-loading, Scholte waves are present. These are indicated by the dashed-dotted lines. Similar as with the Lamb-type modes, there are the fundamental Scholte modes A_0^{Scholte} and S_0^{Scholte} , where A_0^{Scholte} starts at zero phase velocity and S_0^{Scholte} starts at the wave speed in the fluid. Interestingly enough, the higher order Scholte modes appear only if the wave speed of the fluid is higher than the shear wave speed in the plate. Otherwise, S_0^{Scholte} will stay more or less non-dispersive at the wave speed in the fluid.

Now go to the **Through-thickness profiles** (9) panel. This is a useful tool, which allows you to plot the components of **Displacement**, **Stress**, **Strain**, **Energy density**, and **Power flow density** for a selected **Mode** at a selected **Frequency**. All these quantities change through the thickness of the waveguide and with the frequency-thickness product. For instance, Figs. 6(a) and 6(b) show the through-thickness **Displacement** and **Stress** field components of the A_0 Lamb wave at 10 MHz propagating in a 1 mm thick free aluminum alloy 1100 plate, and in Figs. 6(c) and 6(d) the same is plotted if the plate is immersed in water. The latter plots show the behavior also in the half-spaces above and below the plate to a depth of 1 mm on both sides. For the immersed case, the corresponding **Phase** information is plotted in Fig. 7. In all these plots, $x_3 = 0$ mm on the ordinate corresponds to the top surface of the plate, and $x_3 = -d$ (plate thickness d) corresponds to the bottom surface of the plate. The amplitudes, respectively, phase angles are given to the left and right. For the calculation of these amplitudes and phases, the following three conventions are adopted from Disperse:

1. **Phase normalization of amplitudes.** The field components of **Displacement**, **Stress**, and **Strain** vary harmonically both in time and space. Therefore, they have amplitudes and phases. For each component of **Displacement** u_i , **Stress** σ_{ij} , and **Strain** ε_{ij} , $i, j = 1, 2, 3$, the **Phase** at the second point from the top surface is taken and the amplitudes at rest of the points are plotted with this **Phase** (the second point is taken because the amplitude at the surface can be zero sometimes). For instance, suppose that $\varphi_{u_{1(2)}}$ is the **Phase** of $u_{1(2)}$ at the second point from the top surface, then all **Phase** normalized points \hat{u}_1 are calculated by $\hat{u}_1 = u_{1(2)} e^{-i\varphi_{u_{1(2)}}}$. This is done for each component separately, e.g., $\hat{\sigma}_{22} = \sigma_{22} e^{-i\varphi_{\sigma_{22(2)}}}$. If fluid-filled half-spaces are involved, then the second point from the top of the top half-space is used as a reference, except for components which are zero in the fluid, which, for example, is the case in plates for $u_2, \sigma_{23}, \sigma_{13}, \sigma_{12}, \varepsilon_{23}, \varepsilon_{13}, \varepsilon_{12}$. In this case, the second point from the top surface of the immersed plate is used, as we had without fluid-loaded half-spaces. The reference point now has zero **Phase**, i.e., it lies on the positive real axis of the complex plane. The other points, however, are still complex in general. DC plots only their real parts, i.e., their projections onto the real axis in a consistent manner. The **Energy density** and **Power flow density** components are already real-valued because they are calculated using integrals over a complete cycle, according to Eqs. (12), (13), and (14) in Appendix A, so there is no **Phase** information to consider.

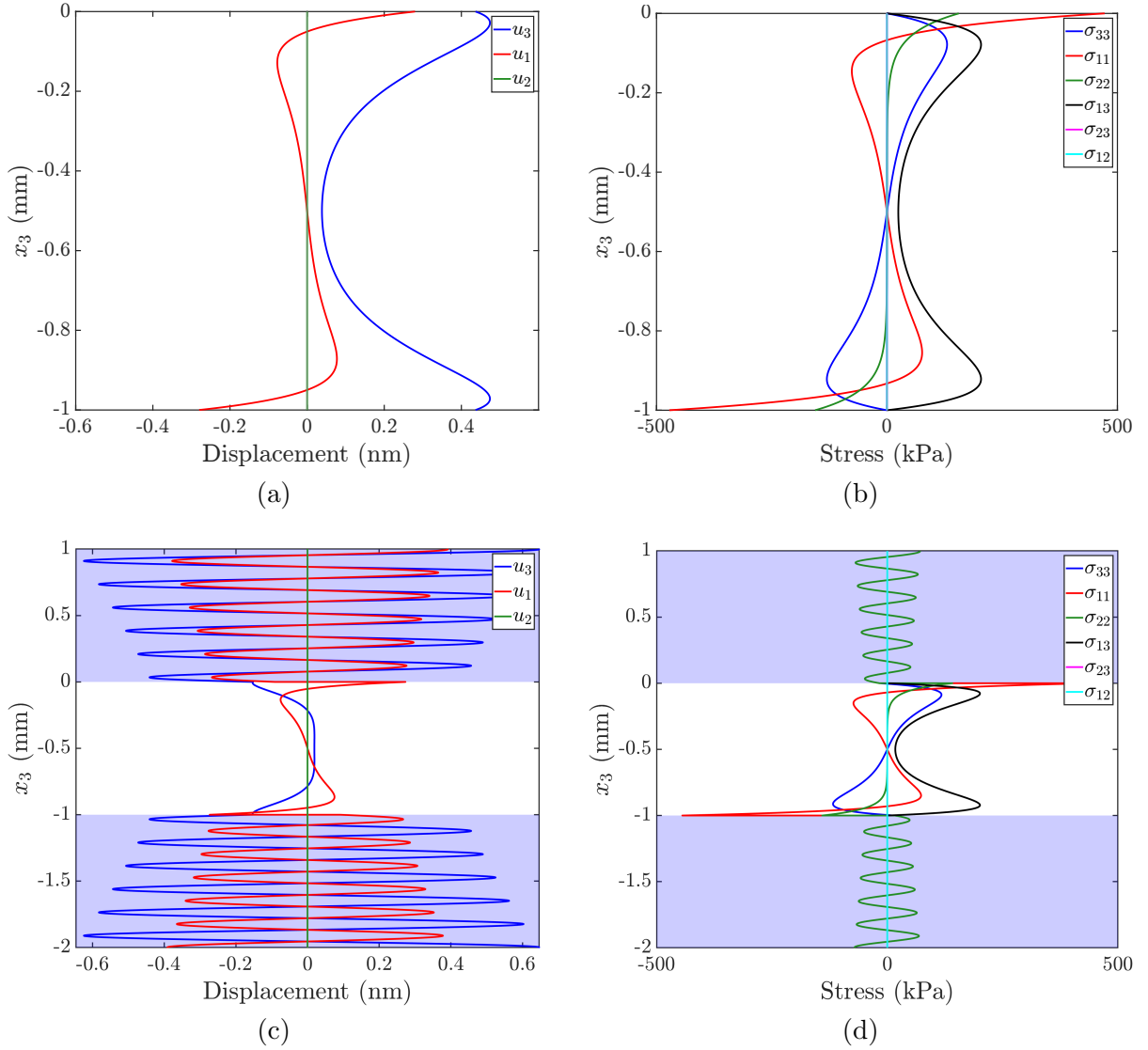


FIG. 6. (a), (c) Displacement and (b), (d) stress field components of the A_0 Lamb wave at 10 MHz in a 1 mm thick aluminum alloy 1100 plate. (a), (b) stress free surfaces (vacuum) and (c), (d) immersed in water.

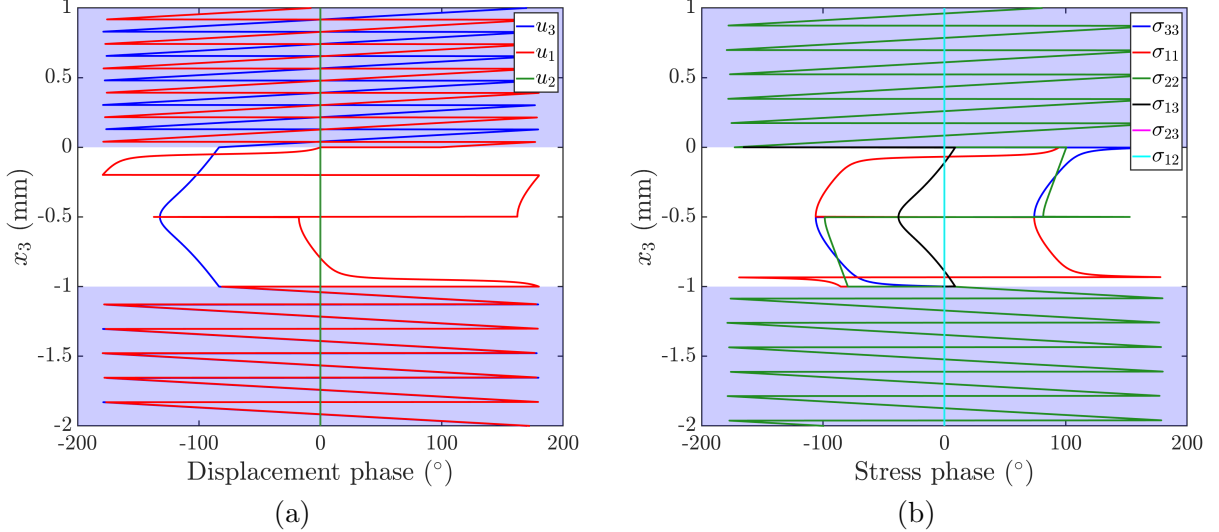


FIG. 7. Phase of the (a) displacement and (b) stress field components of the A₀ Lamb wave at 10 MHz in a 1 mm thick aluminum alloy 1100 plate immersed into water.

2. **Normalization of phases.** The phases of the **Displacement**, **Stress**, and **Strain** components are arbitrary, but the **Phase** differences between them are useful information. As a reference point, the top point of the in-plane **Displacement** component u_1 is taken, no matter if half-spaces are involved or not. The **Phase** at this point is set to zero, and the **Phase** differences of all points of all components are plotted in degrees with respect to it.
3. **Power normalization.** The amplitudes of the field components are calculated by summing up the contributions of the superposing bulk waves, and since their amplitudes are scaled arbitrarily, power normalization is done so that the field components can be compared between different points on the dispersion curves. Therefore, all amplitudes are calculated for guided waves carrying a power flow of one Watt in the propagation direction (x_1 in plates, z in rods and pipes, θ for circumferential waves). The power flow in a plate is per meter normal to the wave propagation direction (x_2). For modes in a rod or pipe, it is for the whole circumference, and for circumferential waves, it is per meter normal to the propagation direction (z). The calculation of the power flow is done using Eq. (14). For instance, to get the power normalized displacements, the displacements are divided through the square root of the power flow in the propagation direction P_1 (in a plate). Similar as in Disperse, the power normalization is not strictly right in case of fluid-loading because the power flow in the fluid is neglected. The developer of Disperse, Prof. Michael Lowe, describes the benefit of power normalization as follows:

“[...] once we normalise the mode shapes to power flow then we can do some meaningful comparison from one point on a curve to another, provided our understanding of the comparison is in that context only - e.g., if the mode has unit power flow, then it has a displacement at frequency xxx that is yyy times bigger than it would be at frequency zzz.”

Asked about the dimensions of the through-thickness energy density and power flow density, Prof. Lowe explains:

“The basis for unit power normalisation is that the steady state guided wave carries 1 Watt of energy past the observation point. Clearly the amount of energy depends on the width of the wavefront, so we choose to say that the 1 Watt is per metre width of wavefront (thus units are W/m). This is how this approach was set up by Auld when he was working on guided wave scattering and how his theory of reciprocity contributes to that. Normalisation of the power flow in this manner simplifies the equations for reciprocity and scattering. More detail of that in his book [55] if you want to follow it up.

The strain energy density is a local quantity that is evaluated at any chosen location in the field of the cross section. So this has to be J/m². If you integrate this through the thickness of the plate and then across 1 m of wavefront, then you get J/m. This is the energy of the wave per metre width. The rate, per second, of this energy passing the observation point is then W/m, i.e. as we had for the paragraph above.”

Displacement is given in nm, **Stress** in kPa, **Strain** is dimensionless, **Energy density** in J/m², and **Power flow density** in W/m.

A note on the accuracy of the **Through-thickness profiles** (9) should be made. Notice that the calculation of the field components depends on the accuracy of the solutions of the dispersion curves. Errors occur if the dispersion curves have not been obtained with high accuracy. These errors become more pronounced at higher frequency-thicknesses. If you need high accuracy profiles, set a smaller value for **Phase velocity accuracy**. Dispersion curve tracing can be slower because it takes more bisections to reach the desired accuracy.

Use the **Quantity** drop-down menu to choose between **Displacement**, **Stress**, **Strain**, **Energy density**, and **Power flow density**. Select the **Mode** you want to analyze from the drop-down list. Set the **Frequency** at which to analyze the selected mode. **Samples x3** determines the number of sample points over the thickness of the waveguide at which the selected quantity is calculated. If you are considering fluid-loading, the **Half-spaces** check box is enabled. With the check box, you can switch the visualization of the **Half-spaces** on and off. In the edit field, you can set how far the **Half-spaces** above

and below the waveguide shall be shown in multiples of the waveguide thickness. For rods and pipes, the bottom of the plot represents the center of the waveguide. Therefore, only the outer half-space is affected by this option. The fluid-filling in a pipe is not a half-space. The **Phase** check box is only enabled if you have selected **Displacement**, **Stress**, or **Strain** in the **Quantity** drop-down menu. Press **Plot** to plot the **Through-thickness profiles** of in a new window. If you have checked the **Phase** check box, an extra plot with the phase angles will be shown in addition to the amplitude plot. To the left of the **Plot** button are six check boxes from which you can select which components of the selected **Quantity** shall be plotted. This facilitates analyzing a single component that is otherwise hidden in a plot crowded with up to six curves. In case you have chosen **Displacement**, **Energy density**, and **Power flow density**, only three check boxes are enabled. The labels of the check boxes change according to the selected **Quantity**. Let us discuss the **Displacement** in a plate. u_1 is the in-plane component along the propagation direction (x_1) of the guided wave. u_2 is in-plane but perpendicular (x_2) to the propagation direction, usually referred to as *shear horizontal*, and u_3 is the out-of-plane or normal **Displacement**. In isotropic materials, there exist only pure Lamb and shear horizontal waves. Pure Lamb waves have only nonzero u_1 and u_3 components (see Fig. 6(a)), and pure shear horizontal modes have only a nonzero u_2 component. A symmetric Lamb wave has the same **Displacement** amplitude u_1 (sign and absolute value) at the top and bottom of the plate, while an anti-symmetric Lamb wave has the same amplitude u_1 at the top and bottom, but with opposite signs, as depicted in Fig. 6(a). The character of a shear horizontal wave is determined by the same rules applied to u_2 . Figure 6(b) displays the four nonzero and the two zero stress components present in a pure Lamb wave. The components σ_{i3} vanish at the surfaces, i.e., the surfaces are traction-free, and no energy can leak into the surrounding vacuum. The **Displacement** component u_1 , the **Stress** component σ_{11} , and the **Strain** component ε_{11} at the top are always taken positive (to the right) as a convention. Let us now consider the fluid-loaded case shown in Figs. 6(c) and 6(d). The **Half-spaces** are shown up to a depth of one plate thickness above and below the plate. The **Stress** component σ_{33} does not vanish anymore at the plate's surfaces, so energy is transmitted into the water. However, σ_{13} and σ_{23} still vanish because non-viscous fluids such as water do not support shear stresses. For the same reason, only σ_{11} , σ_{22} , and σ_{33} are nonzero in the fluid, having all the same amplitude. Although counter-intuitive, the amplitude of leaky waves grows exponentially with the distance normal to the waveguide. Plotting deeper into the **Half-spaces** than in Figs. 6(c) and 6(d) (and in Fig. 8) shows this more clearly. The reason for this is that, the further we go away from the plate, the earlier have the rays been emitted from the plate, when the amplitude of the guided wave propagating in the waveguide was higher (see also Ref. [37]). A shear horizontal wave does not couple to a non-viscous fluid surrounding the plate since its only non-zero stress components are the shear stresses σ_{23} and σ_{12} .

In the **Mode shape** (10) panel, you can visualize the **Displacement** pattern (mode shape) in a waveguide and in the adjacent **Half-spaces** as they are deformed by continuously propagating guided waves. This is particularly helpful to get an idea of how a certain mode looks like at a certain frequency. For example, Fig. 8 shows the mode

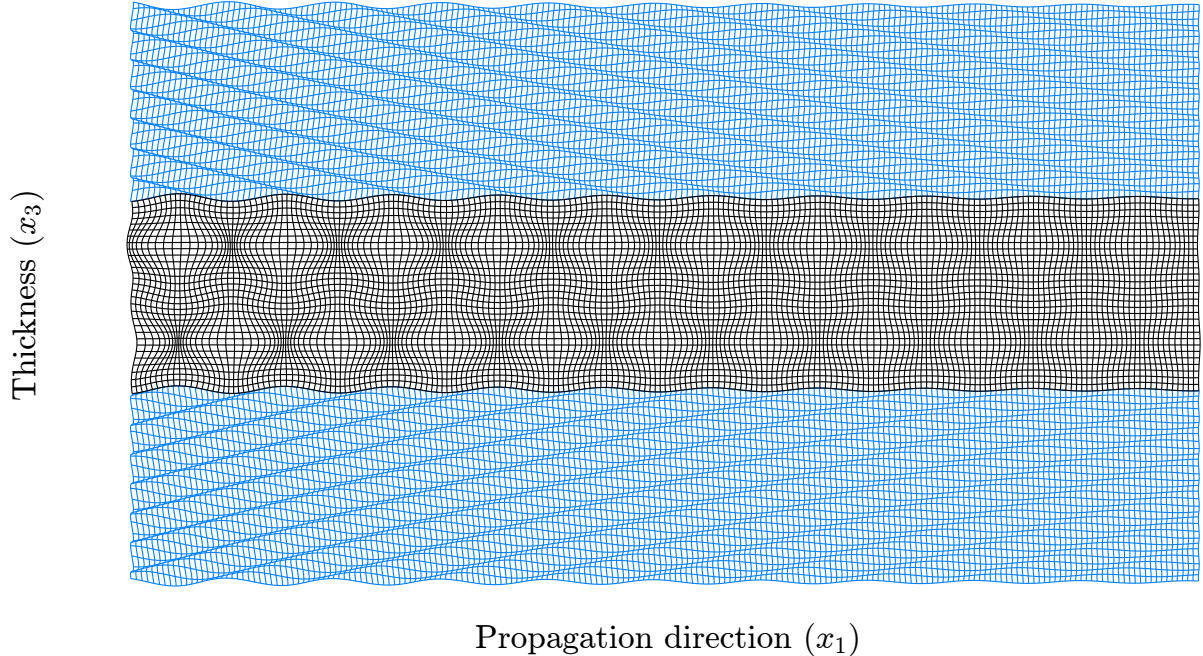


FIG. 8. Mode shape of the A₄ Lamb wave at 10 MHz·mm in an aluminum alloy 1100 plate immersed in water.

shape of ten wavelengths of the A₄ Lamb wave at 10 MHz·mm in an aluminum alloy 1100 plate immersed in water. Notice the wave fronts in the water and how the Lamb wave is damped through the loss of energy to the water. Or check out Figs. 9 (a) and (b), illustrating the mode shape of the L(0,1) mode at 450 kHz in a 10 mm diameter, 1 mm wall thickness aluminum alloy 1100 pipe filled with diesel oil and immersed in water. As in the **Through-thickness profiles** (9), the bottom in Fig. 9 (a) presents the center of the pipe. Again, the guided wave suffers attenuation due to energy leakage into the water (the diesel oil inside the pipe does not cause attenuation). Figure 9 shows a three-dimensional model of the pipe. The outer half-space is not plotted here (although it can be plotted) to see the pipe from outside. Of course, the **Displacement** is highly exaggerated in these plots. First, select the **Mode** you want to analyze from the drop-down list. In case you have selected **Rod** or **Pipe** as a **Geometry**, you can select the view type from the **plane** drop-down menu. Select **r-z** to plot the normal cross-sectional plot through the thickness of the waveguide. Choose **r-θ** for a three-dimensional plot, which is the most realistic representation of the waveguide. Set the **Frequency** at which to analyze the selected mode. **Wavelengths** determines how many wavelengths along the propagation direction are displayed. **Samples x1,x3** determines at how many sample points along the propagation direction, respectively, through the thickness, the mode shape is calculated. If you are considering fluid-loading, the **Half-spaces** check box is enabled. With the check box, you can switch the visualization of the **Half-spaces** on and off. In the edit field, you can set how far the **Half-spaces** above and below the waveguide shall be shown in multiples of the waveguide thickness. For rods and pipes, only the outer half-space is affected by this option. In the **Grid line every** field,

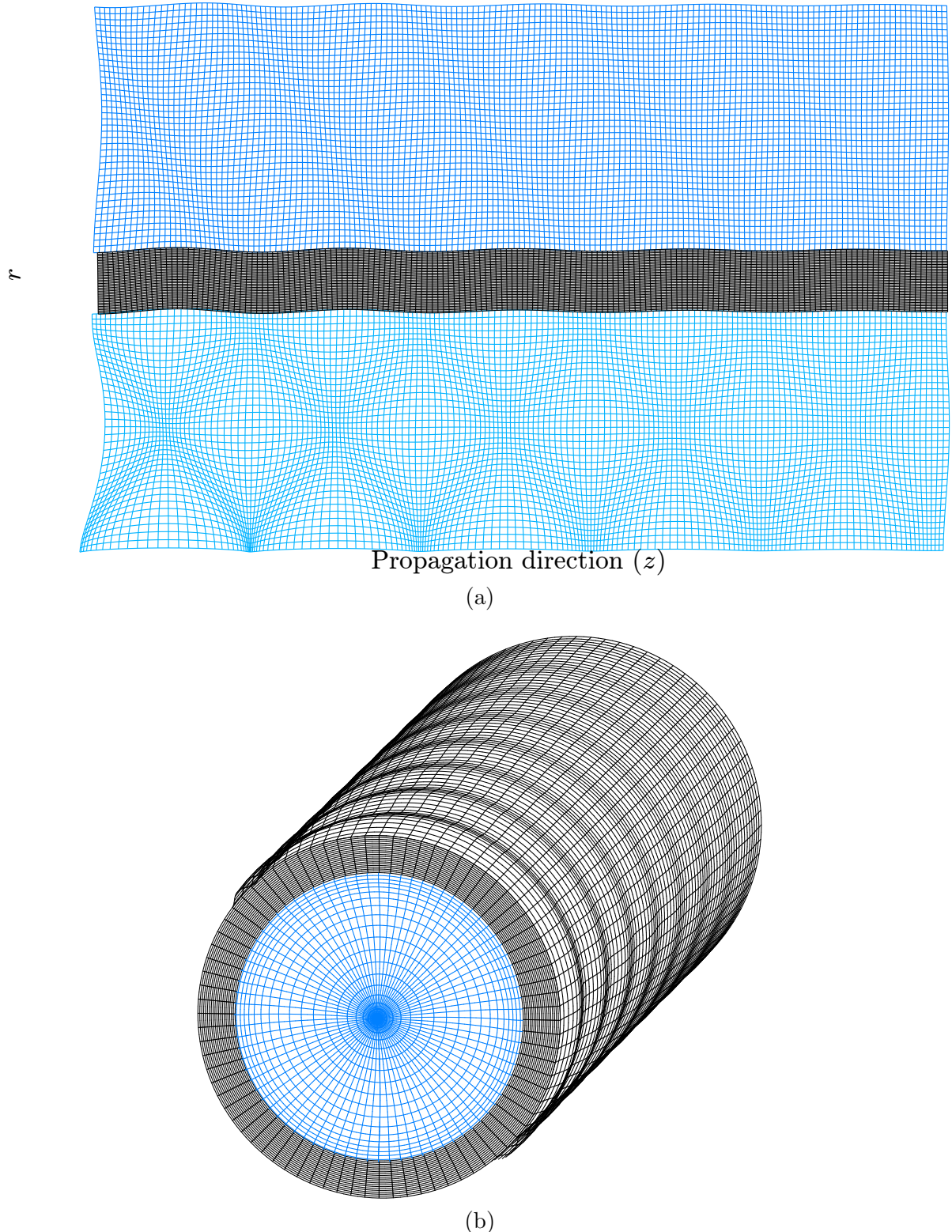


FIG. 9. Mode shape of the L(0,1) mode at 450 kHz in a 10 mm diameter, 1 mm wall thickness aluminum alloy 1100 pipe filled with diesel oil and immersed in water. (a) Cross sectional view ($r - z$). (b) Three-dimensional view ($r - \theta$).

you can specify how many grid lines shall be drawn in the mode shape. This number is updated automatically when you change the number in **Samples x1**. Use **Gain** to magnify the **Displacement** for clarity. Check **Undistorted** to toggle the undistorted grid. Go to the **Animation settings** sub-panel to set up an animation of the grid. The **Cycle duration** determines how long an animated cycle takes. Adjust the **Frame rate** of the movie. The **Movie quality** affects only the quality of the exported movie. Set a value between zero and one hundred. If you check **Animate** and press **Plot**, the animation starts running in an extra window until you close that window. If you leave **Animate** unchecked, only a static grid is plotted.

If you want to export plots and movies in an easy way, you can use the **Export settings** (11). Use the check boxes **PDF** and **PNG** to specify the format of the exported plot. **PDF** is a vectorized graphic that I used for the plots made by DC for this manual. **PNG** in contrast is a rendered graphic for which you can set the **PNG resolution** in dots per inch (dpi). The better performance of a vectorized graphic becomes obvious upon zooming in. Compare Figs. 9 (a) and (b), which are a **PDFs**, to one of the DC screenshots, which are **PNG**. The font in all plots made by DC is the standard L^AT_EX-font “Computer Modern”. Type the **File name** and the **Directory** to specify where the plot/movie is exported to. If you check **Export plots** and then press any of the three **Plot** buttons (their labels change to **Export**), the respective plot will be exported. If you check **Animate** in (10) and then press the **Export** button, the animation is displayed in a new window. Once all frames are captured, the window closes automatically and the movie be exported. The movie consists of 5 repetitions of the calculated cycle.

If you want to perform your own processing on the dispersion curves, you can export them. Enable the **Dispersion curves** check box and select from the top drop-down menu to the right which dimension the frequency axis should have, namely **kHz**, **MHz**, or **MHz·mm**. Then press the ***.mat**, ***.xlsx**, and ***.txt** buttons to export the data in the specific file format. For each mode family, a separate file will be generated in the specified **Directory**, containing all modes belonging to the respective family. For each mode, phase velocity (m/ms), energy velocity (m/ms), propagation time (μ s), co-incidence angle ($^{\circ}$), wavelength (mm), wavenumber (rad/mm), and attenuation (Np/m) are exported. In the second drop-down menu, you can select **Horizontal arrangement** or **Vertical arrangement** of the mode data in the files. You can also export the through-thickness profiles selected in the **Through-thickness profiles** (9) panel. Enable the **Through-thickness** check box and upon pressing the ***.mat**, ***.xlsx**, and ***.txt** buttons, the selected through-thickness **Quantity** of the selected **Mode** at the chosen **Frequency** is exported to the desired file format. If you have checked the **Phase** check box in the **Through-thickness profiles** (9) panel, the phase information will be exported, too.

Adjust the **Plot layout settings** (12) according to your preferences. For the plots in this manual, I switched the **Title** off. Use the **Legend location** drop-down menu to place the legend in the **Through-thickness profiles** (9) inside or outside the axes. You can also adjust the **Box line width** and the **Curve line width**. Only for the dispersion curves, you can adjust the **Dispersion curve colors**, for symmetric modes

in the field **S**, for anti-symmetric modes in the field **A**, and for non-symmetric modes in **B**. If you have selected **Rod** or **Pipe** as a **Geometry**, you can set the color for torsional and longitudinal modes in the **T,L** field and that of the flexural modes with $n = 1$ in the **F** field. If **Geometry** is **Circumferential**, the mode color can be set in the **C** field. You can compose any color by setting the proportions of red, green, and blue. Set a value between zero and one for each proportion, e.g., [1 0 .5]. Change the **Font size** of the **Title**, **Axes labels**, **Axes ticks**, **Mode labels**, and of the **Legend**. Press **Default**, to restore the default settings.

4.3 Anisotropic

In this section, we conduct guided wave modeling in multilayered anisotropic laminates such as the fiber reinforced composite sketched in Fig. 10. **Hybrid** laminates containing layers of different materials and material symmetry classes are also possible. Available material classes are **Orthotropic**, **Transversely isotropic**, **Cubic**, and **Isotropic**. Composite laminates are stackings of m layers with layer thicknesses d_m , consisting of **Orthotropic** or **Transversely isotropic** fiber-epoxy combinations. For each layer, we assign a local (crystallographic) Cartesian coordinate system $x'_{i,m} = (x'_1, x'_2, x'_3)_m$ residing on the top of the m th layer, and we define the layers to lie parallel to the x'_1 - x'_2 -plane. The fibers are oriented along $x'_{1,m}$, while $x'_{3,m}$ is normal to the layer. To describe this system with arbitrary layer orientations in a convenient way, we introduce the nonprimed global coordinate system $x_i = (x_1, x_2, x_3)$. We choose it such that the laminate lies in the x_1 - x_2 -plane, x_1 is the direction of guided wave propagation, and x_3 is the thickness direction of the laminate. With respect to the global coordinate system, the local coordinate systems are yielded by a counterclockwise rotation of an angle Φ_m

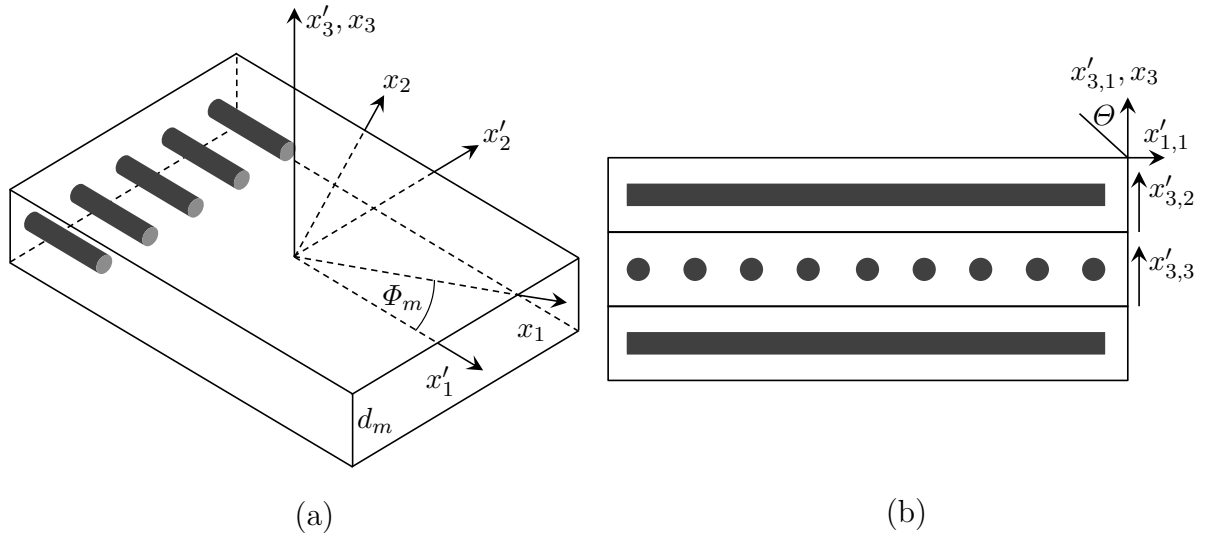


FIG. 10. (a) Single composite layer with local (crystallographic) coordinate system x'_i and global coordinate system x_i , $i = 1, 2, 3$. (b) Layered composite plate with [0/90/0] orientation with respect to the x'_1 -axis.

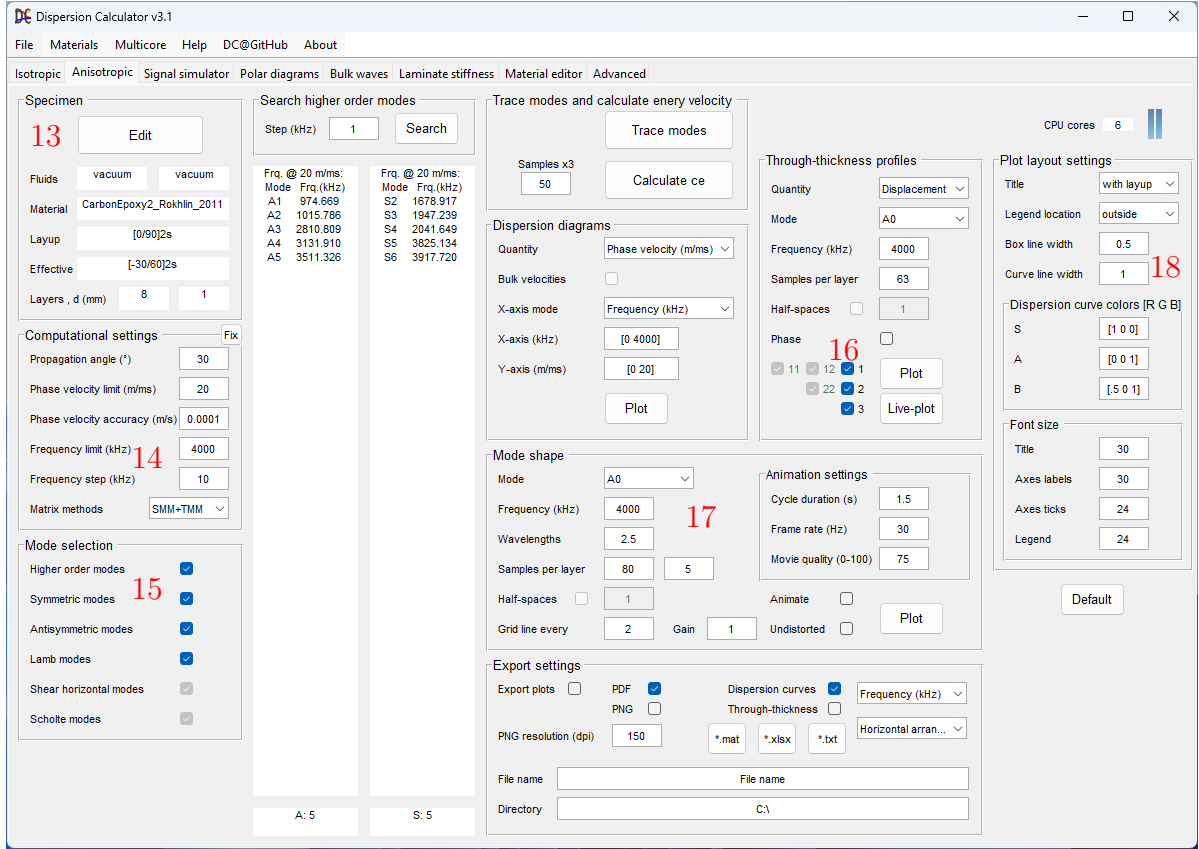
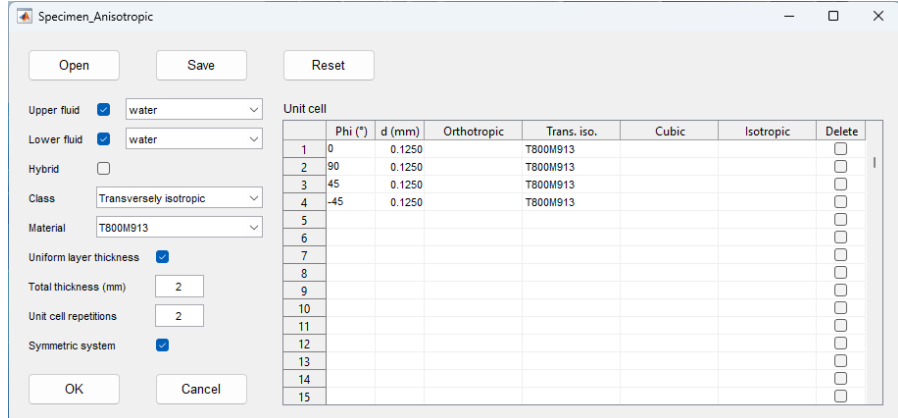


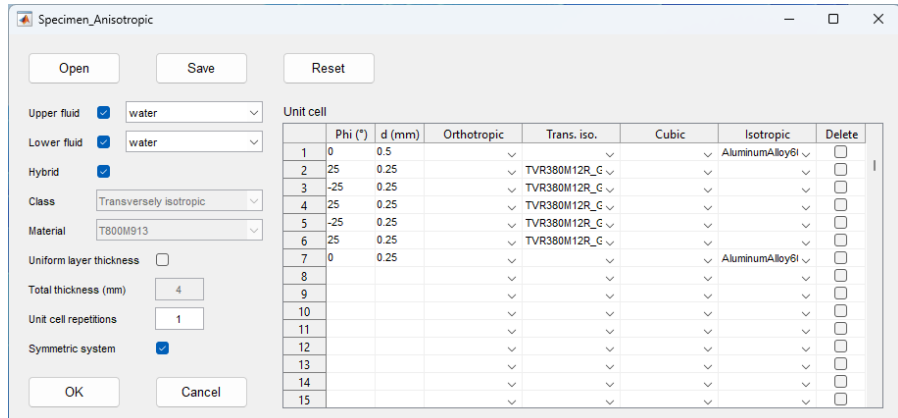
FIG. 11. The tab for the calculation of anisotropic specimens.

between x_1 and $x'_{1,m}$ about the x_3 -axis. Hence, x_3 and $x'_{3,m}$ coincide.

The **Anisotropic** tab looks similar to the **Isotropic** tab. Only panels that are new or different will be explained in this section. First, define the laminate in the **Specimen** (13) panel shown in Fig. 11. Press **Edit** to open the specimen setup depicted for two different situations in Fig. 12. First of all, decide whether you want to consider fluid-loading or not. If you want to add a fluid to the upper half-space, check the **Upper fluid** check box to activate the drop-down menu on the right, and then select a fluid from it. The same goes for the lower half-space via the **Lower fluid** check box and the respective drop-down menu. Leaving a check box unchecked means that the corresponding half-space is filled with a vacuum. You can fill one half-space with a fluid and leave the other one stress free, i.e., filled with a vacuum. Next, decide whether you want to set up a laminate containing layers from only one material, as the case in typical composites, or if you want to create a hybrid laminate containing layers of different materials, like for instance glass laminate aluminum reinforced epoxy (GLARE) [21]. In the first case, leave **Hybrid** unchecked, as shown in Fig. 12(a). Select a material class from the **Class** drop-down menu. According to your choice, the corresponding materials will be listed in the **Material** drop-down menu. Select a material. In the second case, check **Hybrid**, as shown in Fig. 12(b). The **Class** and **Material** drop-down menus become inactive, but the four columns in the **Unit cell** table named **Orthotropic**, **Trans. iso.**, **Cubic**,



(a)



(b)

FIG. 12. The specimen setup. (a) Single material laminate. (b) Hybrid laminate (GLARE).

and **Isotropic** are now active (they are inactive in case **Hybrid** is unchecked). For each layer, represented by one row in the **Unit cell** table, you can select any material from the four drop-down menus. Any selection will overwrite a preceding selection in the same row. Now, decide if the layup should have **Uniform layer thickness** or not. If yes, DC deduces the layer thicknesses from the **Total thickness**, which you can enter below. You will see the layer thicknesses in the **d (mm)** column update automatically when you change the number of layers or the **Total thickness**. Notice that the **Total thickness** is the overall thickness of the laminate, not just of the **Unit cell**. The values in the **d (mm)** column can not be edited if you have checked **Uniform layer thickness**. If you uncheck **Uniform layer thickness**, the **d (mm)** column will be active, and you must enter each layer's thickness in millimeters. In this mode, the **Total thickness** field cannot be edited, but it will show the total thickness calculated from your entries. Complete your definition of the **Unit cell** by filling the **Phi (°)** column with the layers' orientations. Typically, Φ is the fiber direction in composite materials. In order to delete a layer, click the corresponding check box in the **Delete** column. The **Unit**

cell table offers an immense amount of four hundred entries. This ensures that even the largest rocket booster laminates, which can be a nonrepeated unit cell by their own, can be entered. By contrast, unit cells in more common laminates are much smaller, often having only four or eight layers. Note that the uppermost layer in the table refers to the uppermost layer of the laminate. Use **Unit cell repetitions** to specify how many repetitions of the unit cell are contained in the layup. Use only integer numbers. Check **Symmetric system** if the layup is symmetric with respect to the middle plane of the plate/laminate. Now, you can **Save** the specimen definition and **Load** it in future sessions. Press **Reset** to reset the specimen definition to a single orthotropic layer. Press **OK** to accept the specimen definition or **Cancel** to discard it. The setup closes and the specimen definition is displayed below the **Edit**-button.

A few words should be said about setting up a unit cell in a proper way. With reference to the usual composite layup notation, we write the layup as $[unitCell]_{n(s)}$, where $n = 1, 2, \dots$ is the number of unit cell repetitions and “s” stands for symmetric. Basically, the unit cell should be kept as simple as possible in order to maximize efficiency and robustness in the dispersion curve calculation. Let us consider a few examples:

- [0]. Users are tempted to set up a unidirectional laminate by multiple layers, *e.g.*, [0/0/0/0] because this is how the laminate was manufactured. Layups containing layers with all the same orientation and material are not accepted. Replace them by one layer [0] having the total thickness of the four layers. This is equivalent because DC assumes rigid bonding between the layers. Furthermore, it will be more efficient since the computational expense scales with the number of layers.
- [0/90/45/0/0/0/0]. The same thing, but DC does not prevent you from doing this. Avoid adjacent layers with the same layer orientation and material, but group them into one single layer of greater thickness. Uncheck **Uniform layer thickness** and enter the layers’ thicknesses into the **d (mm)** column.
- [0/90]₂. Do not set up the unit cell as [0/90/0/90], but set it to [0/90] and set the **Unit cell repetitions** to two, similarly as shown in Fig. 12(a). This will be more efficient.
- [0/90]_s. DC does not let you define symmetric unit cells like [0/90/90/0] or [0/90/0]. Instead, set [0/90] and check **Symmetric system**, as shown in Figs. 12(a) and 12(b). Only by doing so, DC automatically recognizes that symmetric and anti-symmetric modes can be distinguished. In case of [0/90/0], uncheck **Uniform layer thickness** and divide the thickness of the 90° layer in half in the **d (mm)** column. Such a situation is present in Fig. 12(b). The center layer of this GLARE laminate (taken from Ref. [21]) is a 0.5 mm thick aluminum layer. In row no. 7, it is cut in half.
- [Al/0/0/0/0/Al/0/0/0/0/Al]. This is another GLARE laminate taken from Ref. [21]. Set this up as [Al/0/Al]_s. The corresponding layer thicknesses in this unit cell are 0.5 mm, 1.25 mm, and 0.25 mm, adding up to a 4 mm thick laminate.

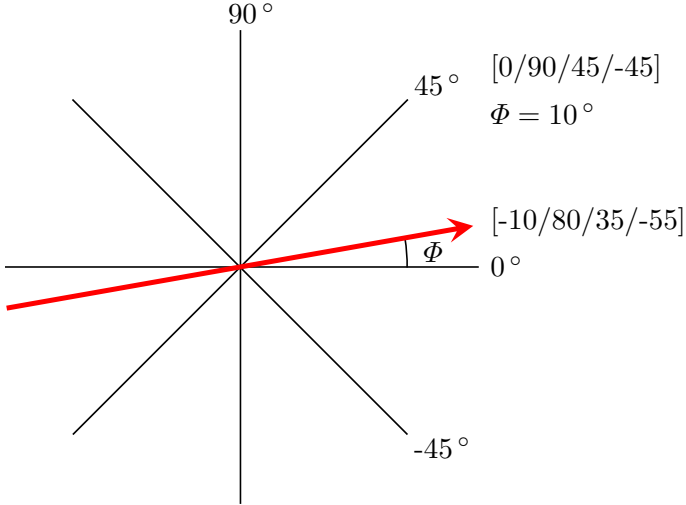


FIG. 13. Wave propagation along a **Propagation angle** of $\Phi = 10^\circ$ in a $[0/90/45/-45]$ layup. A positive Φ results in a counterclockwise rotation of the propagation direction (red arrow) vs. the fiber orientations, yielding the **Effective** layup $[0/90/45/-45]-10 = [-10/80/35/-55]$.

Now, go to the **Computational settings** (14). Define the **Propagation angle** Φ for the guided waves with respect to the layer orientations. Consider for example the $[0/90/45/-45]$ layup sketched in Fig. 13. A positive **Propagation angle** Φ results in a counterclockwise rotation of the propagation direction vs. the fiber orientations, yielding the **Effective** layup, respectively, the angles $\Phi_m [0/90/45/-45]-10 = [-10/80/35/-55]$. The **Phase velocity limit** is set to 20 m/ms by default, and it does not change automatically. The **Frequency limit** is set such that a maximal frequency-thickness product of 4 MHz·mm is covered by default. Starting in DC v3.1, you can use the **Matrix methods** drop-down menu to choose if the transfer matrix method (TMM) shall be used instead of the stiffness matrix method (SMM) whenever there are stable conditions for TMM. Stable conditions for TMM are above the red line in the generic dispersion diagram in Fig. 14. TMM becomes unstable when the bulk waves in the layers turn evanescent. Therefore, before starting dispersion curve tracing, DC performs a phase velocity sweep at the maximum frequency covered by the dispersion diagram (14000 kHz in Fig. 14). DC starts at a high phase velocity, and as the phase velocity decreases, the bulk waves become evanescent and TMM becomes increasingly inaccurate and unstable eventually. DC determines the phase velocity where the inaccuracy sets in and adds a very significant safety on top. This determines the slope of the inclined part of the red line. The slope accounts for the fact that the inaccuracy range extends (from zero) to lower phase velocities at lower frequencies. However, the inaccuracy range can never exceed that phase velocity above which all bulk waves are homogeneous (not evanescent). This phase velocity is indicated by the horizontal part of the red line. There are four benefits of using TMM instead of SMM above the red line. Firstly, TMM computes faster, in particular when there are many layers. Secondly, the dispersion equation amplitudes obtained with TMM do not have maxima, which when using SMM can impede

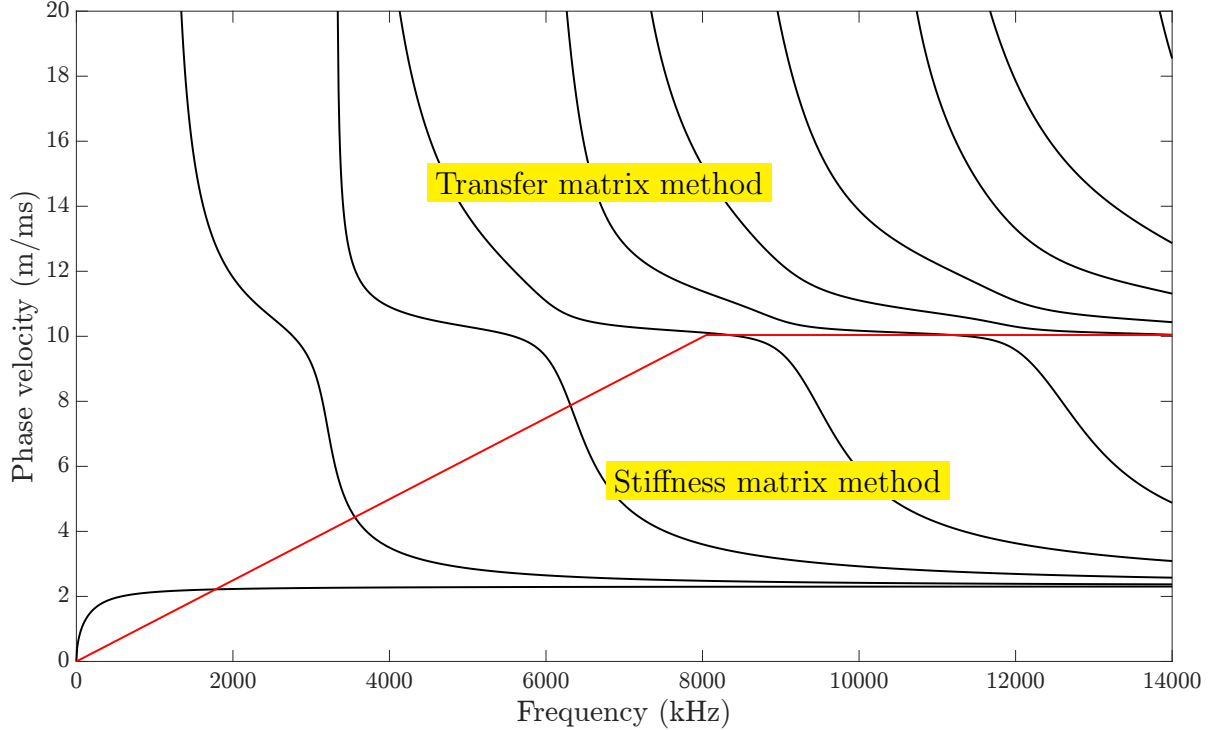


FIG. 14. Generic dispersion diagram. The transfer matrix method is used for dispersion curve tracing above the red line. The stiffness matrix method takes over below the red line.

the tracing algorithm from finding the wanted mimima (see a dispersion equation amplitude minimum in Fig. 30). Third, TMM produces much more pronounced mimima with quasi-SH modes so that it is more robust than SMM in tracing such dispersion curves. And fourth, TMM is stable at very low frequencies and thicknesses where SMM becomes unstable. Therefore, the default setting of the **Matrix methods** drop-down menu is **SMM+TMM**. However, it should be noted that using SMM alone (above and below the red line) brings better results sometimes. Choose **SMM** in this case. Try both options in difficult cases.

In the **Mode selection** (15) panel, some of the check boxes can be inactive. The **Scholte modes** check box will be inactive if you do not consider fluid-loading. The active state of the other check boxes depends on the **Specimen settings** and on the **Propagation angle** in the following way:

Decoupled case

The decoupling into pure Lamb waves (only sagittal motion (x'_1 - x'_3 -plane)) and shear horizontal waves (motion only in x'_2) depends on material symmetries and on the propagation direction of the guided waves. In case of decoupling, both mode families can be traced separately. Otherwise, sagittal and shear horizontal motion are coupled, and no separation into Lamb and guided shear horizontal modes is possible.

- **Orthotropic and transversely isotropic.** Decoupling occurs for wave propagation parallel or normal to the fibers ($\Phi = 0^\circ, 90^\circ$). This is possible in a single layer or in a cross-ply laminate $[0/90]_{n(s)}$, $n = 1, 2, \dots$.
- **Cubic.** Decoupling occurs for guided wave propagation along $\Phi = 0^\circ, 45^\circ, 90^\circ$.
- **Isotropic.** Decoupling occurs for any propagation direction.

In case we have a hybrid layup, the whole system allows decoupling only in case all contributing layers support decoupling in the given situation.

Symmetric system

In symmetric systems, DC traces symmetric and anti-symmetric Lamb, shear horizontal, and, in case of fluid-loading, also Scholte waves separately. If the system is non-symmetric, so are the modes and no separation is possible. The only exception from this are shear horizontal modes. If the laminate is symmetric, but the upper and lower half-spaces are covered by different fluids, the shear horizontal modes are still symmetric and anti-symmetric because shear horizontal modes do not couple to non-viscous fluids.

- A system is symmetric if the top half of the layup mirrors the bottom half in terms of layer (fiber) orientations, layer thicknesses, and layer materials. This is always the case in a single layer. In case of fluid-loading, a symmetric system requires in addition that the upper and lower half-spaces are filled with the same fluid.

The four possible configurations are listed in Table 2. If Lamb and shear horizontal waves are coupled, they are called Lamb waves anyway in reminiscence to Sir Horace Lamb who described Lamb waves mathematically for the first time in 1917 [43]. Lamb dealt only with isotropic media wherein the coupling does not occur. In contrast to pure modes, coupled modes have three nonzero displacement components. If the system is non-symmetric, the modes do not have a clear symmetric or anti-symmetric character, except for shear horizontal modes, as said above. In DC, non-symmetric modes are unconventionally denoted with the letter “B”. To the best of my knowledge, there does not exist an official notation for non-symmetric modes.

TABLE 2. Possible configurations in fluid-loaded anisotropic laminates.

symmetric	decoupled	modes
✓	✓	S, A, S^{SH} , A^{SH} , $S^{Scholte}$, $A^{Scholte}$
✓	✗	S, A, $S^{Scholte}$, $A^{Scholte}$
✗	✓	B, B^{SH} (S^{SH} , A^{SH}) ^a , $B^{Scholte}$
✗	✗	B, $B^{Scholte}$

^a If the half-spaces are covered by different fluids, but the layup is symmetric, S^{SH} and A^{SH} can be distinguished.

If you have a symmetric system, you can choose to calculate the **Symmetric modes** and/or the **Antisymmetric modes**, otherwise the corresponding check boxes will be inactive. If the above described exception for the shear horizontal waves occurs, symmetric and antisymmetric shear horizontal modes will be calculated anyway. In the decoupled case, you can calculate **Shear horizontal modes** separately, otherwise the corresponding check box will be inactive

In the **Through-thickness profiles** (16) panel and in the **Mode shape** (17) panel, the **Samples x3** option is replaced by **Samples per layer**. In coupled cases, i.e., for wave propagation along arbitrary directions in anisotropic media, instead of the energy velocity, it is calculated the energy velocity components, its magnitude, and skew angle. Therefore, if you **Export** the dispersion curves in the **Export settings** panel, you get the energy velocity components c_{e1} and c_{e2} (m/ms), the energy velocity magnitude $|\vec{c}_e|$ (m/ms), and the energy velocity skew angle ($^\circ$). For a discussion on the energy velocity in anisotropic specimens, read Appendix A. In the **Plot layout settings** (18) panel, you can use the **Title** drop-down menu to display the plot title **with layup** or **without layup** or **no title** at all.

4.4 Signal simulator

The **Signal simulator** (see Fig. 15) simulates the temporal and frequency responses of single and multiple guided wave modes after propagating a certain distance in a specimen, based on the dispersion curves obtained in the **Isotropic** and **Anisotropic** tabs (currently limited to plates). Therefore, the tool is valuable to any individual performing NDI or SHM using guided waves. The dispersion diagrams calculated before will help him to excite the desired mode in a specimen. However, it is often difficult to excite only one particular mode, especially when the frequency-thickness product becomes large. In situations where dispersion curves get close to each other in the dispersion diagram, it is very likely that multiple modes will be excited. Then, the inspector has to deal with multiple wave packets appearing in the measured signal of voltage versus time. The **Signal simulator** enables him identifying the modes in the signal. The tool is also useful to interpret signals obtained from acoustical emission experiments. Or suppose you want to perform long-range testing on a pipe or on an aircraft wing structure. The dispersive nature of guided waves leads to a spreading and to a reduction in amplitude of the wave packet with increasing propagation distance because the different frequency components propagate at different phase velocities. Therefore, you would want to excite a weakly dispersive Lamb wave, retaining the shape of its wave packet over long distances. Another effect that becomes evident in the signals is damping due to fluid-loading and/or viscoelasticity. You would prefer a mode that suffers minimal damping loss in the required frequency range. With the **Signal simulator**, you can simulate the wave packets to find an appropriate mode for your task.

Notice that no particular method of excitation and reception is considered here. The assumption is that guided waves are generated *somewhat* at $x = 0$, with the excitation signal plotted on the left-hand side in the signal window (21), starting at $t = 0$. The propagated signal calculation is then based only on the dispersion diagram, which you

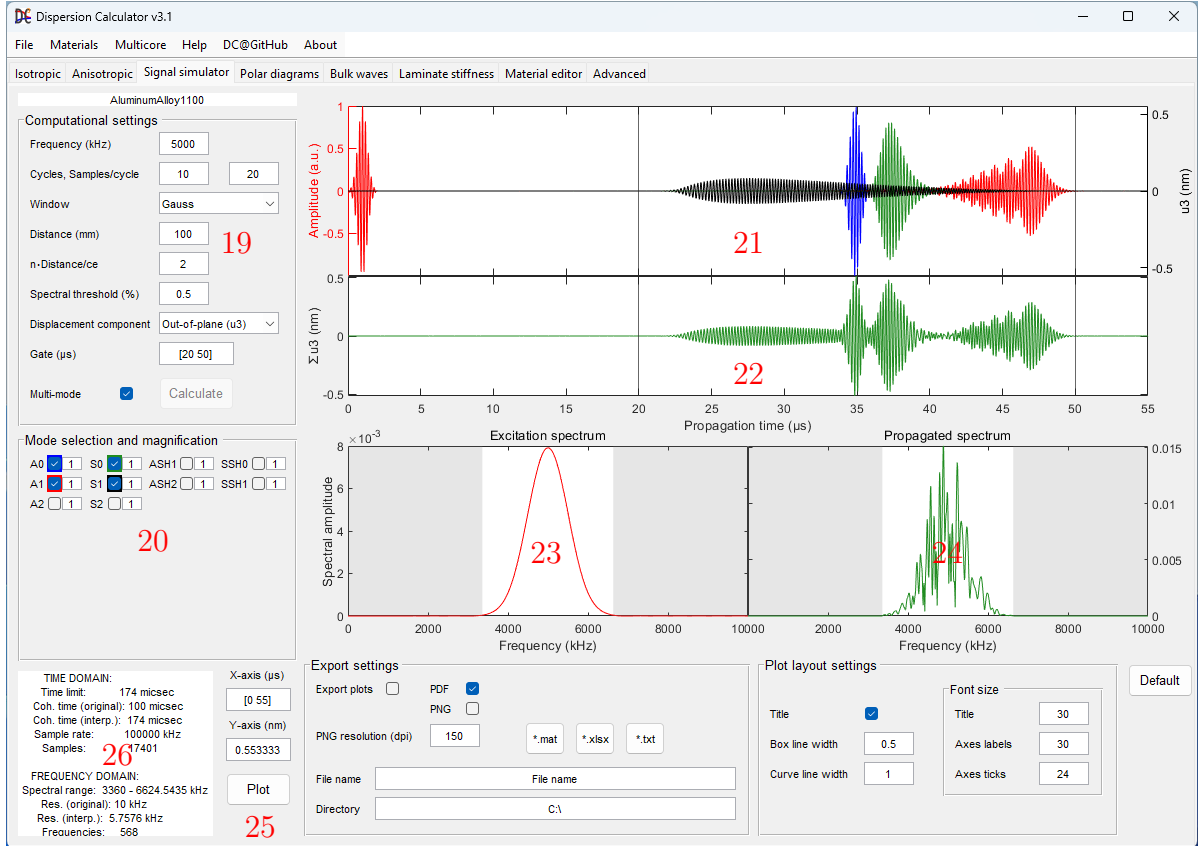


FIG. 15. The Signal simulator.

calculated before, i.e., plane harmonic waves are superposed, having the phase velocities (and attenuation) given by the dispersion curve of the respective mode in the frequency range seen in the **Excitation spectrum** (23). Power-normalization is performed on each contributing plane wave in the same way as done with the through-thickness profiles. The plotted amplitude can be chosen as the out-of-plane displacement (u_3) for Lamb waves or the in-plane displacement (u_1) for Lamb waves or u_2 for shear horizontal waves at the top of the plate, which are assumed to correlate most directly to the detected signal of voltage versus time. The signal is simulated for ideal and simplified conditions, so experimentally measured signals will look more or less different due to many influences present under real conditions. These are, for instance, the specific shape of the ultrasonic beam or a certain angle of incidence, whereas in the simulation, the “perfect” (coincidence) angle (for each contributing phase velocity in the spectrum) is assumed. Furthermore, waveguide imperfections are ignored such as surface roughness, layer debonding or other flaws. Calculating fully realistic signals requires a sophisticated model of the experimental setup, i.e., a detailed model of the sensors as well as of the waveguide to model the generated ultrasonic beam, the propagating wave field, and the received signal. This requires an FEM software such as COMSOL Multiphysics. You can, however, choose to plot the in-plane or the out-of-plane displacement, depending on what component your sensor is more sensitive to. Usually, in non-contact air-coupled ultrasonics, one

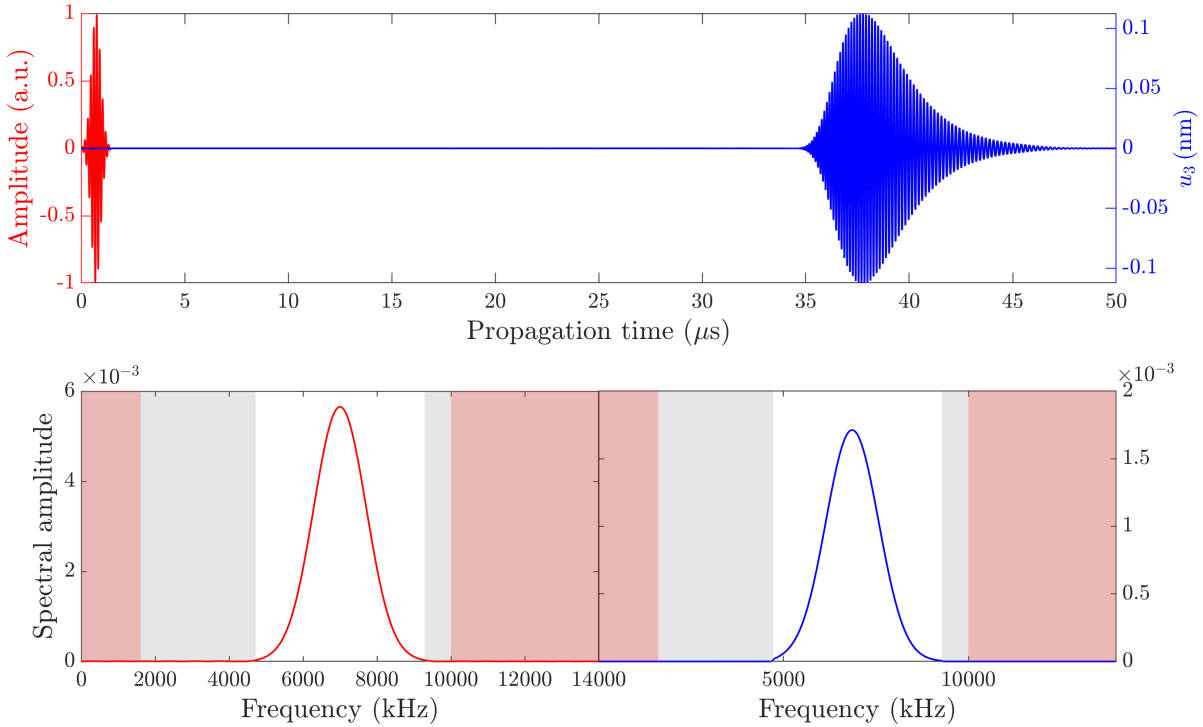


FIG. 16. Top: Simulated out-of-plane signal (ten cycles, Gaussian window) of the A₁ Lamb wave at 7 MHz after propagating a distance of 100 mm in a 1 mm thick free aluminum alloy 1100 plate. Bottom: Excitation spectrum (left) and propagated spectrum (right).

would choose the out-of-plane displacement, whereas in SHM, where you have sensor attached to the component, the in-plane displacement is more favored. In practice, the received signal will map a mixture of both components. The key point is that the **Signal simulator** calculates the displacement caused by the guided waves at the top surface, but the signal displayed on your measurement screen depends on how your sensor reacts to this displacement, and this can obviously not be included in the **Signal simulator**.

Once you have calculated a dispersion diagram in the **Isotropic** and **Anisotropic** tabs, the data will be available in the **Signal simulator**. The field above the **Computational settings** (19) gives the name of the material whose dispersion curves are used. Therefore, notice that whenever you calculate a new dispersion diagram, the prior data will be replaced by the new ones. To set up the simulation, go to the **Computational settings** (19) panel. At first, the excitation signal must be defined. Select the **Frequency** of the sinusoidal carrier wave and the number of **Cycles** within the wave packet. Enter the **Samples per cycle** in the excitation signal. This determines the sample rate, i.e., the resolution of the temporal signal. Then, choose a window function from the **Window** drop-down menu. There are listed four functions, namely **Gauss**, **Hann**, **Hamming**, and **Triangular**¹. By multiplying the carrier wave with the selected window function, the excitation wave packet is obtained. Define the **Distance** which the

¹https://en.wikipedia.org/wiki/Window_function

modes are supposed to propagate in the specimen. The option **n·Distance/ce** defines the temporal length t_{end} of the simulation in multiples n according to

$$t_{\text{end}} = nx/c_{\text{e1}}, \quad (1)$$

where x is the propagation distance and c_{e1} is the energy velocity component in the propagation direction of the chosen mode. n is set to two by default in order to ensure that the temporal axis covers the whole wave packet of a strongly dispersive mode. For short propagation distances, higher multiples n can be necessary. If you have checked **Multi-mode**, the lowest energy velocity among all contributing modes is used for the calculation of t_{end} . The advantage of defining t_{end} in the described way is that an appropriate temporal range is obtained automatically so that the user does not have to try and calculate by himself. Notice that you can edit the temporal axis later in the **X-axis** (25) field. The **Spectral threshold** defines which frequency range shall be used for the construction of the propagated wave packet(s). Only frequencies with spectral amplitudes exceeding this threshold in percent of the maximum spectral amplitude shown in the **Excitation spectrum** (23) will contribute to the simulation. This spectral amplitude maximum in the excitation signal is located exactly at the center **Frequency** defined above. By decreasing the threshold, a wider frequency range will be taken into account. This contributing frequency range is indicated by the white area in the **Excitation spectrum** (23) plot. When the threshold is changed, you will notice that the white area's width changes accordingly. The same happens also in the **Propagated spectrum** (24) plot. If you set a **Frequency** close to a cut-off frequency or to the top frequency in the dispersion diagram, a red area will appear, showing where no data are available (see Fig. 16). Therefore, when you calculate a dispersion diagram, set the top frequency high enough to not miss data for simulating a signal at high frequencies. From the **Displacement component** drop-down menu, you can choose to calculate the **out-of-plane (u3)** displacement or the **In-plane (u1/2)** displacement. Notice that the **Out-of-plane** displacement of shear horizontal waves is zero, so choose **in-plane (u1/2)** in this case. With the **Gate**, you can define the signal range for which the **Propagated spectrum** (24) shall be calculated. This range is indicated by the two vertical black lines in the signal plots (21) and (22). In case you have multiple wave packets in the signal, as shown in Fig. 15, you can put the gate around a particular mode to get its spectral amplitude distribution (24). If **Multi-mode** is unchecked, you can simulate only one propagated mode at a time. The **Mode selection** (20) panel (it is renamed to **Mode selection and magnification** when you check **Multi-mode**) is updated automatically to show the modes available at the **Frequency** defined above. Check a check box to simulate the corresponding mode. In the top window (21), the excitation signal will be plotted in red. Its amplitude is scaled to the LEFT amplitude axis, ranging from -1 to 1. The propagated signal (temporal response) is plotted in blue, and its amplitude is scaled to the RIGHT amplitude axis. The displacement amplitudes are power-normalized and given in nanometers in the same way as are the displacement components drawn in the through-thickness profiles of the **Isotropic** and **Anisotropic** tabs, as explained in Sec. 4.2, **Through-thickness profiles** (9). The middle window (22) appears only if **Multi-mode** is enabled. As mentioned above, you can change

the default temporal axis by editing **X-axis** (25). The displacement axis in the signal window (21) can be changed by editing **Y-axis** (25). We have already discussed the **Excitation spectrum** (23), displayed in the bottom left-hand window. The **Propagated spectrum** (24) (frequency response) is displayed in the bottom right-hand window. For a better view and in order to read values using the data tip tool, you can **Plot** (25) the simulations in a separate window. Figure 16 shows the simulated signal of the A₁ Lamb wave at 7000 kHz after propagating a distance of 100 mm in a 1 mm thick free aluminum alloy 1100 plate. The excitation signal consists of ten cycles multiplied with a Gaussian window. The wave packet arrives after a propagation time of 34.5 μ s. Due to dispersion, it has spread significantly. Its spectrum, shown in the bottom right plot, is shifted to lower frequencies, peaking at a frequency of 6860 kHz, a shift of 140 kHz with respect to the excitation spectrum, shown in the bottom left plot. The output window (26) gives some more information:

Time domain:

- **Time limit:** It is the calculated length of the temporal axis t_{end} .
- **Coherence time:** The coherence time t_c is the time after which the temporal response repeats itself, i.e., we will see a twin of the wave packet at each instant of time $n \cdot t_c$, $n = 1, 2, \dots$, away from the actual wave packet. The coherence time is calculated by

$$t_c = 1/\Delta f, \quad (2)$$

where Δf is the **Frequency step**, i.e., the frequency resolution of the calculated dispersion curves. Therefore, to avoid unwanted wave packet twins, we require that $t_c > t_{\text{end}}$. You can satisfy this by setting a small enough value for **Frequency step**, but you don't have to. If you have $t_c < t_{\text{end}}$, DC will interpolate the dispersion curves with a value of Δf small enough to meet $t_c > t_{\text{end}}$. In this case, the output window will read **Coh. time (original)**, giving the coherence time resulting from the native frequency resolution, followed by **Coh. time (interp.)**, giving the coherence time resulting from the interpolated frequency resolution.

- **Sample rate:** It is calculated by multiplying the **Frequency** with the **Samples per cycles**.
- **Samples:** It gives the total number of sample points contained in the temporal signal.

Frequency domain:

- **Spectral range:** This is the frequency range contributing to the construction of the propagated wave packets. It is indicated by the white areas in the spectral amplitude plots in the windows (23) and (24).
- **Resolution:** It is the frequency resolution of the dispersion curves, as set by **Frequency step**. In case of $t_c < t_{\text{end}}$, the output window will read **Res. (original)**,

giving the native frequency resolution, followed by **Res.** (**interp.**), giving the interpolated frequency resolution.

- **Frequencies:** This is the total number of frequency sample points contained in the **Spectral range**.

In the example shown in Fig. 16, the spectral range is from 4720 kHz to 9290 kHz. The red areas indicate where no dispersion curve data are available. The cut-off frequency of A_1 at a phase velocity of 20 m/ms is 1615 kHz so that no data are available below this value. The top frequency in the dispersion diagram is 10000 kHz, just high enough to not cut the white area contributing to the simulation.

If you enable **Multi-mode**, as shown in Fig. 15, you must first **Calculate** all modes present at the selected **Frequency**. You can terminate the calculation by pressing the **Stop**-button. After the calculation is finished, all modes will be plotted. You can show/hide any particular mode to see only those you want. The background colors of the checkboxes in the **Mode selection and magnification** (20) panel match the line colors of the corresponding modes plotted in the top window (21). To the right of each check box, the amplitude magnification can be entered. The (displacement) amplitudes are calculated for modes carrying a power flow of unity. However, in reality, each of the modes will carry a different power flow because they are excited at different efficiency. To account for that, the user can magnify the amplitude of each mode individually. Notice again that the amplitudes of the propagated wave packets are scaled to the right amplitude axis, whereas the excitation signal (red) scales to the left one. The middle window (22) shows the sum amplitude of all simulated modes, thereby representing the signal which the user measures in his experiment. By comparing it with the top window (21), he can ascribe particular modes to the contributions in window (22). The lower right-hand window now shows the **Propagated spectrum** (24) of the sum amplitude shown in window (22).

4.5 Polar diagrams

Often it is useful to have the guided wave dispersion versus the propagation direction in a laminate at a certain frequency rather than versus the frequency for a certain propagation direction. In the **Polar diagrams** tab (see Fig. 17), you can calculate polar diagrams that give a very intuitive picture of the anisotropic propagation characteristics of the fundamental modes in a laminate. These are set up as usual except that only unit cells that contain at least one zero degree layer are accepted. Notice that fluid-loading and viscoelasticity cannot be considered here. Then use the **Computational settings** (27) panel. The dispersion curves are traced in the frequency space, as usual, up to the **Frequency limit** with a certain **Frequency step**. Notice that after calculating the polar dispersion diagram(s), data are available not only at the **Frequency limit** but at each **Frequency step** from zero to **Frequency limit**. With the **Propagation angle limit** drop-down menu, you can choose to calculate the dispersion curves for propagation angles ranging from 0° to 180° or only to 90° . In the first case, to obtain the full polar diagram, the data will be copied to the third and fourth quadrant. In

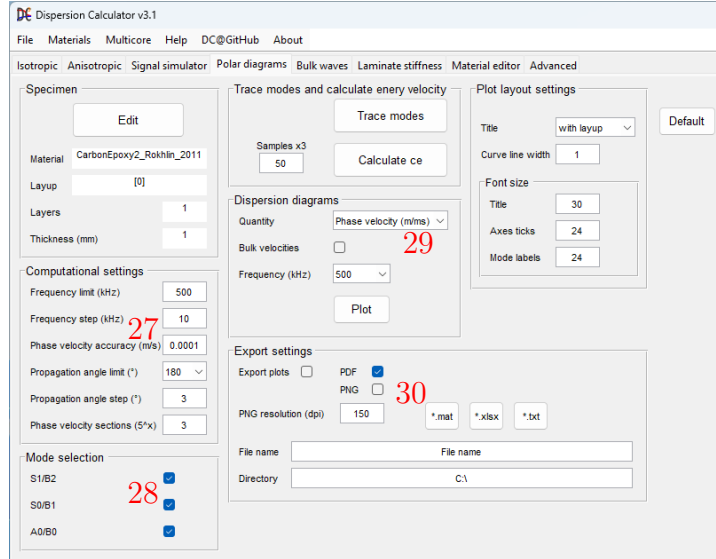


FIG. 17. The tab for the calculation of polar dispersion diagrams of the fundamental modes.

the second case, the data of the first quadrant will be copied to the three remaining ones. Notice that the second option is insufficient for unit cells such as [0/45]. This will become obvious by kinks in the polar diagrams at the quadrant borders. Use

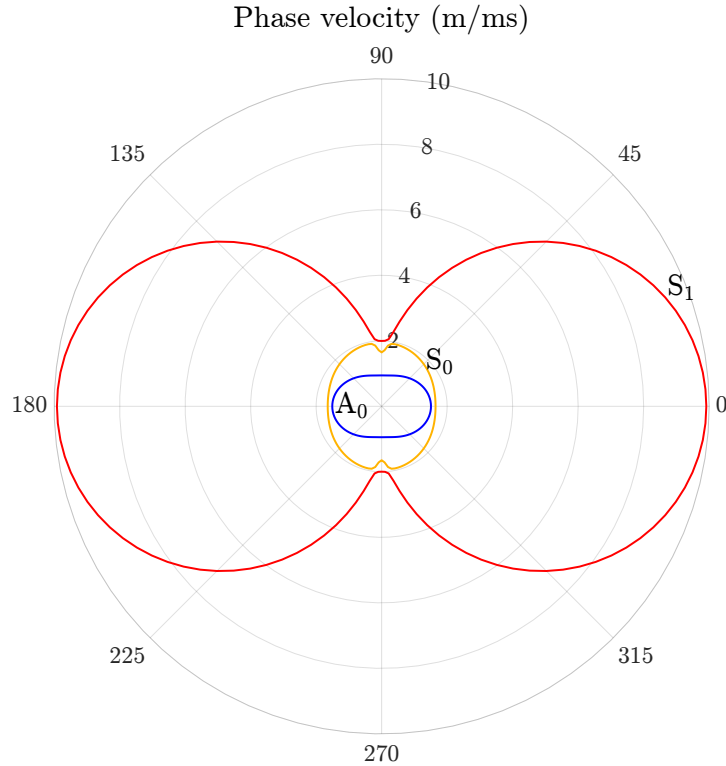


FIG. 18. Polar dispersion diagram at 500 kHz for 1 mm thick unidirectional T800M913.

Propagation angle step to define the propagation angle increments for which the dispersion curves will be calculated. In the **Mode selection** (28) panel, you can choose which ones of the fundamental modes A_0/B_0 , S_0/B_1 , and S_1/B_2 shall be calculated. In the **Dispersion diagrams** (29) panel, you can choose which **Quantity** to plot, namely the phase velocity, energy velocity, propagation time, coincidence angle, wavelength, and wavenumber versus the propagation direction. From the **Frequency** drop-down menu, select a frequency for which to plot the polar diagram. Upon pressing **Plot**, a new window will open with a polar diagram like the one displayed in Fig. 18. In the **Export settings** (30) panel, you can export the plots. Press the ***.mat**, ***.xlsx**, and ***.txt** buttons to export the polar dispersion curves at the selected **Frequency** to the desired file format.

4.6 Bulk waves

In the **Bulk wave** tab (see Fig. 19), you can model the behavior of elastic waves (bulk waves) in bulk material and their scattering on interfaces. In isotropic materials, the phase velocity of bulk waves is independent from the propagation direction, and the polarization is along the wave propagation direction for longitudinal waves (L) and

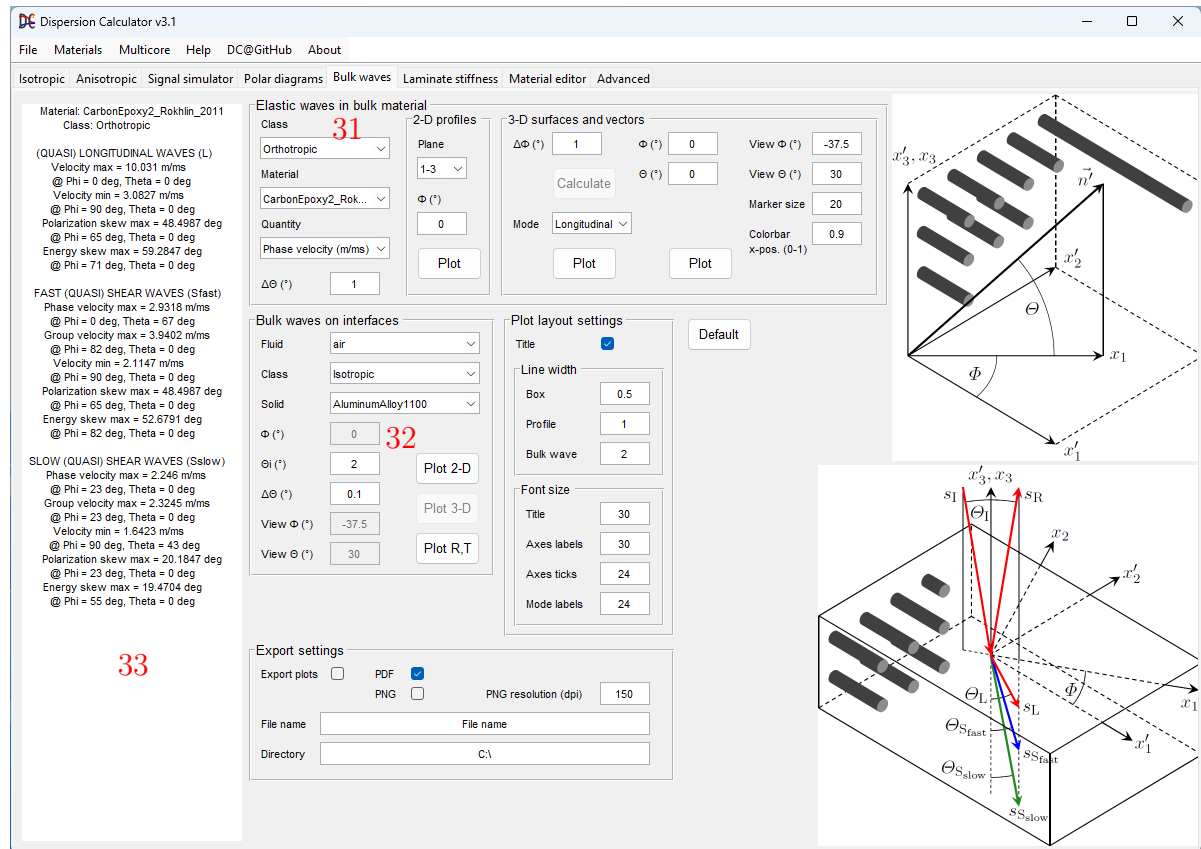


FIG. 19. The Bulk waves tab.

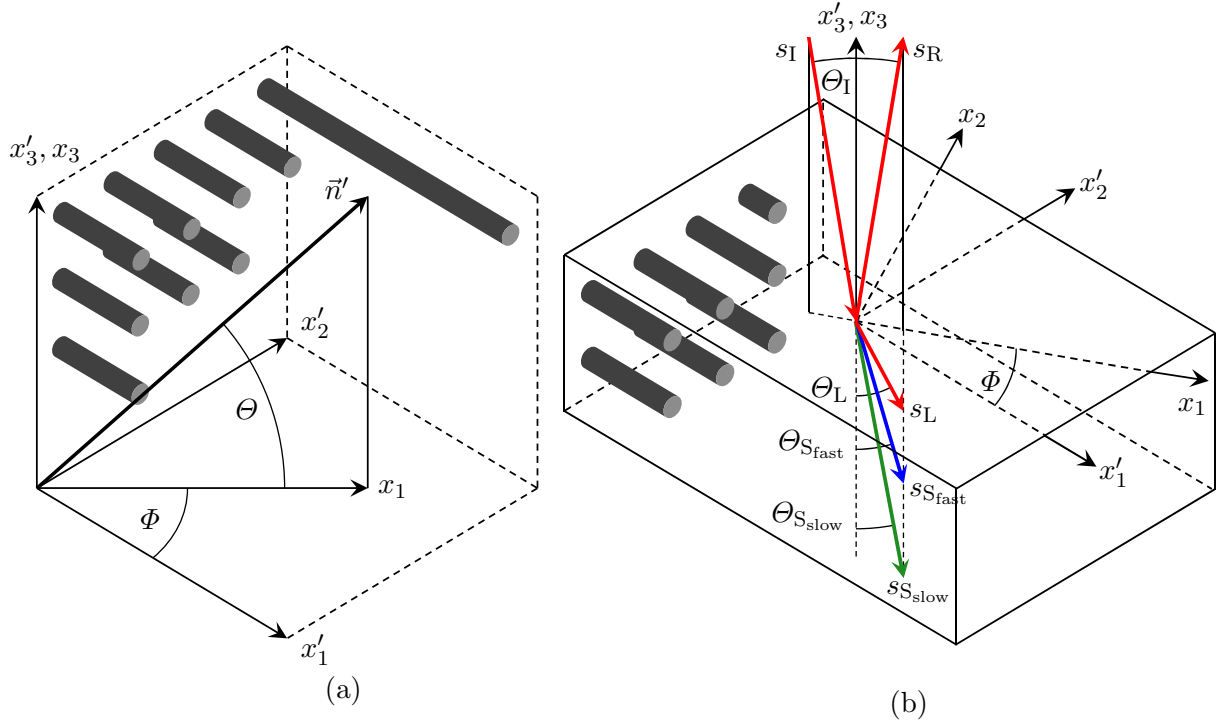


FIG. 20. Crystallographic and global coordinate systems x'_i , x_i and fiber orientation in transversely isotropic material. (a) Elastic wave propagation in the bulk material as treated in the **Elastic waves in bulk material** (31) panel. (b) A plane wave impinging from a fluid generates three bulk waves in transversely isotropic material propagating in the x_1 - x_3 -plane of the global coordinate system. This topic is covered in the **Bulk waves on interfaces** (32) panel.

perpendicular for shear vertical (SV) and shear horizontal waves (SH). Therefore, if we consider bulk waves emanating from a point source in an isotropic bulk material, the phase velocity surfaces for both wave types are spherical with the radii being the longitudinal velocity for L waves and the transverse velocity for SH and SV waves. These velocities are given in the **Material editor** (Sec. 4.8) tab. The group velocity surfaces coincide with the phase velocity surfaces. L waves are polarized along the radial direction, and SH and SV waves normal to it. In anisotropic materials, however, each of the three bulk wave types has its own phase velocity, which depends on the propagation direction \vec{n}' in Fig. 20(a), and the group velocity surface does not coincide with the phase velocity surface. In general, the group velocity vector deviates from the phase velocity vector, where the latter is parallel to the propagation direction unit vector \vec{n}' . In absence of attenuation, the group velocity is the same as the energy flow velocity, and its vector represents the actual direction of the acoustic beam. See Appendix A for information on the similar problem of the group velocity of guided waves in anisotropic media. This situation leads also to differences in the magnitude of the phase and group velocities. The bulk waves' polarization is either along or perpendicular to the propagation direction, respectively, only in case of propagation along or perpendicular to the fibers (in these cases, the modes are called ‘pure’), except for one shear type bulk wave in transversely

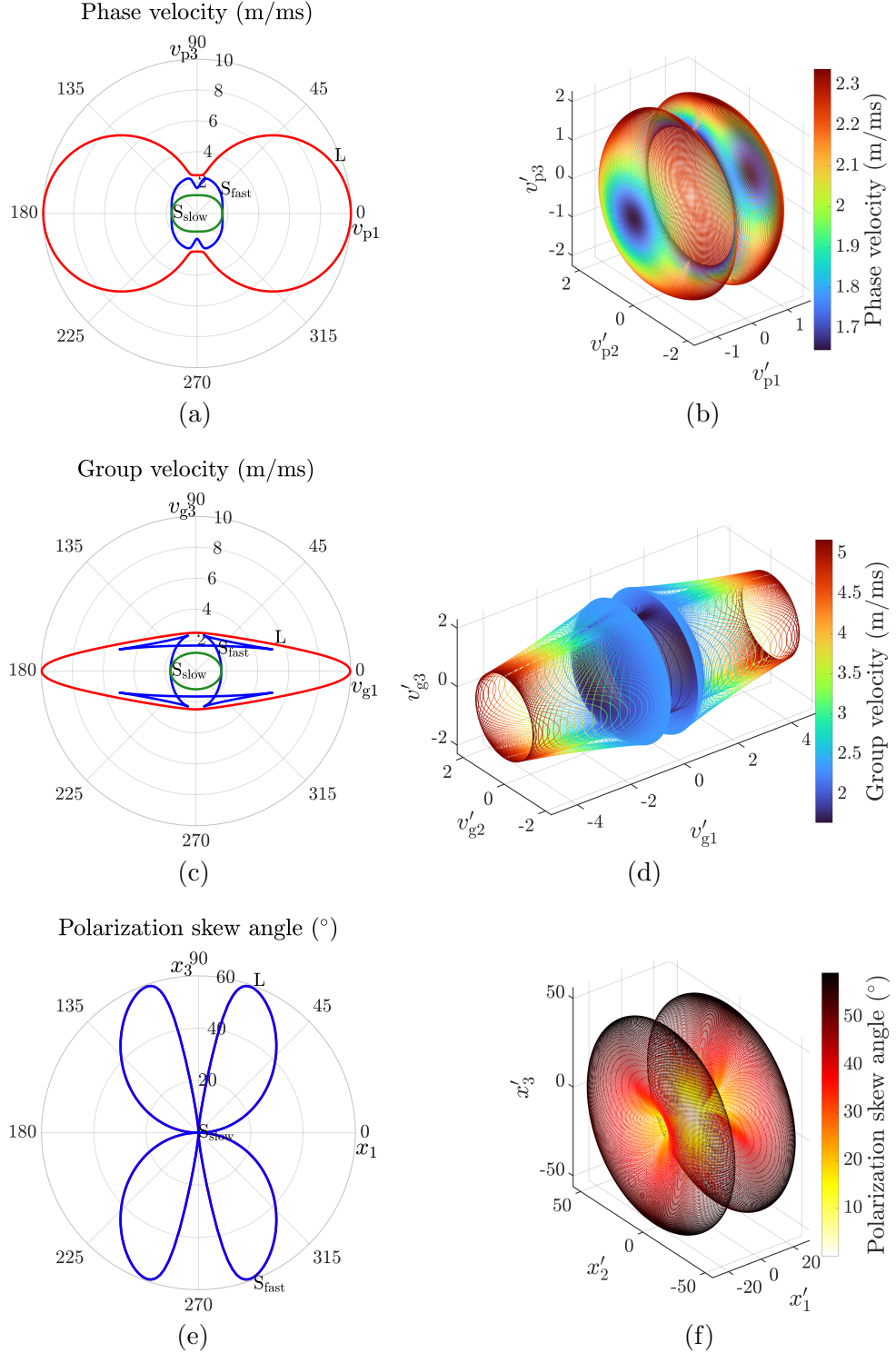


FIG. 21. Bulk waves in T800M913. (a) Phase velocity, (c) group velocity, and (e) polarization skew angle profiles at $\Phi = 0^\circ$, and (b) S_{fast} phase velocity, (d) S_{fast} group velocity, and (f) L and S_{fast} polarization skew angle surfaces.

isotropic materials, which has pure character for any propagation direction. The shear waves do not have the same phase velocity anymore. Because of that, the bulk waves in anisotropic materials are called quasilongitudinal waves (L), fast quasishear waves (S_{fast}), and slow quasishear waves (but slow shear waves in transversely isotropic material) (S_{slow}). Figure 20(a) displays the conventions used for the elastic wave propagation in a fiber-epoxy system. Here, x'_1 is along the fiber direction, and x'_2 and x'_3 are normal to it. Θ defines the wave propagation angle with respect to the x'_1 - x'_2 -plane (elevation), and Φ is the angle between the propagation direction projected into the x'_1 - x'_2 -plane and x'_1 (azimuth).

In the **Elastic waves in bulk material** (31) panel, you can plot the phase velocity, group velocity, the corresponding slownesses s , the energy skew angle γ between the bulk waves' phase velocity vectors and the group velocity (or energy) vectors, and the polarization skew angle δ of bulk waves in anisotropic materials in 2-D and 3-D. The slowness is the inverse phase velocity, and the polarization skew angle is the deviation angle from transverse polarization ($\beta = 90^\circ$) in case of S_{fast} and S_{slow} , and longitudinal polarization ($\beta = 0^\circ$) in case of L . In transversely isotropic material, δ for S_{slow} is always zero since it is a pure mode for any propagation direction in this material class. From the **Class** drop-down menu, select which material class you want to consider. The **Material** drop-down menu will be updated accordingly. Select a material from the **Material** drop-down menu. Choose the **Quantity** to be plotted and use $\Delta\Theta$ to determine the Θ resolution. In the **2-D profiles** sub-panel, you can plot the quantity for a given angle Φ , as shown in Figs. 21(a), 21(c), and 21(e) for T800M913 at $\Phi = 0^\circ$. By using the **Plane** drop-down menu, you can select to plot the 1-3-plane or the 1-2-plane. This is useful for orthotropic materials where the modules E_2 and E_3 are not equal. If you select the 1-2-plane, the axes x'_2 and x'_3 in Fig. 20(a) are swapped. In the **3-D surfaces and vectors** sub-panel, you can plot the complete surface. Now, you have to set $\Delta\Phi$ to determine also the Φ resolution. Upon pressing **Calculate**, the point cloud made up by $\Delta\Theta$ and $\Delta\Phi$ will be calculated and the key data be displayed in the output window (33). Use the **Mode** drop-down menu to select which one of the three bulk wave mode surfaces you want to plot. Figures 21(b) and 21(d) show the phase and group velocity surfaces of S_{fast} in T800M913, respectively, and Fig. 21(f) shows the (coinciding) polarization skew angle from pure mode polarization of L and S_{fast} . It can readily be seen that the skew angle becomes zero for wave propagation parallel and normal to the fibers. These are the propagation directions for which pure L and S_{fast} modes occur. In the center column of the **3-D surfaces and vectors** sub-panel, you can plot the slowness and polarization vectors of bulk waves propagating along a specific direction. Define the propagation direction using Φ and Θ , and press **Plot** to get an image like the one shown in Fig. 22. In addition to the **Plot layout settings**, which apply to all plots on the current tab, you find some additional layout settings in the **3-D surfaces and vectors** sub-panel, which apply only to the 3-D plots. You can adjust the view by using **View Φ** and **View Θ** . Of course, you can also use the **Rotate 3-D** tool inside the plot window. You can also change the **Marker size** and the x-position of the colorbar.

In the **Bulk waves on interfaces** (32) panel, you can model the bulk waves that

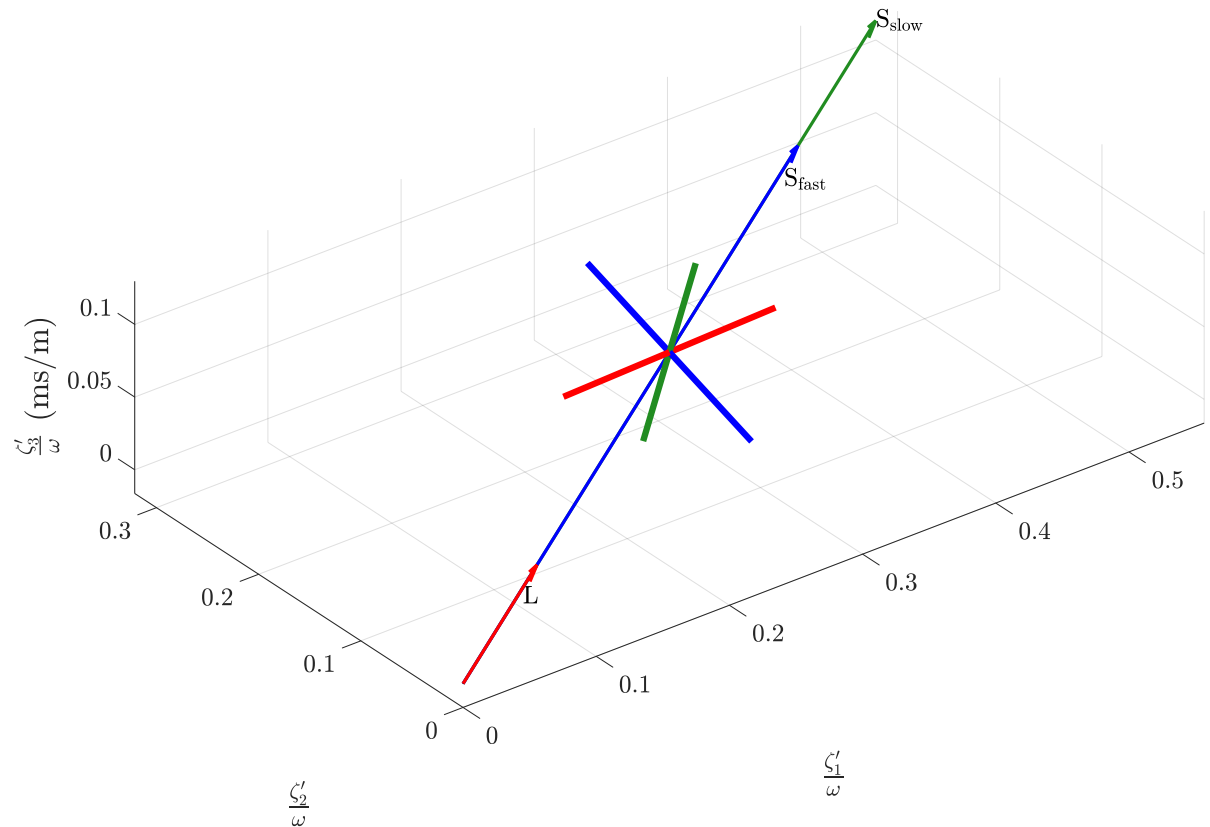


FIG. 22. Bulk wave slownesses and polarizations in T800M913 for propagation along $\Phi = 30^\circ$, $\Theta = 10^\circ$. The polarization vectors are always mutually orthogonal.

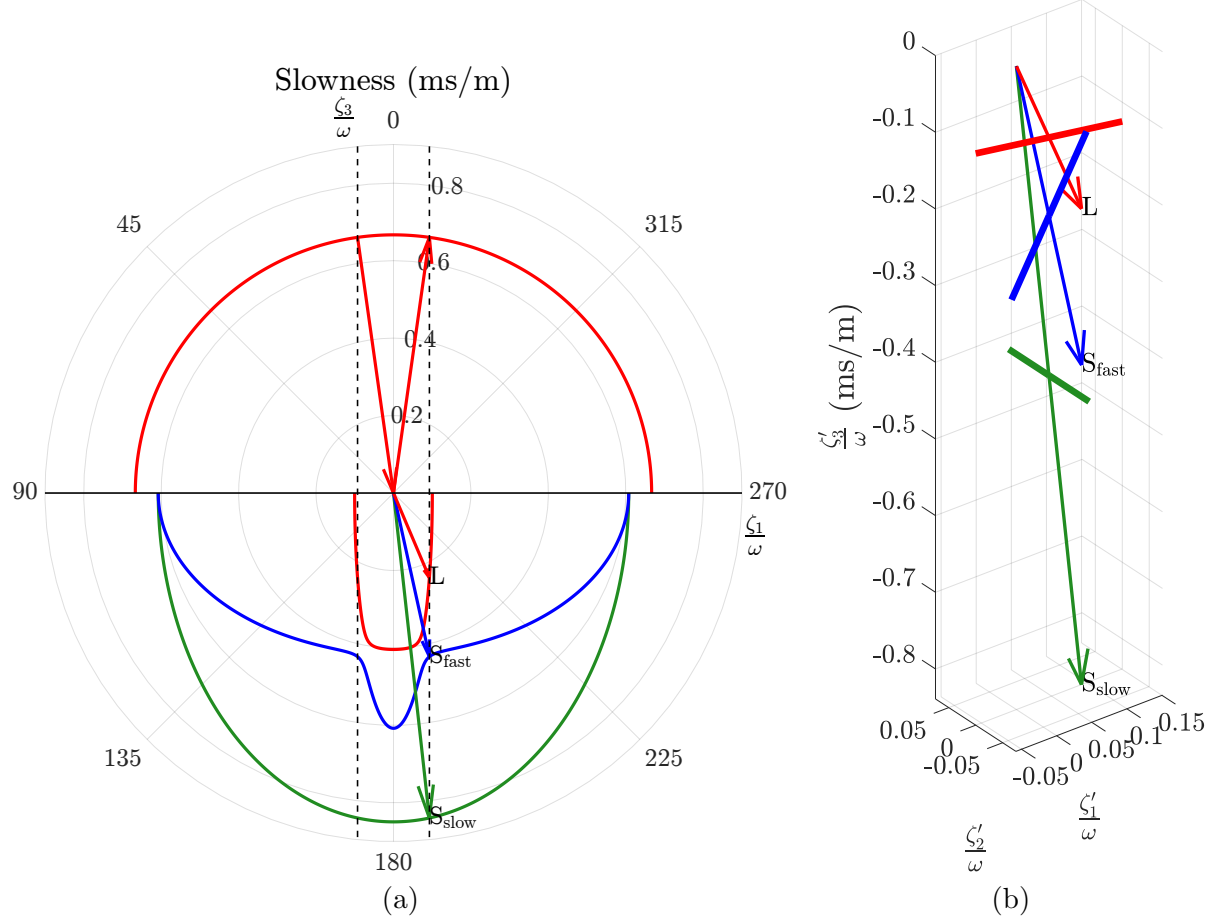


FIG. 23. Bulk waves generated in T800M913 through plane wave incidence from water at $\Phi = 0^\circ$, $\Theta_I = 8^\circ$. The upper half-space is covered by water, the lower half-space by T800M913. (a) Construction of the bulk wave slownesses based on Snell's law. (b) Slownesses and polarizations of the generated bulk waves.

are generated in an isotropic or anisotropic material when a plane wave impinges from a fluid. This situation is depicted in Figs. 20(b) and 23(a). Here, the upper half-space is covered by water and the lower half-space by transversely isotropic T800M913. The incident as well as the reflected and transmitted waves propagate in the $\Phi = 0^\circ$ plane, i.e., $x_1 = x'_1$. The curves represent the slownesses in water and T800M913. Water as well as any other nonviscous fluid supports only the longitudinal wave type (because the shear modulus is zero), represented by the red vectors in the upper half-space. The plane wave is incident under an angle of $\Theta_I = 8^\circ$. Its wavenumber ζ_I is given by

$$\zeta_I = \frac{\omega}{v_I} = \omega s_I, \quad (3)$$

where ω is the angular frequency $2\pi f$, with the frequency f , and v_I is the phase velocity in water. At the boundary to the solid, a certain proportion of energy is reflected, and the rest is transmitted into T800M913 where three bulk waves with the wavenumbers

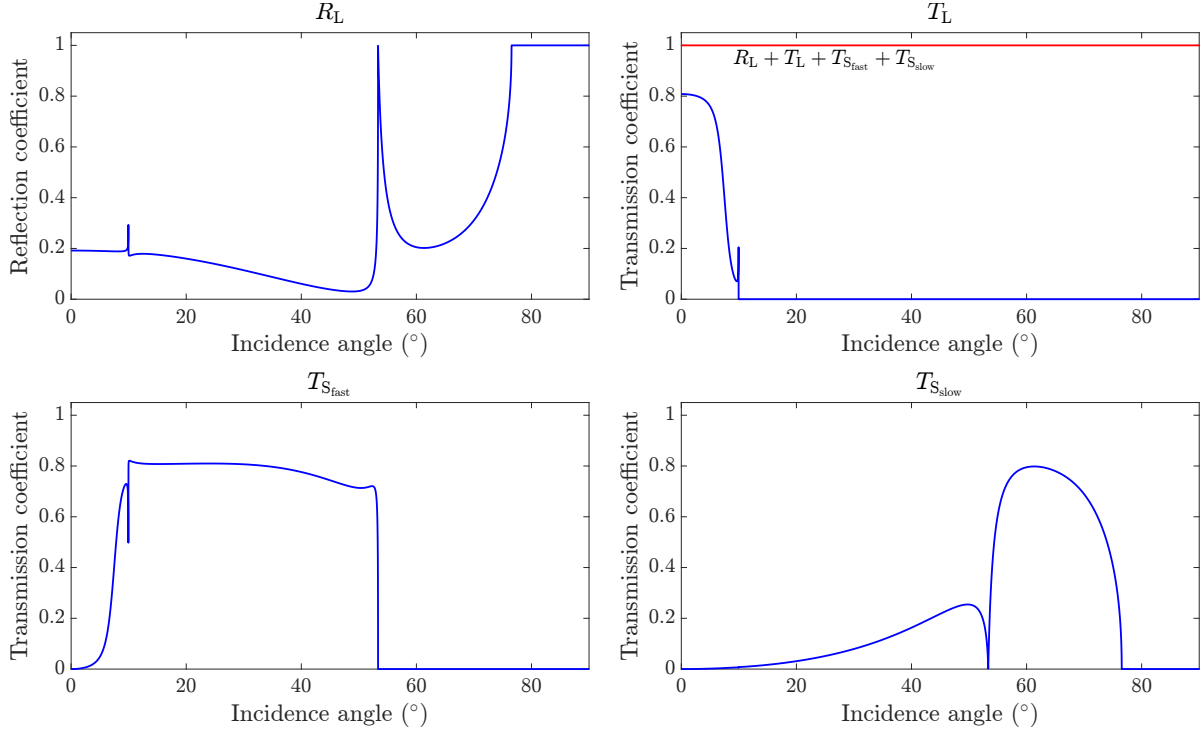


FIG. 24. Reflected and transmitted energy scattering coefficients versus incidence angle for the bulk waves scattered on the interface between water and T800M913 at $\Phi = 30^\circ$

$\zeta_L, \zeta_{S_{\text{fast}}}, \zeta_{S_{\text{slow}}}$ are generated. For these waves, Eq. (3) applies with their respective phase velocities and slownesses $v_L, v_{S_{\text{fast}}}, v_{S_{\text{slow}}}, s_L, s_{S_{\text{fast}}}, s_{S_{\text{slow}}}$. According to Snell's law, all scattered waves (reflected and transmitted ones) must have the same projected wavenumber along the boundary ζ_{Ix_1} as the incident wave, i.e.,

$$\zeta_I \sin \Theta_I = \zeta_{(k)} \sin \Theta_{(k)} = \zeta_{I1}, \quad k = 1, 2, \dots, 4, \quad (4)$$

where $\zeta_{(k)}$ stands for the wavenumber of any scattered wave, and $\Theta_{(k)}$ is the corresponding reflection or refraction angle, respectively. With the use of Eq. (3), we can write Eq. (4) in terms of the slownesses of the scattered waves $s_{(k)}$ as

$$s_I \sin \Theta_I = s_{(k)} \sin \Theta_{(k)} = s_{I1}. \quad (5)$$

This important constraint is indicated by the two vertical guide lines in Fig. 23(a). The utility of this picture is that the wave slowness vectors $\vec{\zeta}_{(k)}/\omega$ can be constructed simply by drawing lines from the origin to the points, where the right guide line intersects the slowness profiles. Then, by assigning a frequency, the actual wavenumber can be obtained. From Fig. 23(a), it becomes also clear that, as the incidence angle increases, critical angles will be reached beyond which a slowness vector for a given bulk wave cannot be constructed anymore. Physically, these waves are evanescent, i.e., their amplitude decays exponentially with depth, and they are confined to a certain area below the boundary. Basically, these are surface waves (Rayleigh waves). By contrast, below

the critical angles, we have propagating bulk waves. Now, let us look at Fig. 23(b) to find out more about the polarization of the bulk waves in T800M913. Here, only the lower half-space from Fig. 23(a) is displayed. The bold lines emanating from the middle of the wave vectors indicate their polarization.

The final question is how much energy each of the scattered waves carries. Clearly, the conservation of energy has to be satisfied, so the sum of the energies of the reflected and transmitted waves must be the same as that of the incident wave. Figure 24 displays the reflected and transmitted energy scattering coefficients versus incidence angle for the bulk waves scattered on the interface between water and T800M913 at $\Phi = 30^\circ$. Four subplots represent the reflected longitudinal wave (upper left), the transmitted longitudinal wave (upper right), the transmitted fast quasishow wave (lower left), and the transmitted slow shear wave (lower right). The red line in the upper right subplot indicates the summation of all four energy scattering coefficients, confirming the result of unity. The kinks and peaks in the blue curves mark exactly the critical angles. Consider for instance the upper right subplot showing the transmitted longitudinal wave. There is a notable peak at 9.9° . Beyond this angle, L will not be generated in the solid anymore. The other critical angles are 53.4° and 76.6° . Beyond the latter, total reflection occurs, i.e., the reflected energy coefficient reaches unity.

To do your modeling, select a **Fluid** from the drop-down menu. Then select the **Class**. Depending on your choice, you can now select an isotropic, a cubic, a transversely isotropic, or an orthotropic **Solid**. All other parameters in this panel work similarly to those in the **Elastic waves in bulk material** (31) panel. Whenever you make an entry, information about the generated bulk waves in the solid, including critical angles and energy scattering coefficients, will be displayed in the output window (33). Press **Plot 2-D**, **Plot 3-D**, and **Plot R,T** to generate (and export) the kind of plots shown in Figs. 23 and 24.

4.7 Laminate stiffness

The **Laminate stiffness** tab depicted in Fig. 25 is an additional tool that allows to calculate the laminate stiffness matrix, which is also referred to as the *homogenized stiffness tensor*. The laminate stiffness matrix is the stiffness matrix of a layered, anisotropic laminate. It is calculated using the *classical laminate theory* (CLT). First, the layer stiffness matrices are transformed into the global coordinate system to account for their individual fiber orientations, and then the transformed stiffness matrices are multiplied by their respective layer thickness-to-unit cell thickness ratio and summed up to obtain the unit cell stiffness matrix. Since every unit cell has the same stiffness matrix, and because of the multiplication with the thickness ratios, the laminate stiffness matrix does not depend on the repetitions of the unit cell, i.e., it is equal to the unit cell stiffness matrix.

The **Specimen** (34) setup is reduced accordingly. The **Laminate stiffness components** (35) are displayed for the chosen **Azimuthal angle**. This matrix has the form of monoclinic material symmetry. In the polar diagram (36), every laminate stiffness component can be plotted with respect to the wave propagation angle in the defined laminate. Use the check boxes on the left accordingly. You can export the laminate

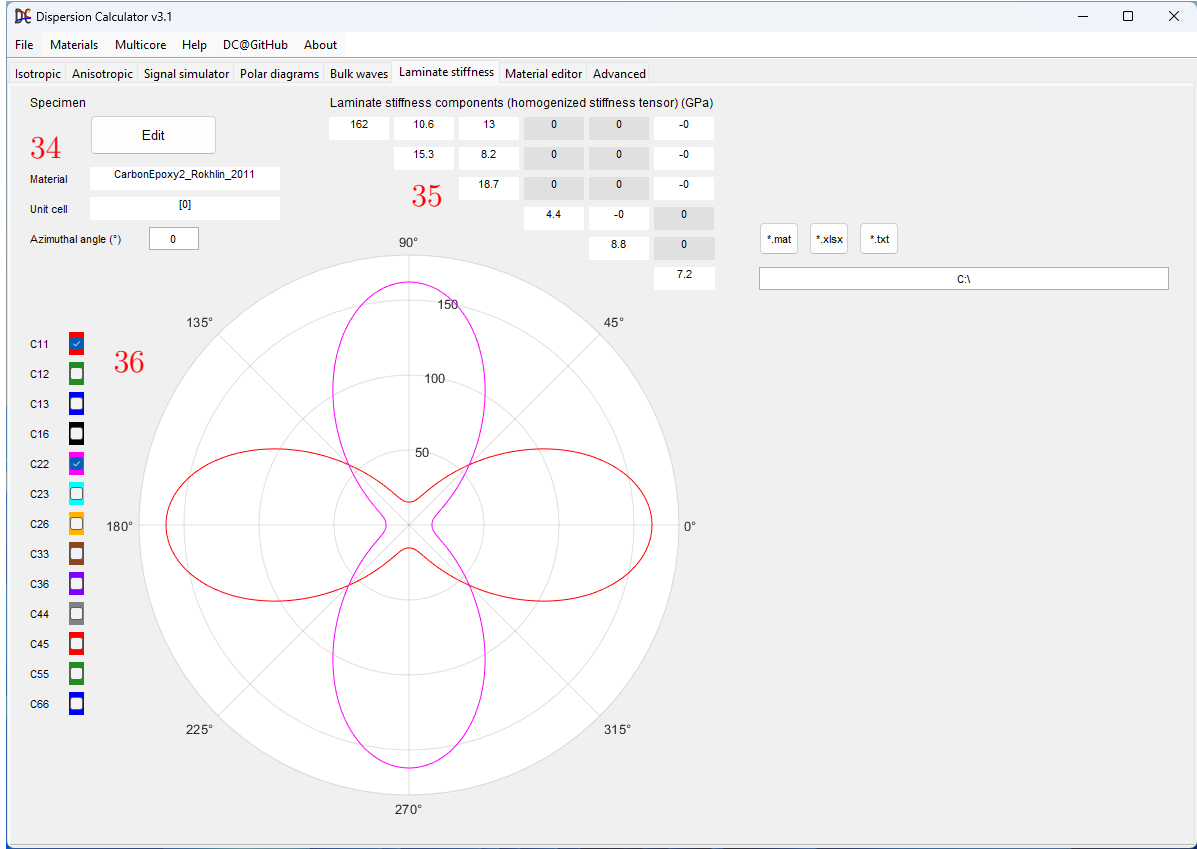


FIG. 25. The Laminate stiffness tab.

stiffness matrix displayed in (35) to the desired file format.

4.8 Material editor

Starting in DC v2.1, viscoelastic damping can be considered. To account for this, the **Engineering constants** and **Stiffness components (GPa)** are complex. With only non-zero **Real parts**, one describes a perfectly elastic material, as it was prior to DC v2.1. To consider viscoelastic damping, you need to enter non-zero **Imaginary parts**. Many complex default materials are available in DC. These are listed in Appendix C. To distinguish them from the perfectly elastic materials, they carry the suffix “_viscoelastic”. For the guided wave modeling in viscoelastic materials, DC uses the hysteretic damping model, corresponding to a linear increase of attenuation with frequency, i.e., a constant loss per wavelength.

In the **Material editor** tab, you can view the parameters of the available materials and add or remove materials. In the **Isotropic materials** (37) panel shown in Fig. 26, you can choose an isotropic **Material** from the drop-down menu. If you want to add a new material, enter its **Mass density**, and then you can choose one of the following three options:

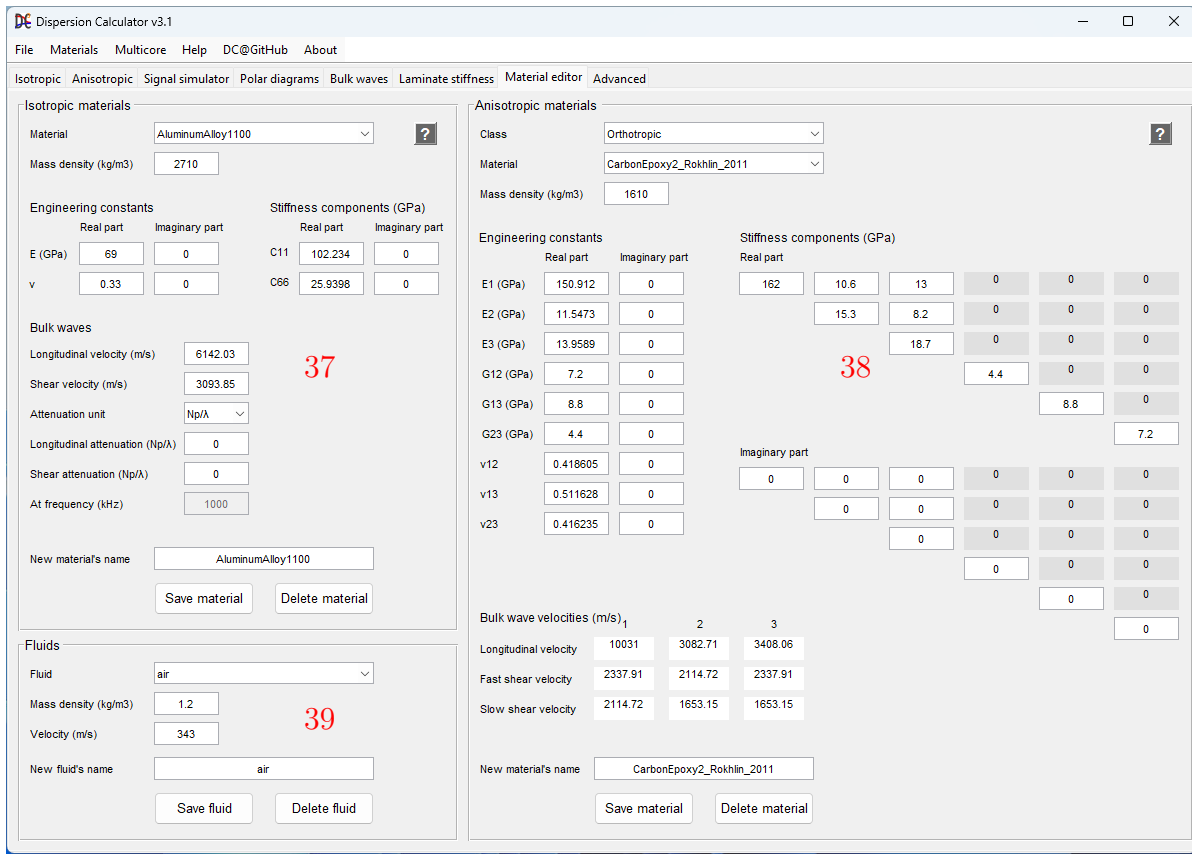


FIG. 26. The Material editor.

- Engineering constants.** Enter Young's modulus **E (GPa)** and Poisson's ratio **v**. In case you want to consider viscoelastic damping, enter non-zero **Imaginary parts** in addition to the **Real parts**.
- Stiffness components (GPa).** Enter **C11** and **C66**. Similarly as for the above, enter non-zero **Imaginary parts** for viscoelastic damping.
- Bulk waves.** Enter the **Longitudinal velocity (m/s)** and the **Shear velocity (m/s)**. To consider viscoelastic damping, you also need to fill **Longitudinal attenuation** and **Shear attenuation**. From the **Attenuation unit** drop-down menu, you can choose one of four units in which you enter the attenuation values. These are **Np/λ**, **dB/λ**, **Np/m**, and **dB/m**. If you choose **Np/m** or **dB/m**, the **At frequency (kHz)** field becomes active. Enter the frequency at which the **Longitudinal attenuation** and the **Shear attenuation** were measured.

Notice that if you change a material parameter, all parameters which depend on it are updated automatically. After you have edited your material, assign a **New material's name** and press **Save material**. If you want to remove a material from the list, select it from the **Material** drop-down menu and press **Delete material**.

The **Anisotropic materials** (38) panel works in the same way except that you can only enter the **Engineering constants** or the **Stiffness components (GPa)**, but not the **Bulk wave velocities (m/s)**. These are calculated from the **Stiffness components (GPa)** and the **Mass density** by using the equations listed in Appendix B. Notice, that the direction 1 is along the fibers, while 2 and 3 are normal to it. 2 is in-plane and 3 is out-of-plane. You can use the **Class** drop-down menu to choose between **Orthotropic**, **Transversely isotropic**, and **Cubic** materials. If you select **Transversely isotropic**, four of the nine engineering constants and four of the nine stiffness components will be inactive so that you just need to enter the remaining five independent engineering constants or stiffness components. If you select **Cubic**, six engineering constants and six stiffness components will be inactive so that you just need to enter the remaining three independent engineering constants or stiffness components.

In the **Bulk wave velocities** section, you get the **Longitudinal velocity**, **Fast shear velocity**, and the **Slow shear velocity** of the three bulk wave types for propagation along the three principal axes 1, 2, and 3. Notice that in transversely isotropic materials, the bulk wave velocities are equal for propagation along the axes 2 and 3 (normal to the fibers), i.e., for propagation in the plane of (transverse) isotropy. In cubic materials, all longitudinal velocities are equal and all transverse velocities are equal. In Appendix B, it is shown how to calculate those velocities.

In the **Fluids** (39) panel, you can add fluids or solid coupling media like the Olympus wedge. The latter is meant for the calculation of the coincidence angle dispersion diagrams available in the **Isotropic**, **Anisotropic**, and **Polar diagrams** tabs. Fluids are currently treated as non-viscous.

4.9 Advanced

The **Advanced** tab offers options, which do not need to be changed on a regular basis, but which help to overcome specific dispersion curve tracing problems. There are three panels. The **Phase velocity sweeps** (40) panel affects the most part of the dispersion curves tracing whereas the **Frequency sweeps...** (41) panel affects only the dispersion

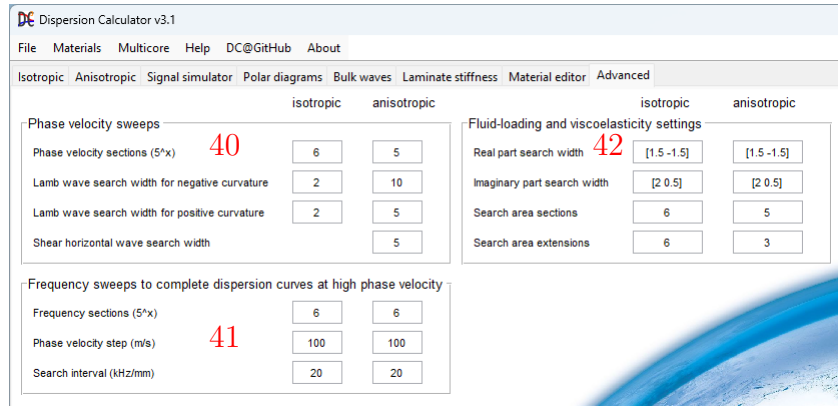


FIG. 27. The Advanced tab.

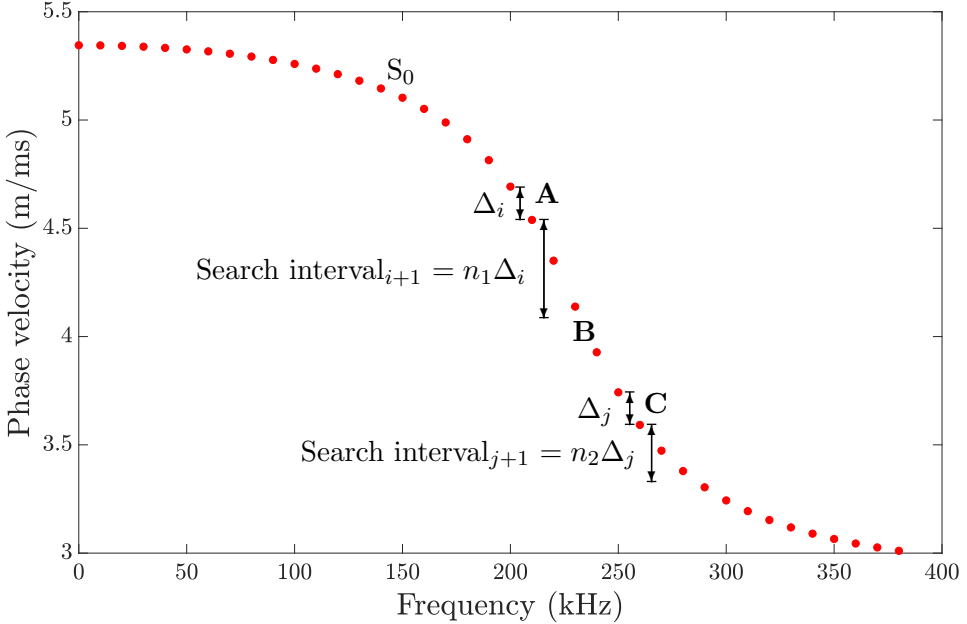


FIG. 28. The search interval as it is applied by the phase velocity sweeps.

curve tracing used to complete the higher order modes around the cut-off frequency. The **Fluid-loading and viscoelasticity settings** (42) panel adjusts the dispersion curve tracing algorithm used in case of fluid-loading and viscoelasticity. For each option, you have two fields. The left field is for isotropic materials, and the right field is for anisotropic materials.

Let us discuss the **Phase velocity sweeps** (40) panel. The number of **Phase velocity sections** determines the ability to find a modal solution. At each frequency step, starting at low frequency, a first guess is made in which phase velocity search interval the modal solution for a particular mode should lie. This is necessary to avoid an extremely slow curve tracing. It is then checked, whether there is a modal solution in the search interval. A modal solution is defined by a simultaneous sign change and minimum in the characteristic function amplitude. If yes, then a bisection algorithm starts to converge upon the root until the desired **Phase velocity accuracy** is reached. If no root is found, an x -loop starts to divide the search interval into 5^x sections, until a root in a section is found, and then the bisection of the critical section starts unless the desired **Phase velocity accuracy** has already been reached. At this point, if symmetric and anti-symmetric modes can be distinguished (see Table 2), a final check is made whether the modal solution has the right symmetry. The in-plane displacement component u_1 is calculated at the top and at the bottom surfaces of the plate. If they have the same sign, the mode is symmetric, otherwise it is anti-symmetric. If the search interval covers any previously traced lower mode(s), those solution(s) will be ignored in the tracing of the current mode. The number of **Phase velocity sections** x as the power of five sets the maximum number of sections into which the search interval is divided. In order to understand the **Lamb wave search width for negative curvature**, please have a

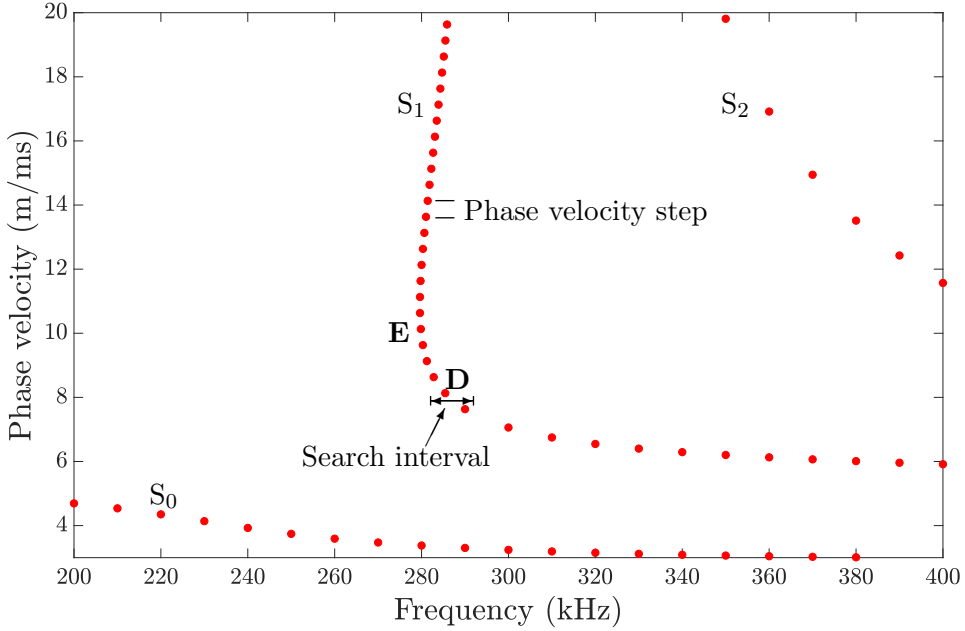


FIG. 29. The search interval and the phase velocity step as used by the frequency sweeps.

look at Fig. 28. It shows the tracing of the S_0 Lamb wave in a 10 mm thick free aluminum alloy 1100 plate. Consider situation **A**. Suppose the sample at 210 kHz has already been obtained, and we are now searching for the 220 kHz sample. It is expected at a lower phase velocity. It is therefore taken the difference of the phase velocities between the 200 kHz and the 210 kHz sample Δ_i . The curvature is determined to be negative here. The 220 kHz sample is expected to lie within the search interval $i+1$, which reaches from the 210 kHz sample's phase velocity down by the multiple $n_1 \cdot \Delta_i$, where n_1 is the **Lamb wave search width for negative curvature**. The 220 kHz is indeed found there. As the tracing progresses, we pass the turning point **B** and reach situation **C**. Since the curvature is now positive, DC uses the **Lamb wave search width for positive curvature** n_2 , which is smaller than the value for negative curvatures n_1 . The **Shear horizontal wave search width** is used for shear horizontal waves in anisotropic media only. In isotropic materials, the shear horizontal modes are calculated by an analytic equation so that dispersion curve tracing is unnecessary.

Since the higher order modes are more or less parallel to the phase velocity axis at high phase velocities, the usual phase velocity sweeps at fixed frequencies do not work there very well, and the dispersion curves are often incomplete. Therefore, **Frequency sweeps to complete dispersion curves at high phase velocity** (41) are performed up to the top phase velocity required in the dispersion diagram. The **Frequency sections** work similarly to the **Phase velocity sections**. Higher values in **Phase velocity sections** and **Frequency sections** increase the chance to find modal solutions, and therefore accomplish the tracing successfully at the cost of processing time. However, setting low numbers does not necessarily cause problems in the curve tracing because there is a routine involved that replaces missing samples. This routine

fits the already known samples and extrapolates them to the current frequency step. However, if more than five consecutive samples have been missed, the tracing of the current curve stops and continues with the next mode. Please consider Fig. 29. After the tracing of the fundamental modes, the higher order modes are traced. S_1 comes first. The cut-off frequency at 20 m/ms is 286.129 kHz. Since we have a **Frequency step** of 10 kHz, the phase velocity sweeps starts at 290 kHz, leaving the curve incomplete below 290 kHz. The frequency sweeps continue the curve at point **D**, which is above the 290 kHz sample by an amount of **Phase velocity step**. This point is within a search interval spanning from a certain offset above 290 kHz to 290 kHz–**Search interval** in kHz/mm. The aforementioned offset is needed to overcome point **E**, where the curve turns to higher frequencies again. This procedure continues until the cut-off frequency is reached. A more detailed description of this dispersion curve tracing algorithm can be found in Ref. [40].

Prof. Lowe describes a different tracing routine in Refs. [29, 56, 57], which he applies in Disperse. An extrapolation method is used to make a guess for the next sample point. This works well in the wavenumber space since the curves are more straight there than in the frequency space.

Let us now move to the dispersion curve tracing algorithm used in case of fluid-loading and viscoelasticity, causing attenuation of elastic waves. It was mentioned earlier that in this case, the wavenumber of guided waves turns complex, i.e., it has a real part and an imaginary part, whereas without attenuation, the wavenumber remains real. The phase velocity c_p of an attenuated guided wave is given by

$$c_p = \frac{\omega}{\xi_{\text{real}}}, \quad (6)$$

where ω is the angular frequency ($= 2\pi f$) and ξ_{real} is the real part of the complex wavenumber. The attenuation α in Nepers per wavelength is given by

$$\alpha = 2\pi \frac{\xi_{\text{imag}}}{\xi_{\text{real}}}, \quad (7)$$

or, more simple, in Nepers per meter by

$$\alpha = \xi_{\text{imag}}. \quad (8)$$

Hence, dispersion curve tracing in the attenuated case requires a two-dimensional search for the modal solutions in the complex wavenumber plane rather than a one-dimensional search only on the real axis. Programming a two-dimensional dispersion curve tracing algorithm is particularly difficult. It took me many months to develop that used by DC, and it has to be very complex, almost to the point where it is intelligent, to enable a robust dispersion curve tracing with descent speed. More important than speed is robustness. Therefore, the algorithm performs extensive search for the solutions if they are not found immediately, and since a two-dimensional search is much more computationally expensive than a one-dimensional, obtaining a dispersion diagram can take

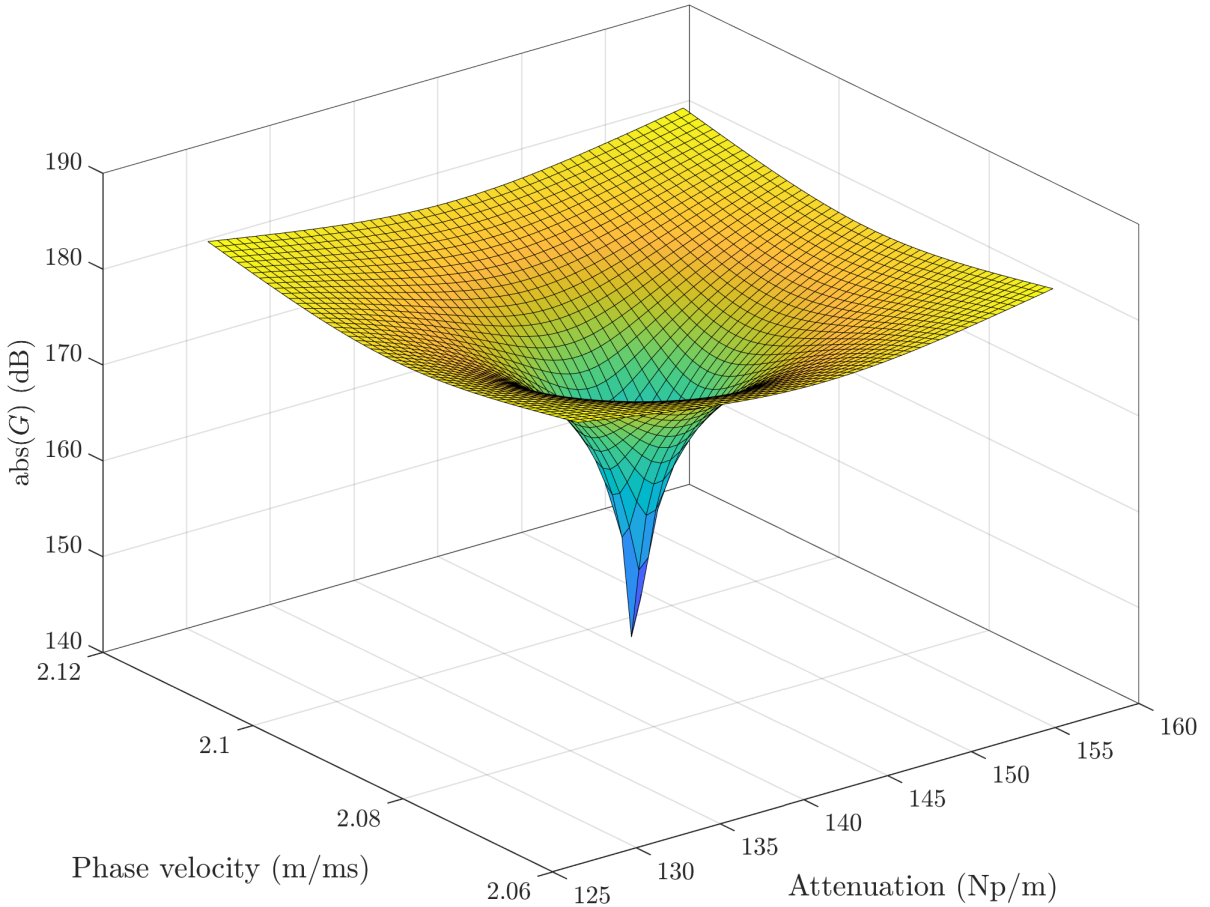


FIG. 30. Absolute values of the complex symmetric Rayleigh-Lamb equation calculated for a 1 mm thick viscoelastic epoxy plate (DC material: “Epoxy_Disperse_Viscoelastic”) immersed in water at 400 kHz. The equation is evaluated on a 51-by-51 point raster in the complex wavenumber plane and plotted in the phase velocity-attenuation space. The minimum indicates the modal solution of the S_0 Lamb wave, which is located at $c_p = 2.09008$ m/ms, $\alpha = 143.175$ Np/m. A denser raster makes the “singularity” deeper.

much longer in the attenuated case than in the nonattenuated case. I tried in particular that actually no advanced adjustments have to be done by the user to get the dispersion curve tracing working in a particular case. For instance, usual code requires that the user sets an appropriate range for the imaginary wavenumber part. In the **Fluid-loading and viscoelasticity settings** (42) panel, this can be adjusted by the **Imaginary part search width** and **Search area extensions** options. However, the dispersion curve tracing algorithm is designed in such a way that a reasonable guess for the imaginary search range will be done automatically, and in case a solution is not found anyway, the search range will be extended step by step. A good software should not bother the user with such specific adjustments, requiring knowledge which an unexperienced user does not have. Of course though, the dispersion curve tracing algorithm is far from being

perfect, and there is no guarantee that all modes will be found and traced from the start to the end (see Secs. 5.4 and 5.5). Notice that, unlike in the nonattenuated case, it is possible that dispersion curves can stop at certain points for physical reasons. In these cases, the dispersion curve tracing algorithm did not fail. See for instance Fig. 4. A_0 stops at a point where its attenuation approaches zero. The same for the higher order modes when they drop below the wave speed in water.

The two-dimensional dispersion curve tracing algorithm starts with an initial guess for the phase velocity as well as for the attenuation, based on the solutions found at previous frequencies. In damped systems, it is normal that dispersion curves can tend towards higher and lower phase velocities with increasing frequency. Therefore, for the calculation of the phase velocity search interval $_{i+1}$ wherein we expect the solution at the current frequency, it is taken the difference of the phase velocities between the two preceding samples Δ_i . The upper bound of the search interval $_{i+1}$ is at a multiple of $n_1 \cdot \Delta_i$ above the phase velocity of the last found solution, where n_1 is the left number in **Real part search width**. Similarly, the lower bound is at a multiple of $n_2 \cdot \Delta_i$ below the phase velocity of the last found solution, where n_2 is the right number in **Real part search width**. The attenuation can also increase or decrease with frequency. The upper bound of the attenuation search interval lies at the previous solution's attenuation multiplied by the left number in **Imaginary part search width**, and the lower bound is at the previous solution's attenuation multiplied by the right number in **Imaginary part search width**. The phase velocity and attenuation search intervals are divided into five equally spaced samples. From these, a square raster of twenty-five complex wavenumbers are calculated, and the characteristic function is evaluated at these samples. Figure 30 shows the absolute values of the characteristic function amplitude G , evaluated at 51-by-51 sample points in this example. For better visualization, the amplitude is drawn on a logarithmic scale. Since we are evaluating the absolute value, a modal solution is indicated by a minimum. This is clearly visible in Fig. 30. Next, the algorithm takes the outer border of the four squares adjacent to the minimum and evaluates another raster of twenty-five samples within these borders. This process continues until the desired resolution (**Phase velocity accuracy**) has been reached for both the phase velocity and for the attenuation.

There are two possible reasons why the algorithm does not find a solution with the initial search. Either the solution lies outside the complex search area, or the five-by-five raster is too coarse to detect a minimum. The algorithm has strong and sophisticated measures to find even difficult-to-find solutions. In short, in case a solution has not been found, the search will be repeated with a finer raster, i.e., with a higher density of samples, but with an increase in size (phase velocity and attenuation), too. There exist different strategies for how the number of samples is increased, and whether the raster will be square or rectangular. These strategies are applied to solve various complicated situations that can occur. **Search area sections** gives the number of how many times a yet unsuccessful search is repeated with an ever finer raster covering an ever larger complex plane area. **Search area extensions** gives the number of how many times the above repeated searches are repeated with an extra increase in the size of the search raster. Suppose you have five **Search area sections** and three **Search area exten-**

sions. In case a modal solution is not found, the search will be repeated five times, every time with a finer and larger raster. After that, the size of the raster will be extra enlarged by a factor of three in both phase velocity and attenuation so that it will be nine times larger. At the same time, the number of samples will be increased also, but only a little bit so that the density of the previous raster will not be reached anymore. The five searches will be repeated a second time, followed by a third time with an again nine times larger raster. If the solution is still not found, the previous found solutions for phase velocity and attenuation will be fitted and extrapolated. If solutions have not been found at more than five consecutive frequency steps, the dispersion curve tracing stops and continues with the next mode.

The described routine enables a high robustness, but it can also be slow, in particular when the first solution around the cut-off frequency of a higher order mode is sought. Here, in case the algorithm does not find the solution at the cut-off frequency, it will continue the search at the next frequency step until a frequency/thickness range of 50 kHz/mm has been covered. Remember that, even if you are considering fluid-loading and/or viscoelasticity, the initial frequency sweep for the cut-off frequencies is always performed for the nonattenuated case, i.e., without fluid-loading and viscoelasticity. The resulting cut-off frequencies will be the starting points for the search of the higher order modes also in the attenuated case. In this case, the dispersion curves start at more or less shifted cut-off frequencies, and some modes, which are present without attenuation, are not present at all otherwise. In the latter case, it will take some time for the algorithm to complete the search and then go to the next mode. However, it is better to wait some time longer and then have a more complete dispersion diagram rather than getting the diagram fast but missing dispersion curves or parts of them. If you want to increase the speed of computation anyway, you can reduce the values of **Search area sections** and **Search area extensions**.

To improve robustness, the algorithm has quite some flexibility in dealing with complicated situations. Only some prominent features can be described here briefly:

- DC ignores any minimum in the raster that coincides with any previously traced dispersion curve.
- If a found solution lies too far from the current dispersion curve in terms of phase velocity or attenuation, it is discarded as an outlier.
- In case multiple minima are found in the raster, DC will pick the one which lies closest to the last solution found on the currently traced dispersion curve.
- If DC does not find a minimum, it checks if there are border minima, i.e., valleys in the characteristic function amplitude, which cut into one of the four borders of the raster and which get deeper towards the border. Such a valley points towards a full minimum. The raster is therefore extended towards the suspected minimum until it is found. Border minima on the four corners are ignored.
- In case multiple border minima are found in the raster, DC will extend the raster towards the one which lies closest to the last solution found on the currently traced dispersion curve.

5 Examples

5.1 T800M913 single layer plate @ 45°

We want to obtain the dispersion diagram for a unidirectional layer of the fiber-matrix system T800M913. The thickness shall be 2 mm and the wave propagation along an angle of 45° with respect to the fiber orientation. Since a single layer is symmetric, we can determine symmetric and anti-symmetric modes. Lamb and shear horizontal waves are coupled. Using the default settings, there are two problems:

1. Take a look at situation **A** in Fig. 31. If you are using the default **Step** of 0.5 kHz for the frequency sweep in the **Search higher order modes** panel, the cut-off frequency of A_{16} is not found and the mode not traced. Set a smaller **Step** of 0.05 kHz. A_{16} will now appear in the upper left output window below the **Search higher order modes** panel and can be traced.
2. Consider situation **B**. If you are using the default **Frequency step** of 5 kHz, the tracing of A_{12} fails to cross through the lower order modes at point **B** so that the part beyond 4.5 MHz is missing. To solve the problem, set a **Frequency step** of 2 kHz.

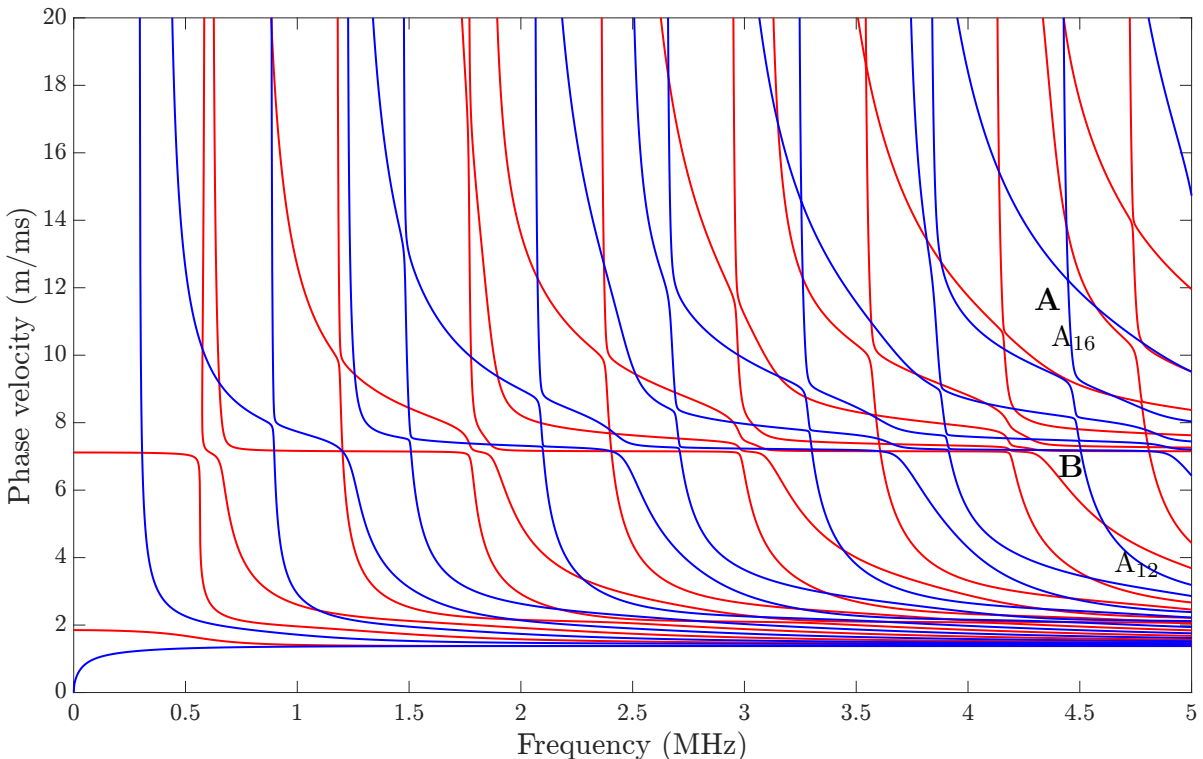


FIG. 31. Dispersion diagram for wave propagation along 45° with respect to the fiber direction in 2 mm thick unidirectional T800M913.

5.2 T800M913 [0/90]₄ plate @ 45°

Now, let us compute a 2 mm thick layup [0/90]₄ from the same material, and again we let the guided waves propagate along 45°. Since the layup is non-symmetric, symmetric and anti-symmetric waves cannot be distinguished. Lamb and shear horizontal waves are coupled. The dispersion diagram in Fig. 32 poses a significant challenge to the dispersion curve tracing algorithm because dispersion curves are very close to each other over wide frequency ranges, and there are difficult mode crossings. Using the default **Frequency step** of 5 kHz and **Lamb wave search width for negative curvature** of 10 and **Lamb wave search width for positive curvature** of 5 in the **Advanced** tab, dispersion curves are incomplete in many occasions. However, DC can master the challenge by setting a small **Frequency step** of 1 kHz and **Lamb wave search width for negative curvature** of 5 and **Lamb wave search width for positive curvature** of 2. The latter two options narrow down the phase velocity search range for each modal solution so that more neighboring modes are excluded and the modal solutions are found faster. The risk is that the tracing cannot follow a mode through sections where it bends abruptly (as the case in Sec. 5.1), but this is not the case here; the curves bend rather smoothly.

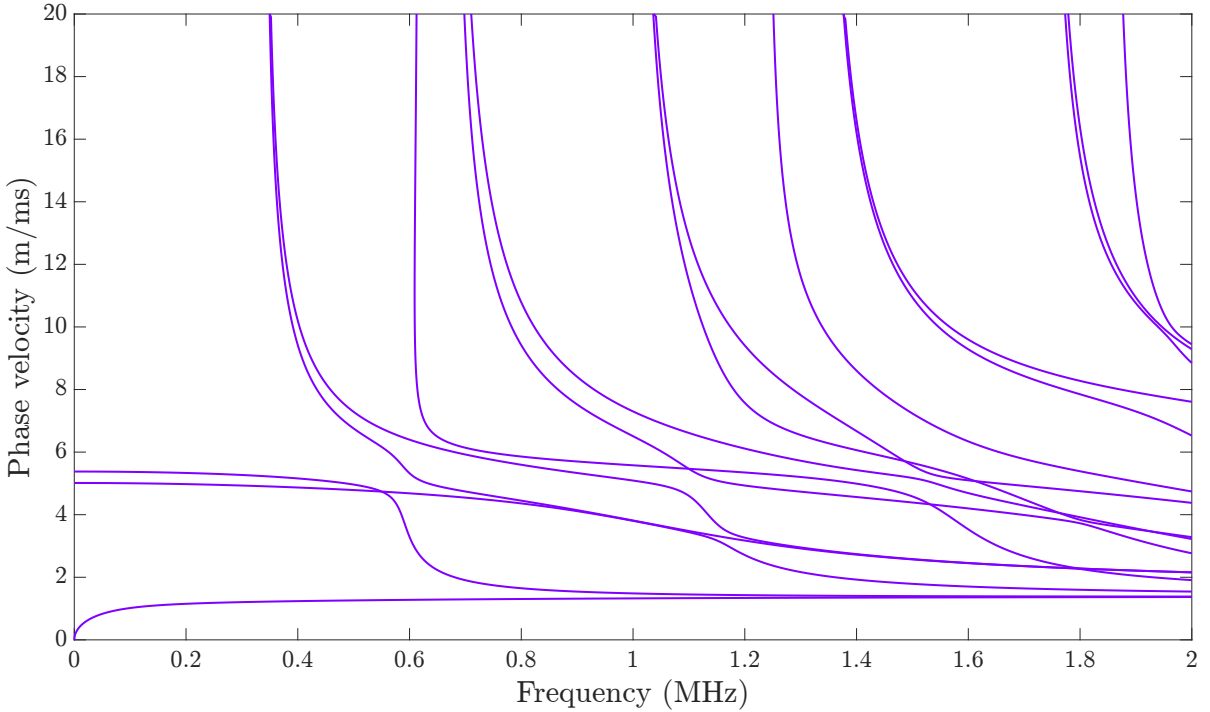


FIG. 32. Dispersion diagram for wave propagation along 45° in a 2 mm thick layup [0/90]₄ T800M913.

5.3 T800M913 [0/90]_{100s} plate @ 0°

It was mentioned in the introduction that modern rocket booster pressure vessels can consist of up to 400 layers in certain areas. Now, we want to calculate such kind of laminate. We assume a layup [0/90]_{100s} with layer thicknesses of 0.125 mm yielding a 50 mm thick laminate. Despite the 400 layers, the dispersion diagram in Fig. 33 computes in just seven seconds on my notebook (using multicore computing (**Multicore → Enable**)), thanks to optimizations done in DC v3.0. Lamb and shear horizontal waves decouple and can therefore be calculated separately. Figure 34 shows the displacement and stress field components of the S₀ Lamb wave at 50 kHz. The periodicity of the layup becomes obvious in the displacement u_1 and in the stresses σ_{11} and σ_{22} .

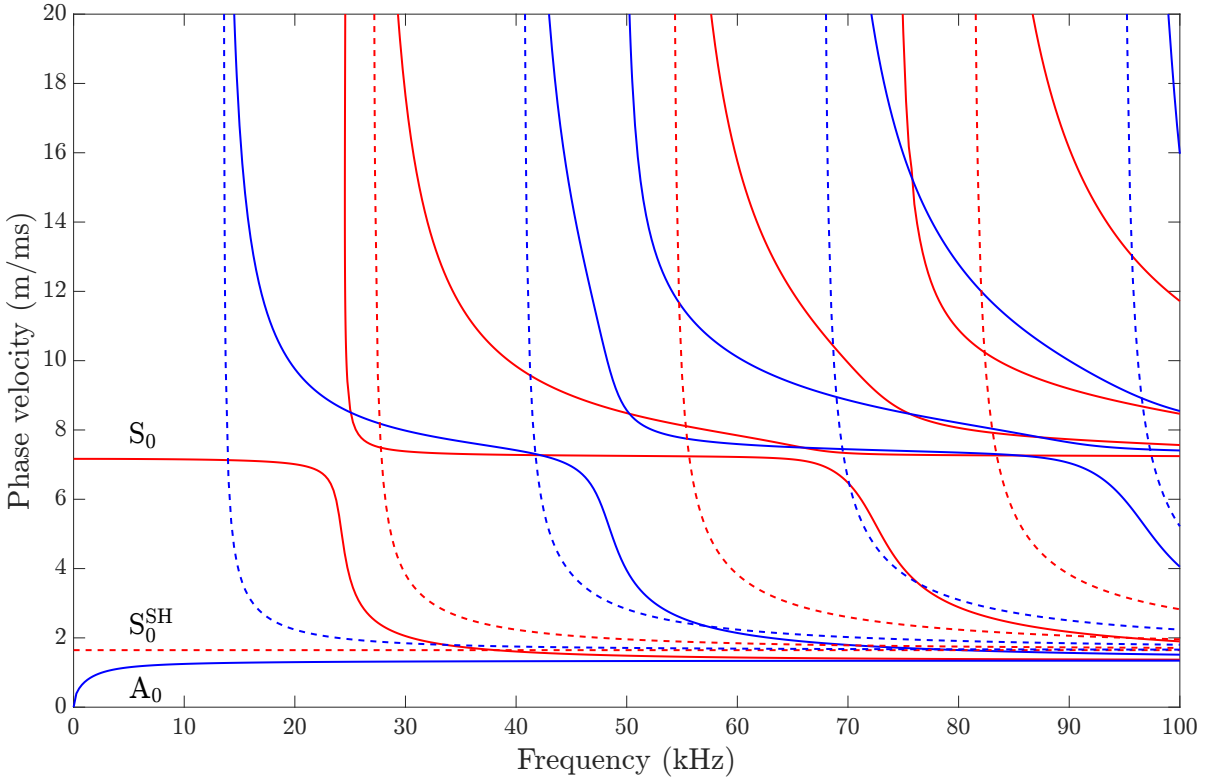


FIG. 33. Dispersion diagram for wave propagation along 0° in a 50 mm thick layup [0/90]_{100s} T800M913.

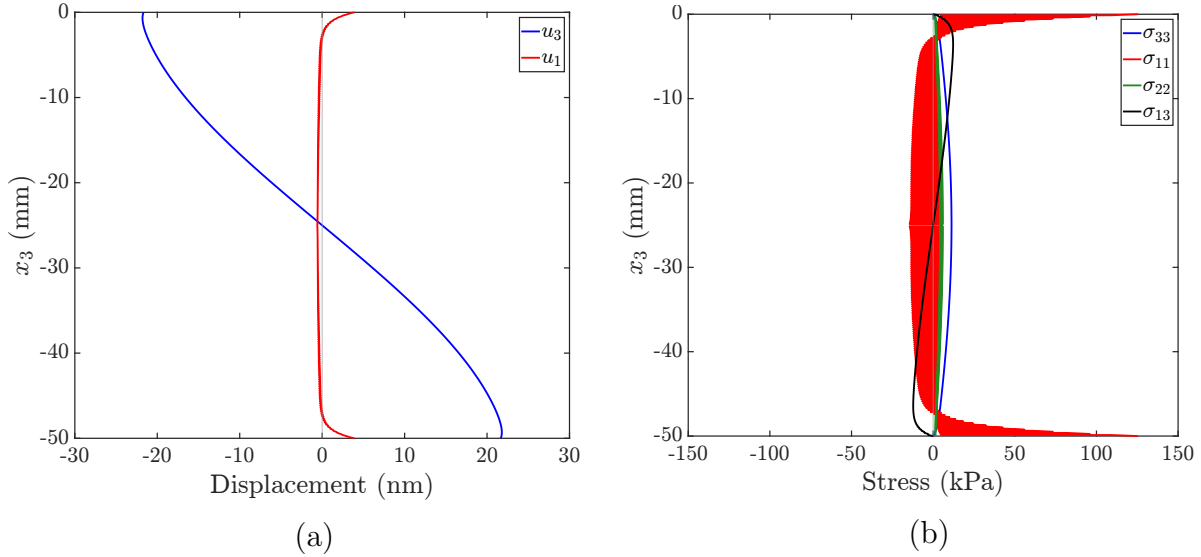


FIG. 34. (a) Displacement and (b) stress field components of the S_0 Lamb wave at 50 kHz in a 50 mm thick layup $[0/90]_{100s}$ T800M913.

5.4 CarbonEpoxy_Hernando_2015_Viscoelastic single layer plate @ 30°

Let us consider now a viscoelastic case. We want to obtain the dispersion diagram for a unidirectional layer of the fiber-matrix system CarbonEpoxy_Hernando_2015_Viscoelastic. The thickness shall be 1 mm and the wave propagation be along 30°. If you use the default **Frequency step** of 10 kHz, the tracing has two problems. In point A, A₁ makes a small kink, and in point B, S₂ jumps to S₃ and vice versa. Both issues are solved by setting the **Frequency step** to 5 kHz. You may have noticed that many problems can be solved by reducing the **Frequency step**. S₂ is incomplete at high phase velocity.

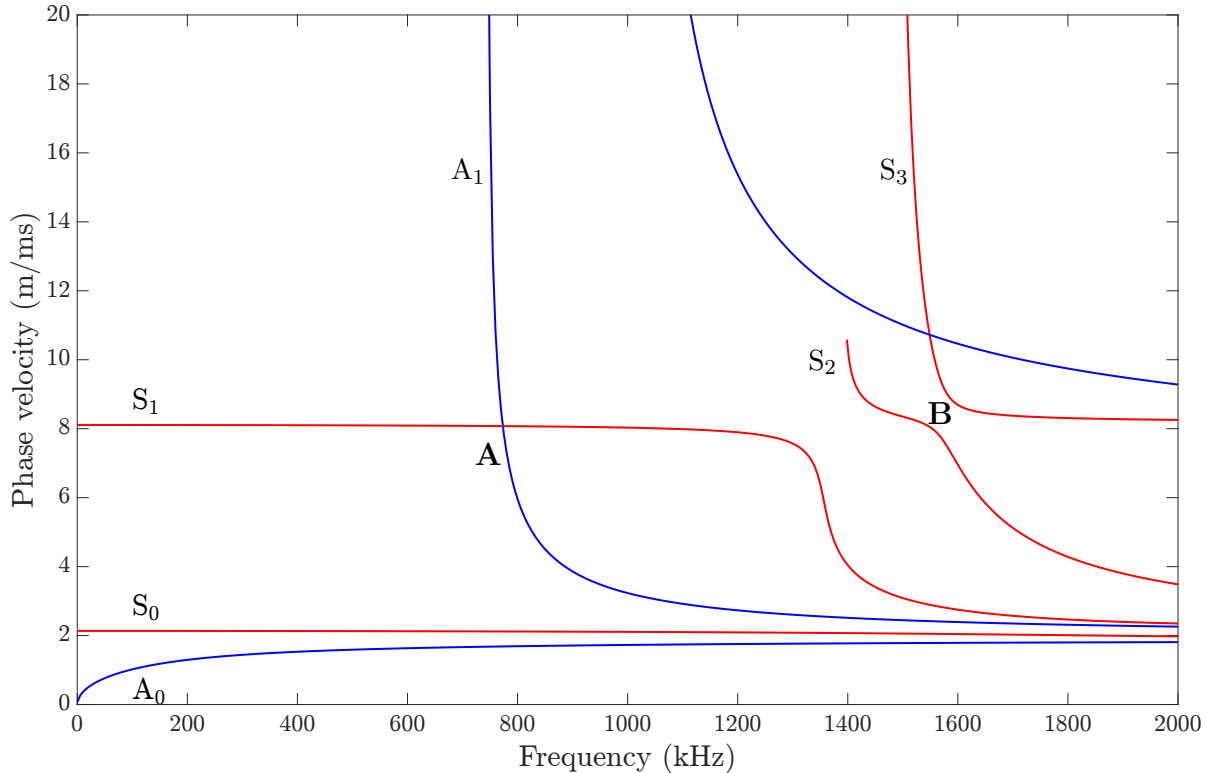


FIG. 35. Dispersion diagram for wave propagation along 30° in 1 mm thick unidirectional CarbonEpoxy_Hernando_2015_Viscoelastic.

5.5 AS4M3502 [0/90]_{2s} plate @ 45° in water

Let us compute the dispersion diagram for a 1 mm thick [0/90]_{2s} layup of AS4M3502 immersed in water. Wave propagation shall take place in the 45°-direction. Due to the water-loading, the two fundamental Scholte modes S_0^{Scholte} and A_0^{Scholte} are present. These are indicated by the dashed-dotted lines. Notice that S_0^{Scholte} starts at the wave speed in water. Higher order Scholte modes do not occur in this situation. The problem is that S_2 cannot be traced when the propagation direction is exactly 45°. To help with this, we change the propagation direction slightly to 45.1°. While this has hardly any impact on the dispersion curves themselves, dispersion curve tracing seems to become easier. Also the tracing of S_0 starts much faster. A small error is present at the cut-off frequency of S_2 . It is connected to S_3 .

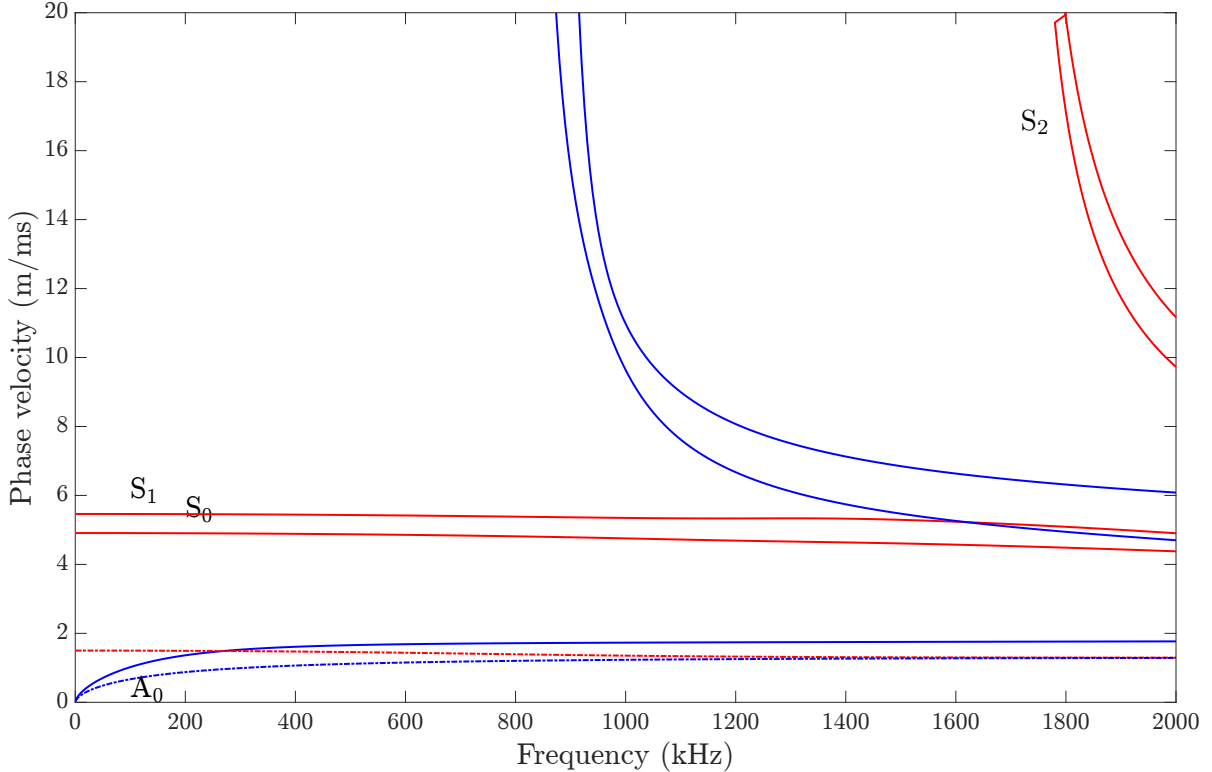


FIG. 36. Dispersion diagram for wave propagation along 45° in a 1 mm thick [0/90]_{2s} layup of AS4M3502 immersed in water.

5.6 Aluminum alloy 1100 pipe filled with water

We now consider an aluminum alloy 1100 pipe with an outer diameter of 10 mm and with an inner diameter of 8 mm. The pipe is filled with water. We calculate the dispersion diagram twice, and we only plot the longitudinal modes (red curves) and the flexural modes with the circumferential order $n = 1$ (blue curves). In the first run, we do not place a sink at the center (use a **Frequency step** of 1 kHz instead of 1.25 kHz to avoid a small problem in the tracing). This system has no attenuation. The dispersion diagram is shown in Fig. 38 (a). In the second run, we place a sink at the center. This adds damping to the system. The result is in Fig. 38 (b). Comparing both dispersion diagrams, we notice that, when the sink is placed, far less modes are present compared to the case without sink. Most of the modes in Fig. 38 (a) are propagating almost entirely in the fluid-filling, with hardly any energy transport in the pipe wall. Different from these are a few modes which carry most of their energy in the pipe wall. These pipe modes remain when we put a sink at the center, which suppresses the bulk waves propagating from one side of the pipe wall through the fluid to the opposite side of the pipe wall. Usually, in pipe inspection, we are interested only in modes which propagate predominantly in the pipe wall. Let us compare for example F(1,12) and F(1,13) at 1.7 MHz from Fig. 38 (a). The through-thickness displacements are plotted in Fig. 37. From Fig. 37 (a), we see clearly that F(1,12) is a pipe mode, whereas F(1,13) in Fig. 37 (b) is a fluid mode, which is rather unsuitable for inspecting a pipe. Hence, for this task, it is advantageous to suppress the fluid-modes by placing the sink.

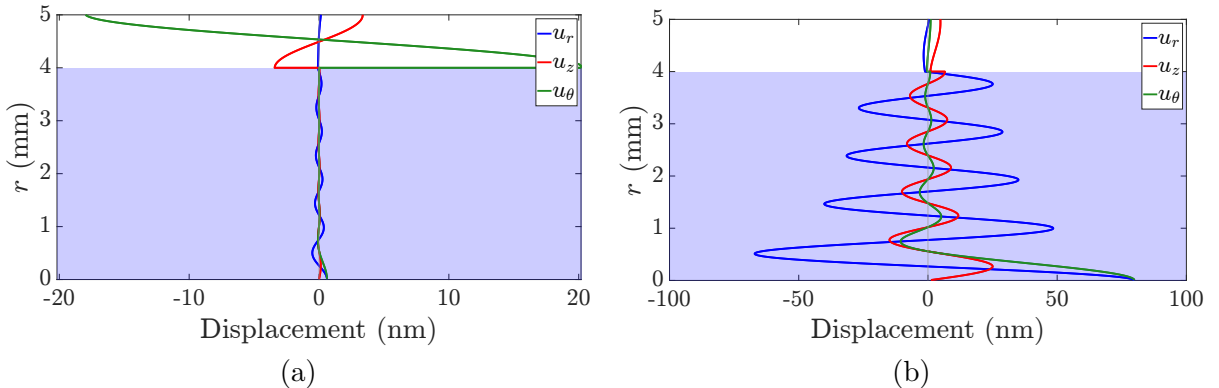


FIG. 37. Through-thickness displacements at 1.7 MHz for a 10 mm diameter, 1 mm wall thickness aluminum alloy 1100 pipe filled with water (no sink at the pipe center). (a) F(1,12). (b) F(1,13).

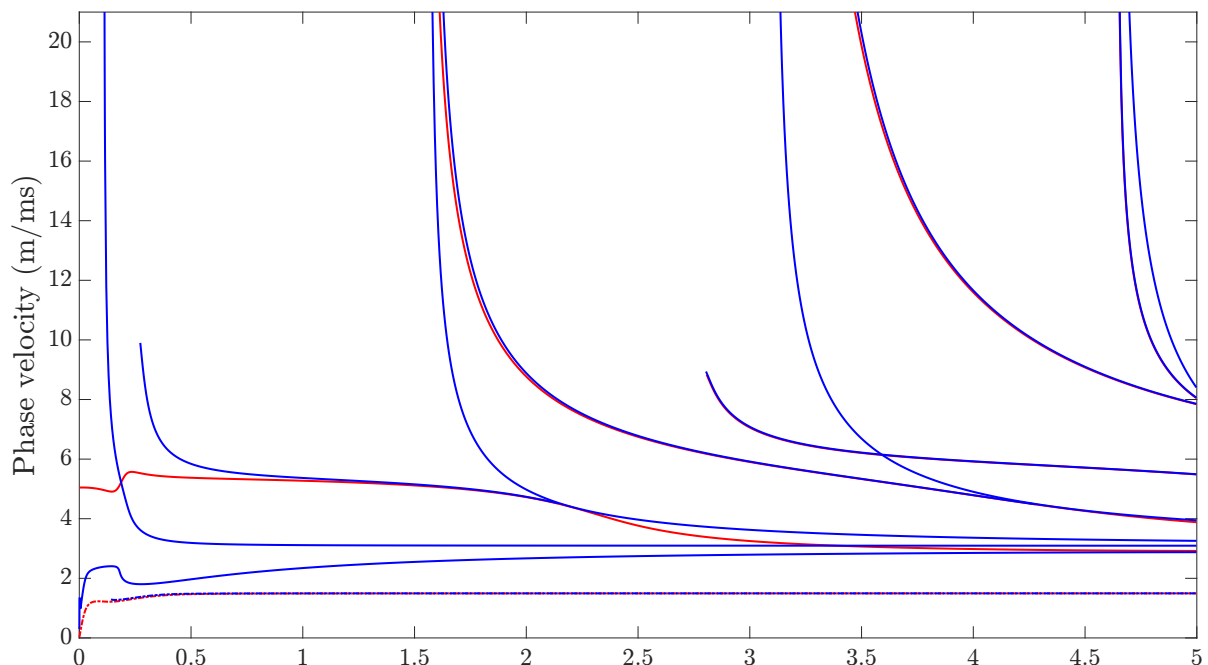
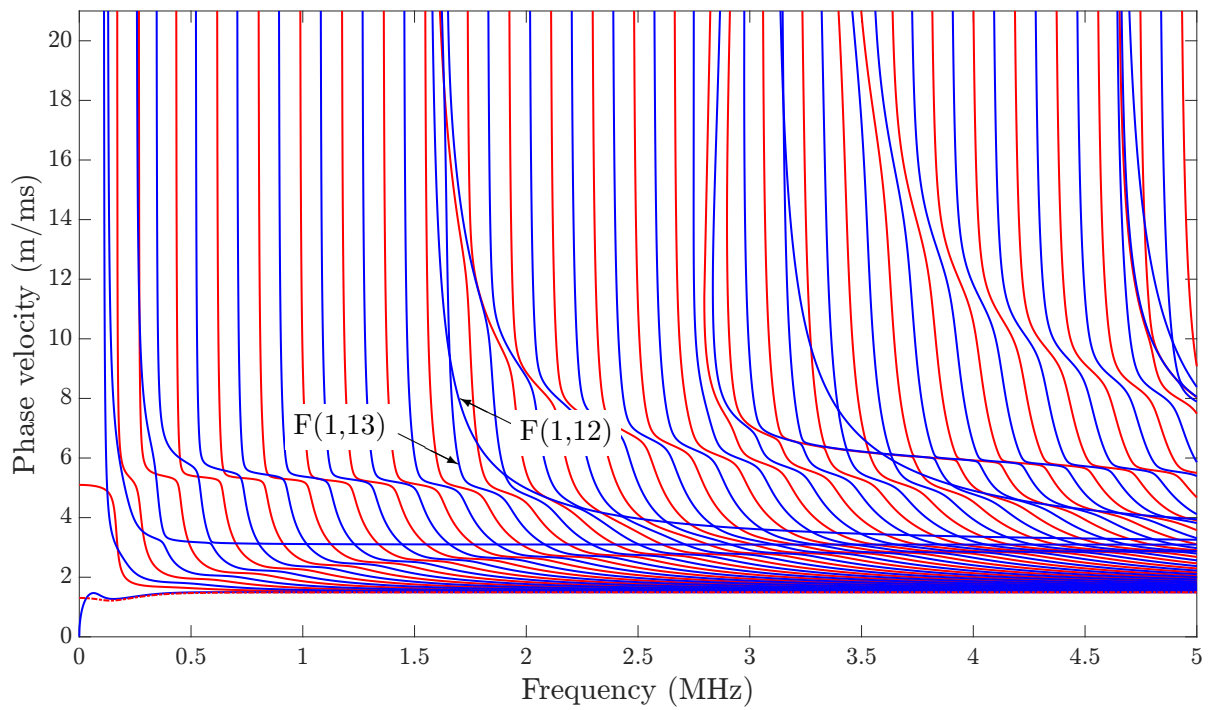


FIG. 38. Dispersion diagrams for a 10 mm diameter, 1 mm wall thickness aluminum alloy 1100 pipe filled with water. (a) No sink at the center. (b) Sink at the center.

5.7 Aluminum alloy 1100 circumference

Consider an aluminum alloy 1100 pipe with an outer diameter of 100 mm and with an inner diameter of 60 mm. We are interested in the Lamb-type and shear horizontal-type guided waves propagating in the circumferential direction. As the waveguide is, from the point of view of the guided waves, like a curved plate, the circumferential waves are non-symmetric. The phase velocity of circumferential waves is a function of the radius, and in DC, the phase velocity at the outer pipe surface (outer diameter, d_o) is displayed in the dispersion diagram, see Fig. 39. Notice that the fundamental shear horizontal mode C_0^{SH} is dispersive, unlike the case for S_0^{SH} in a flat plate. Also, what is S_0 in a flat plate turns out to be a higher order mode C_1 in a circumference.

Now consider an aluminum alloy 1100 pipe with an outer diameter of 100 mm and with an inner diameter of 98 mm. This is a thin-walled pipe. The dispersion diagram for circumferential waves is displayed in Fig. 40 (a). Notice how the cut-off frequency of C_1 has shifted to very low frequency. As the ratio of the inner diameter to the outer diameter approaches unity, the waveguide behaves more and more like a flat plate. In the case considered here, the ratio is 0.98, and starting at this value, DC issues a recommendation to calculate a flat plate with a thickness of the wall thickness of the assumed pipe. Figure 40 (b) shows the dispersion diagram for a 1 mm thick aluminum alloy 1100 plate for comparison. Already at a ratio of 0.98, both dispersion diagrams look very similar. As the ratio increases further, the equations for the circumferential become numerically unstable so that calculating a plate becomes absolutely necessary.

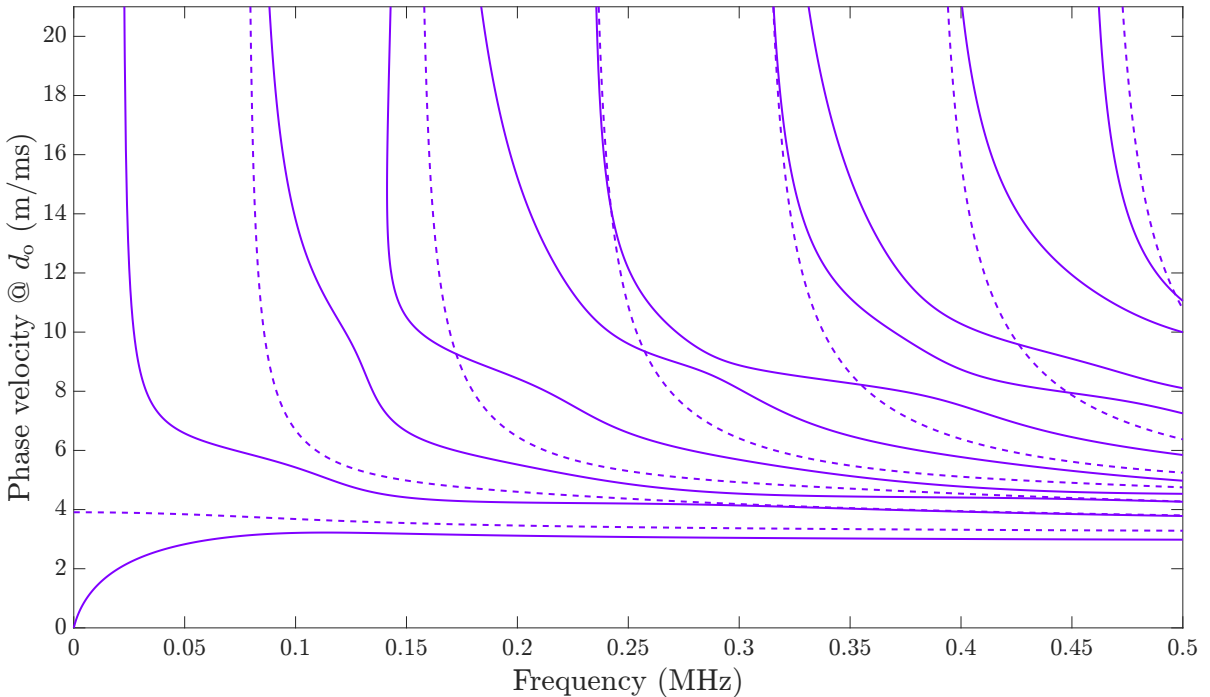
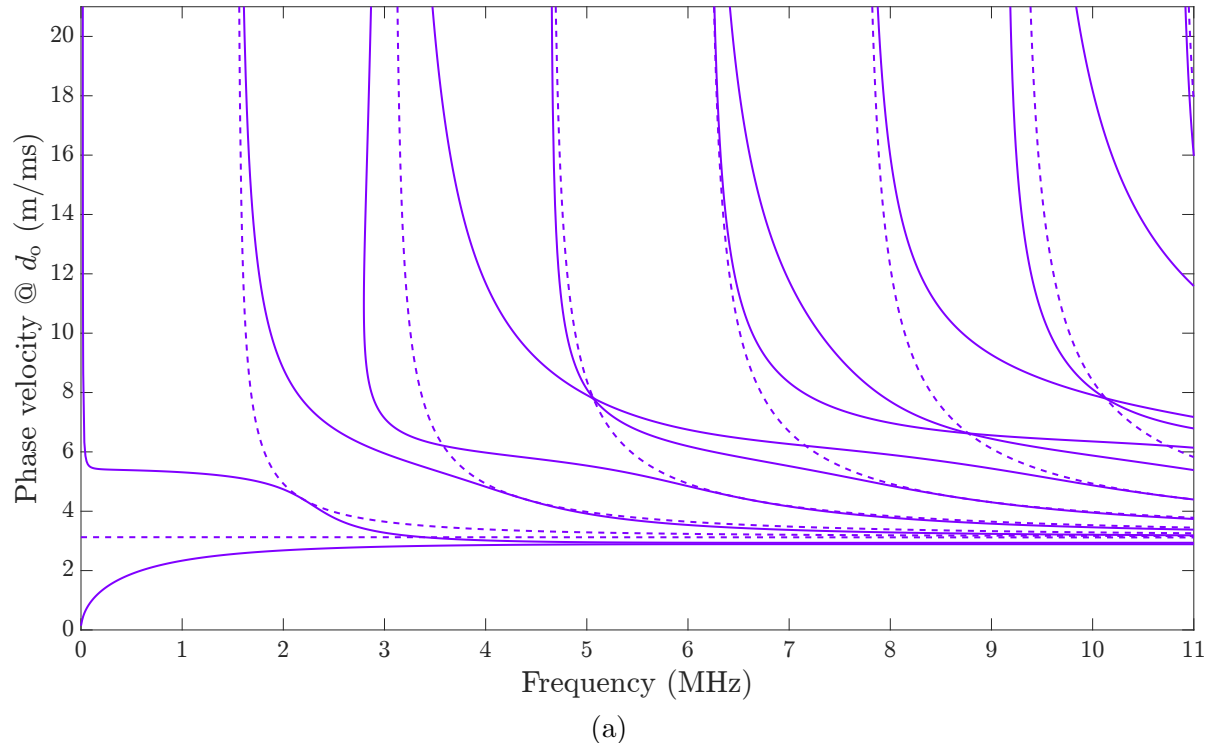
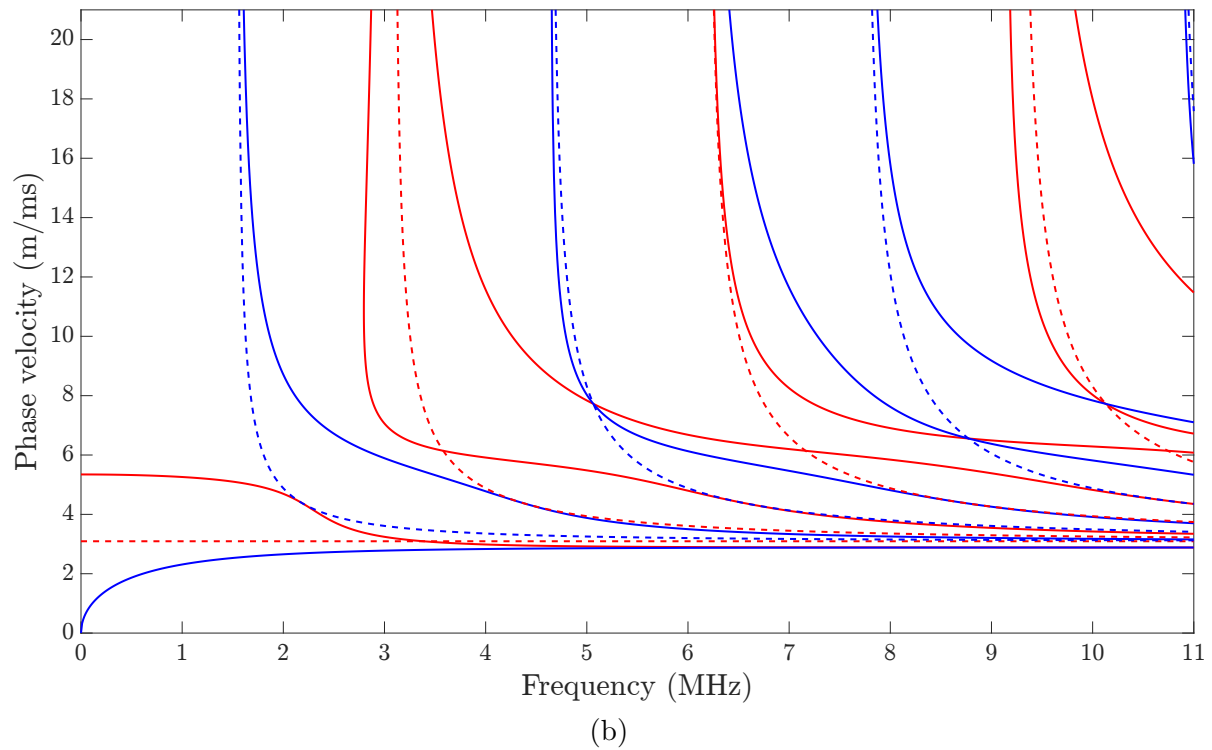


FIG. 39. Dispersion diagram for circumferential waves in a 100 mm diameter, 20 mm wall thickness aluminum alloy 1100 pipe.



(a)



(b)

FIG. 40. (a) Dispersion diagram for circumferential waves in a 100 mm diameter, 1 mm wall thickness aluminum alloy 1100 pipe. (b) Dispersion diagram for a 1 mm thick aluminum alloy 1100 plate.

A Group velocity and energy velocity of guided waves

The group velocity of a guided wave is the speed at which a wave packet propagates, i.e., the speed at which energy is transported. It is calculated by the well-known equation

$$c_g = \frac{\partial \omega}{\partial \xi}, \quad (9)$$

where ω is the circular frequency ($= 2\pi f$), and ξ is the wavenumber of the guided wave. For simple dispersion equations like the Rayleigh-Lamb equations, it is possible to derive analytic equations using

$$c_g = -\frac{\partial c_p / \partial \xi}{\partial c_p / \partial \omega}, \quad (10)$$

with the phase velocity c_p , as shown by Bernard et al. [58]. Otherwise, Eq. (9) can be manipulated into

$$c_g = c_p^2 \left(c_p - f \frac{\partial c_p}{\partial f} \right)^{-1}. \quad (11)$$

To carry out Eq. (11) programmatically, the phase velocity dispersion curve is fitted so that its derivative can be taken from the fitted function. Although Eq. (10) is used in DC where possible, Eq. (11) is not applied as a general solution for two reasons. Firstly, the group velocity has physical significance only in non-dissipative systems, i.e., without attenuation caused by viscoelasticity or energy leakage to the surrounding medium (fluid-loading). With attenuation, the wavenumber turns complex so that Eq. (9) does not make sense anymore. The energy velocity is the more generic quantity. It is valid both with and without attenuation, where in the latter case, group and energy velocity are equivalent. Secondly, Eq. (9) gives only the group velocity component in the direction of wave propagation. Therefore, DC calculates the energy velocity whenever Eq. (10) cannot be used.

Let us introduce a coordinate system $x_i = (x_1, x_2, x_3)$, where a plate lies in the x_1 - x_2 -plane, x_1 is the propagation direction of the guided wave, and x_3 is normal to the plate. The total energy E_{total} is the energy per unit volume carried by a guided wave. It has two contributions, namely the strain energy E_{strain} and the kinetic energy E_{kin} so that $E_{\text{total}} = E_{\text{strain}} + E_{\text{kin}}$, where

$$E_{\text{strain}} = \frac{1}{2} \int_S \text{Re}(\varepsilon_{ij} \sigma_{ij}^*) dS, \quad i, j = 1, 2, 3, \quad (12)$$

with the stress tensor σ_{ij} and the strain tensor ε_{ij} , and

$$E_{\text{kin}} = \frac{1}{2} \rho \int_S v_i^2 dS, \quad (13)$$

where integration of the respective energy densities is performed over the cross section S of the laminate, and where ρ is the material density and $v_i = u_i$ is the particle velocity vector.

The power flow P_j is the energy flow per unit volume and unit time carried by a guided wave. It is obtained by integration of the power flow density (*Poynting vector*) p_j , indicating the magnitude and direction of the power flow

$$P_j = \int_S p_j dS = -\frac{1}{2} \int_S \operatorname{Re}(\sigma_{ij} v_i^*) dS = -\frac{1}{2} \int_S \operatorname{Re} \begin{bmatrix} \sigma_{11} v_1^* + \sigma_{21} v_2^* + \sigma_{31} v_3^* \\ \sigma_{12} v_1^* + \sigma_{22} v_2^* + \sigma_{32} v_3^* \\ \sigma_{13} v_1^* + \sigma_{23} v_2^* + \sigma_{33} v_3^* \end{bmatrix} dS. \quad (14)$$

The star (*) indicates the complex conjugate. In absence of attenuation, there is only power flow along the propagation direction P_1 , (and P_2 in coupled cases in anisotropic media) while P_3 (normal to the plate) is zero.

The energy velocity components c_{e1} and c_{e2} are calculated from the ratios of the power flow P_j to the total energy E_{tot} as

$$\vec{c}_e = \frac{1}{E_{\text{tot}}} \begin{bmatrix} P_1 \\ P_2 \\ 0 \end{bmatrix} = \begin{bmatrix} c_{e1} \\ c_{e2} \\ 0 \end{bmatrix}, \quad (15)$$

where the total energy is obtained with Eqs. (12) and (13) by

$$E_{\text{tot}} = \frac{1}{2} \int_S \operatorname{Re}(\varepsilon_{11} \sigma_{11}^* + \varepsilon_{33} \sigma_{33}^* + \varepsilon_{23} \sigma_{23}^* + \varepsilon_{13} \sigma_{13}^* + \varepsilon_{12} \sigma_{12}^*) dS, \quad (16)$$

$$+ \frac{1}{2} \rho \int_S (v_1^2 + v_2^2 + v_3^2) dS,$$

(ε_{22} is zero in a plate), and the power flow components are calculated from Eq. (14) by

$$P_1 = -\frac{1}{2} \int_S \operatorname{Re}(\sigma_{11} v_1^* + \sigma_{12} v_2^* + \sigma_{13} v_3^*) dS, \quad (17)$$

$$P_2 = -\frac{1}{2} \int_S \operatorname{Re}(\sigma_{12} v_1^* + \sigma_{22} v_2^* + \sigma_{23} v_3^*) dS.$$

Obviously, Eq. (15) describes a vector with a component c_{e1} along and a component c_{e2} normal to the wave propagation direction x_1 . The magnitude of the energy velocity vector is given by

$$c_e = |\vec{c}_e| = \sqrt{c_{e1}^2 + c_{e2}^2}. \quad (18)$$

\vec{c}_e points in the direction of energy flow so that it indicates the actual direction of the guided wave beam (ray angle Φ_r). In general, Φ_r deviates from the wave propagation angle Φ by the skew angle γ , given by

$$\gamma = \Phi - \Phi_r. \quad (19)$$

With the energy velocity vector components obtained from Eq. (15), we can calculate

$$\gamma = -\tan^{-1} \frac{c_{e2}}{c_{e1}}. \quad (20)$$

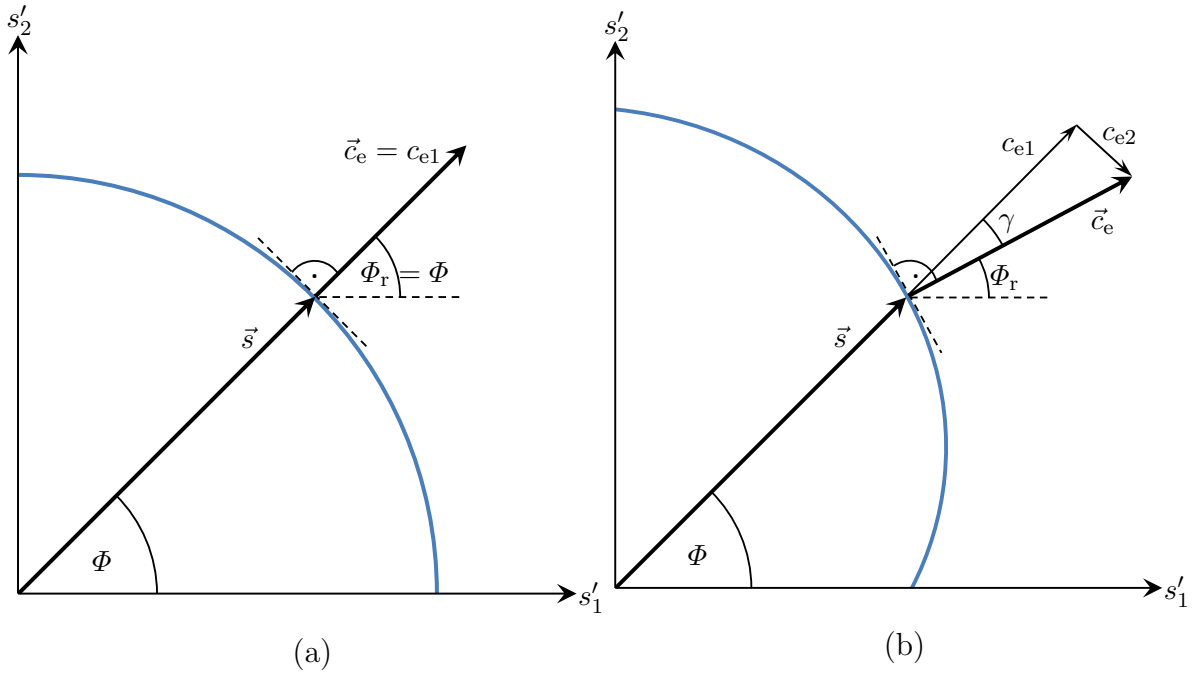


FIG. 41. The energy velocity vector. (a) In the decoupled case such as in an isotropic medium, the energy velocity direction coincides with wave propagation direction. (b) In the coupled case in anisotropic media, the energy velocity direction skews from the wave propagation direction.

The negative sign in Eq. (20) accounts for the fact that the guided wave beam, i.e., the energy flow, skews towards the fiber direction because energy can be transported more efficiently in that direction.

In decoupled cases such as in isotropic media or in anisotropic media for wave propagation along or normal to the fibers, Φ_r is equal to Φ . This situation is illustrated in Fig. 41(a), where the slowness is plotted versus the wave propagation angle in an isotropic medium. The slowness is the inverse phase velocity $s = c_p^{-1}$, and the energy velocity vector \vec{c}_e is oriented perpendicular to the slowness profile. Since the slowness profile in an isotropic medium is a circle, the energy velocity vector is always aligned with the slowness vector and with the wave propagation direction, i.e., $\gamma = 0$ so that $c_{e2} = 0$ and $\vec{c}_e = \vec{c}_{e1}$. By contrast, in coupled cases, i.e., for wave propagation other than along axes of symmetry in an anisotropic medium, the energy velocity direction is not anymore aligned with the wave propagation direction, but skews by an angle $\gamma \neq 0$, as illustrated in Fig. 41(b).

DC applies Eqs. (15) to (20) to every sample point in every phase velocity dispersion curve to obtain results as those presented in Fig. 43. Therein, the energy velocity components are illustrated for a coupled case, namely for wave propagation along an angle of $\Phi = 45^\circ$ in a 1 mm thick layer T800M913. Figure 43(a) shows the energy velocity component along the wave propagation direction c_{e1} . The plot is useful for scenarios like air-coupled ultrasonic inspection where you send a guided wave in a certain (wave propagation) direction, and detect the signal after propagating a certain distance

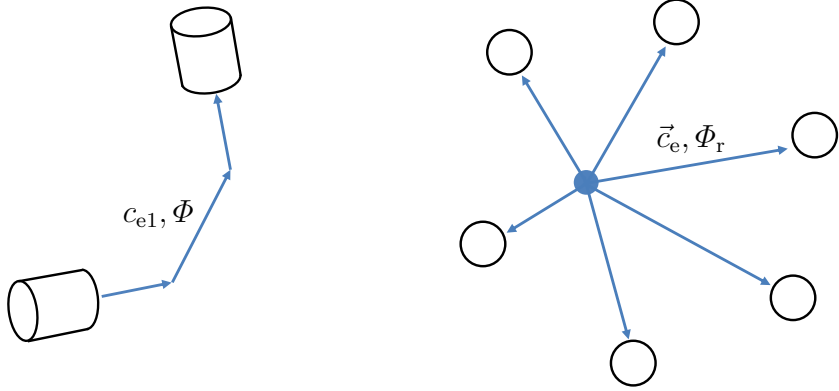


FIG. 42. The two main scenarios encountered in guided wave-based non-destructive inspection. Left: A guided wave is sent along a chosen propagation angle Φ , like in air-coupled ultrasonic inspection. Right: Guided waves are emanating outwards from a point source such as from a crack to be detected by a sensor array.

in that direction (see on the left in Fig. 42). Figure 43(b) shows the energy velocity component c_{e2} normal to the propagation direction. It can take positive and negative values, meaning that the energy velocity vector, i.e., the energy flux, can skew at some angle γ to the left and to the right side with respect to the wave propagation direction. This relates to the negative and positive skew angles seen in Fig. 43(d). The energy velocity magnitude c_e is displayed in Fig. 43(c). It is the speed at which energy is transported in the direction determined by the ray angle Φ_r , in this case $\Phi_r = 45^\circ - \gamma$. Figure 43(e) displays a propagation time dispersion diagram for a propagation distance of 100 mm. These kind of diagrams are useful for acoustical emission experiments to identify modes in the measured signals of voltage versus time. The propagation time diagram is calculated based on c_{e1} , namely $t_{\text{prop}} = \text{distance}/c_{e1}$. Similarly, the signals simulated in the **Signal simulator** correlate with the energy velocity component c_{e1} . The onsets of the wave packets appear as predicted by the propagation time dispersion diagram. Similarly as stated for the energy velocity component c_{e1} , the propagation time dispersion diagram is valid for modes excited and detected in a chosen wave propagation direction angle Φ .

The difference between c_{e1} and \vec{c}_e becomes even more striking when we look at polar dispersion diagrams. Figure 44(a) shows the energy velocity component c_{e1} of the fundamental modes at 200 kHz versus the wave propagation angle Φ in 1 mm thick T800M913. By contrast, Fig. 44(b) shows the energy velocity magnitude c_e versus the ray angle Φ_r . This plot, also called wavecrest plot, shows how the guided waves generated by a point source advance outwards with time. Therefore, these plots are useful for scenarios like acoustical emission where an array of sensors is placed on a specimen to detect ultrasonic signals emitted from a point source (see on the right in Fig. 42). It is striking how different the profiles of the extensional modes in Fig. 44(a) look compared to those in Fig. 44(b). They are equal only at $\Phi = 0^\circ, 90^\circ$ because these are the axes of symmetry where the skew angle and c_{e2} become zero so that $c_e = c_{e1}$. It shows how much the fiber direction $\Phi = 0^\circ$ is preferred for the actual transport of energy. In the profile of

S_0 , we notice that multiple energy velocity values are possible for a given ray angle. This is closely related to the skew angle plotted versus the wave propagation direction in Figure 44(c). Finally, Fig. 45 presents the corresponding polar propagation time for a propagation distance of 100 mm. Figure 45(a) is calculated from c_{e1} , so use it only for directed signals, whereas Fig. 45(b) is deduced from c_e and appropriate for point sources radiating outwards.

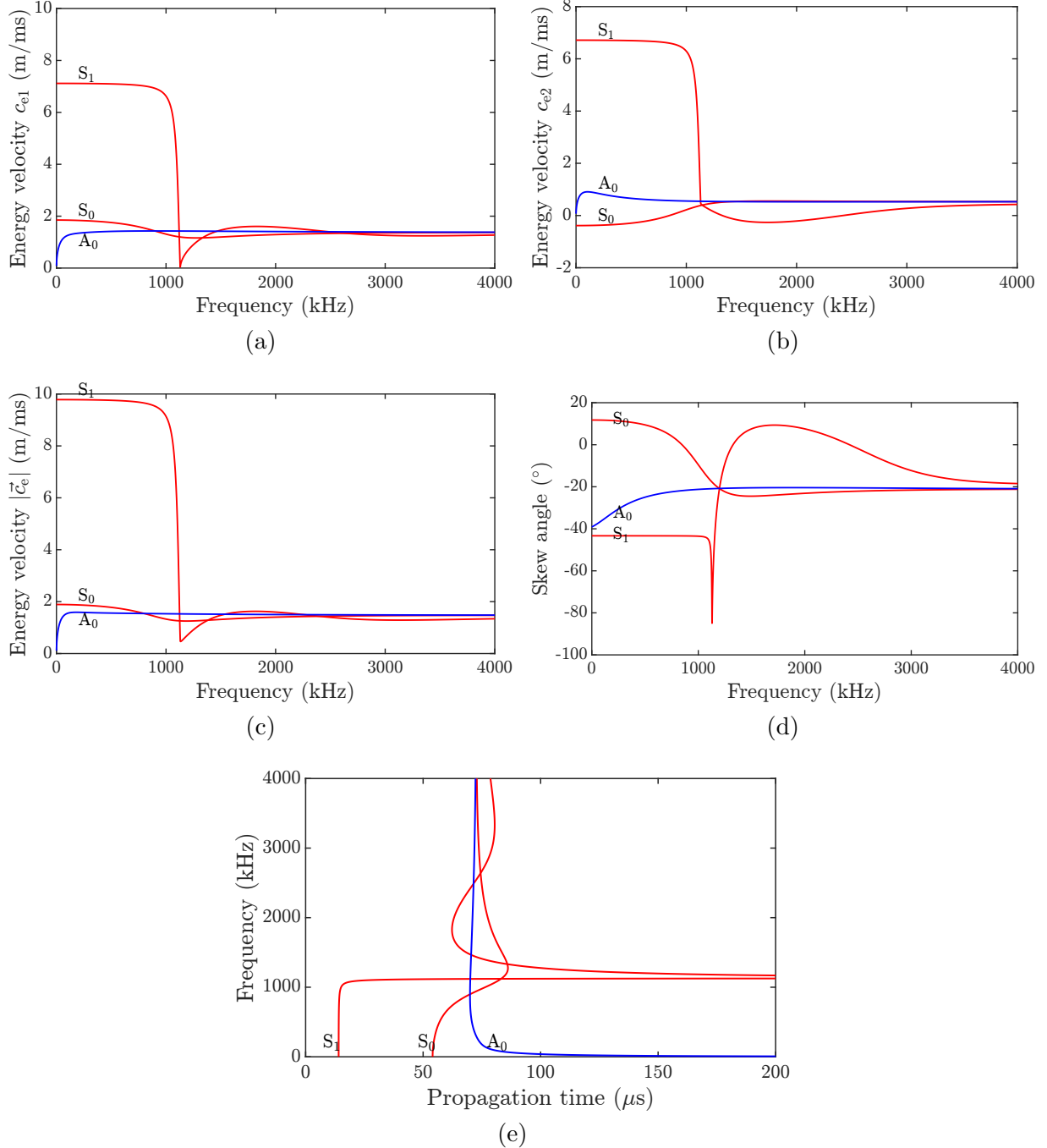


FIG. 43. Energy velocity and propagation time dispersion diagrams of the fundamental modes for propagation along $\Phi = 45^\circ$ in a 1 mm thick layer T800M913. (a) Energy velocity component c_{e1} , (b) component c_{e2} , (c) magnitude $|c_e|$, and (d) skew angle γ . (e) The propagation time for a distance of 100 mm is calculated from c_{e1} .

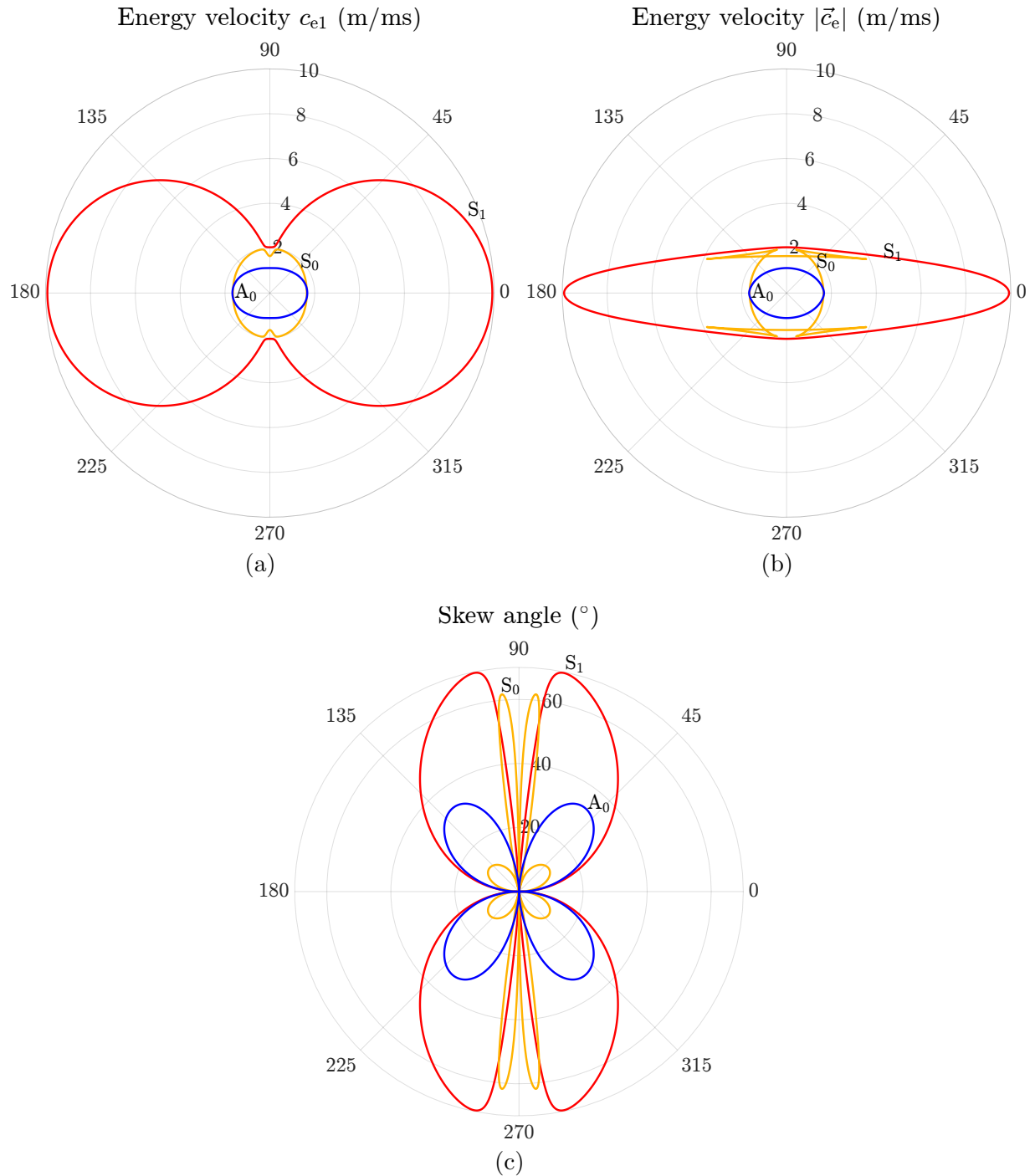


FIG. 44. Polar energy velocity dispersion diagrams of the fundamental modes at 200 kHz in a 1 mm thick layer T800M913. (a) Energy velocity component c_{e1} , (b) magnitude $|\vec{c}_e|$, and (c) skew angle γ .

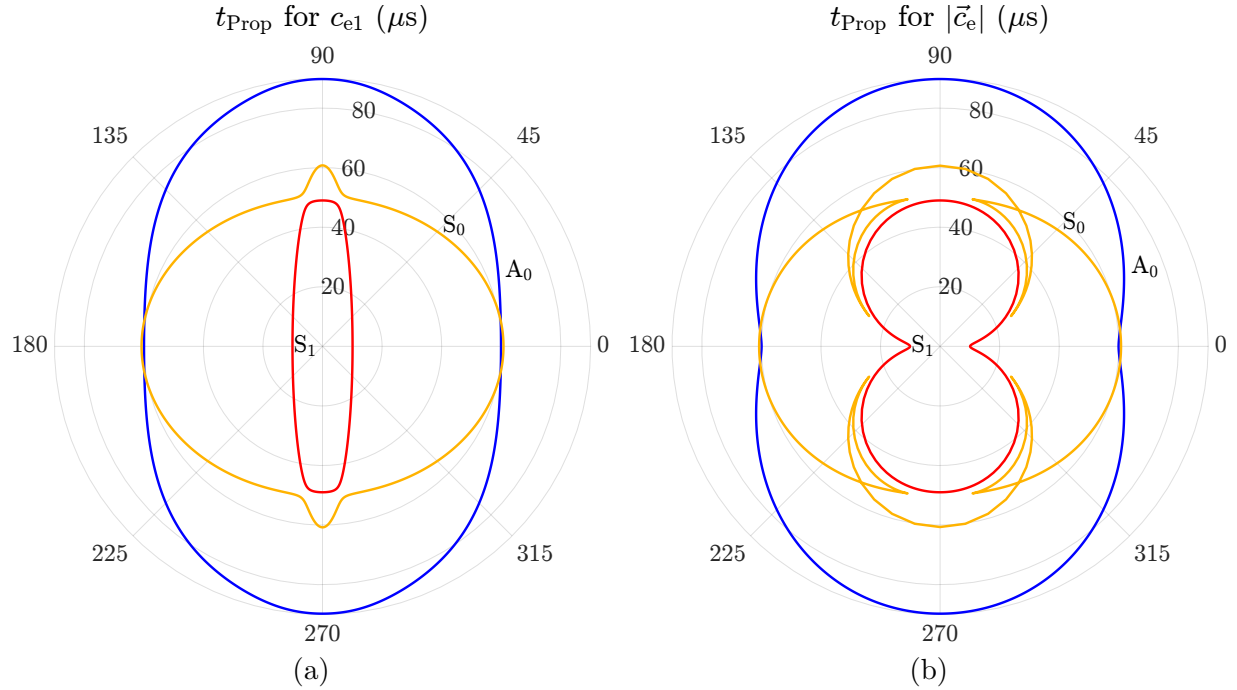


FIG. 45. Propagation time dispersion diagrams of the fundamental modes at 200 kHz in a 1 mm thick layer T800M913. (a) Propagation time based on c_{e1} and (b) based on $|\vec{c}_e|$.

B Bulk wave velocities in elastic media

Of particular significance are the bulk waves' phase velocities for propagation along the principal axes in elastic media. The Table 3 lists the velocities as function of the stiffness components C_{ij} and of the density ρ . The direction 1 is along the fibers, while 2 and 3 are normal to it. In transversely isotropic media, the velocities are equal for propagation along 2 and 3 (and in fact for any direction within the 2-3-plane) since $C_{33} = C_{22}$ and $C_{55} = C_{66}$. In cubic materials, all longitudinal velocities are equal since $C_{11} = C_{22} = C_{33}$, and all shear waves are also equal because $C_{44} = C_{55} = C_{66}$. Both is true also in isotropic media with the specialty that $C_{44} = C_{55} = C_{66} = 0.5(C_{11} - C_{12})$. Notice that in case of complex stiffnesses C_{ij} , only the real parts are used in the below equations.

TABLE 3. Bulk wave velocities along principal axes.

Velocity	1	2	3
Longitudinal	$= \sqrt{\frac{C_{11}}{\rho}}$	$= \sqrt{\frac{C_{22}}{\rho}}$	$= \sqrt{\frac{C_{33}}{\rho}}$
Fast shear	$= \sqrt{\frac{C_{55}}{\rho}}$	$= \sqrt{\frac{C_{66}}{\rho}}$	$= \sqrt{\frac{C_{55}}{\rho}}$
Slow shear	$= \sqrt{\frac{C_{66}}{\rho}}$	$= \sqrt{\frac{C_{44}}{\rho}}$	$= \sqrt{\frac{C_{44}}{\rho}}$

C List of default materials

More material data are found on MatWeb <http://www.matweb.com/>. For a list of more than two hundred viscoelastic material data sets, consult the work by Ono [59–61].

C.1 Isotropic

If not stated otherwise, the materials are taken from Ref. [62].

	ρ (kg/m ³)	E (GPa)	ν	α_L (Np/ λ)	α_T (Np/ λ)
AluminumAlloy1100	2710	69	0.33	0	0
AluminumAlloy2011_Ono_2020_Viscoelastic [60]	2830	72.64	0.3355	0.0046	0.0075
AluminumAlloy2024	2770	72.4	0.33	0	0
AluminumAlloy2024_Ono_2020_Viscoelastic [60]	2770	71.56	0.3442	0.0012	0.0011
AluminumAlloy6061	2700	69	0.33	0	0
AluminumAlloy6061_Ono_2020_Viscoelastic [60]	2700	73.53	0.3298	0.0105	0.0092
AluminumOxide	3980	380	0.22	0	0
Aluminum_Disperse [2]	2700	70.76	0.3375	0	0
Aluminum_Disperse_Viscoelastic [2]	2700	70.76	0.3375	0.003	0.01
CastIronG3000	7300	101.5	0.26	0	0
CastIronG4000	7300	124	0.26	0	0
Concrete	2400	31	0.2	0	0
Copper110_Ono_2020_Viscoelastic [60]	8940	135.7	0.3174	0.0222	0.0244
CopperAlloyBrass260_Ono_2020_Viscoelastic [60]	8500	112.1	0.3382	0.0311	0.0191
CopperAlloyBrass360_Ono_2020_Viscoelastic [60]	8530	108.1	0.3333	0.0136	0.0092
CopperAlloyC17200BerylliumCopper	8250	128	0.3	0	0
CopperAlloyC26000CartridgeBrass	8530	110	0.35	0	0
CopperAlloyC36000FreeCuttingBrass	8500	97	0.34	0	0
CopperAlloyC71500CopperNickel30	8940	150	0.34	0	0
CopperAlloyC93200BearingBronze	8930	100	0.34	0	0
CopperAlloyCuAgZr_Ono_2020_Viscoelastic [60]	9920	149.7	0.3324	0.0132	0.025
CopperAlloyCuAl2O3_Ono_2020_Viscoelastic [60]	8900	137.6	0.2982	0.0122	0.0116
CopperOFHC_Ono_2020_Viscoelastic [60]	8960	171.8	0.1323	0.013	0.0389
DiamondNatural	3510	950	0.2	0	0
DiamondSynthetic	3360	863	0.2	0	0
Epoxy_Disperse [2]	1170	3.94	0.39	0	0
Epoxy_Disperse_Viscoelastic [2]	1170	3.94	0.39	0.04	0.1
Epoxy_Ono_2020_Viscoelastic [60]	1390	7.039	0.3319	0.0867	0.1636
GlassBorosilicate	2230	70	0.2	0	0
GlassCeramic	2600	120	0.25	0	0
GlassQuartz	2200	73	0.17	0	0
GlassQuartz_Ono_2020_Viscoelastic [60]	2560	69.06	0.2538	0.0126	0.0178

GlassSodaLime	2500	69	0.23	0	0
GlassSodaLime_Ono_2020_Viscoelastic [60]	2480	74.29	0.2227	0.0059	0.0065
Gold	19320	77	0.42	0	0
Ice [2]	900	9.55	0.33	0	0
Inconel625	8440	207	0.31	0	0
Inconel625_Ono_2020_Viscoelastic [60]	8440	209.2	0.3064	0.0104	0.0075
Inconel718_Ono_2020_Viscoelastic [60]	8190	199.5	0.3005	0.0144	0.0278
Inconel738_Ono_2020_Viscoelastic [60]	8110	199.4	0.2958	0.0122	0.0262
Iron_Ono_2020_Viscoelastic [60]	7870	211.4	0.304	0.09	0.0606
Lead	11340	13.5	0.44	0	0
MagnesiumAlloyAZ31B	1770	45	0.35	0	0
MagnesiumAlloyAZ61_Ono_2020_Viscoelastic [60]	1800	42.31	0.3147	0.0013	0.0014
Magnesium_Ono_2020_Viscoelastic [60]	1740	43.95	0.2974	0.0044	0.0056
Molybdenum	10220	320	0.32	0	0
Monel400	8800	180	0.32	0	0
Monel400_Ono_2020_Viscoelastic [60]	8800	179.3	0.3276	0.0214	0.0065
Nickel200	8890	204	0.31	0	0
Nickel200_Ono_2020_Viscoelastic [60]	8910	206.7	0.3156	0.0398	0.1029
NickelAlloyNi3Al_Ono_2020_Viscoelastic [60]	8100	214.7	0.2261	0.1178	0.1292
Nylon	1140	2.69	0.39	0	0
Nylon_Ono_2020_Viscoelastic [60]	1140	4.506	0.3735	0.0827	0.0991
Platinum	21450	171	0.39	0	0
Plexiglass	1190	2.74	0.31	0	0
Plexiglass_Ono_2020_Viscoelastic [60]	950	4.625	0.2421	0.0253	0.0408
Polycarbonate	1200	2.38	0.36	0	0
Polycarbonate_Ono_2020_Viscoelastic [60]	1200	3.178	0.383	0.1653	0.2008
PolyethyleneHighDensity_Ono_2020_Viscoelastic [60]	940	3.499	0.3613	0.0642	0.136
PolyethyleneLowDensity_Ono_2020_Viscoelastic [60]	910	3.825	0.3483	0.133	0.1785
Polypropylene_Ono_2020_Viscoelastic [60]	900	4.465	0.3062	0.1358	0.2002
Polystyrene	1050	2.78	0.33	0	0
PolyvinylChloride	1440	3.28	0.38	0	0
PolyvinylChloride_Ono_2020_Viscoelastic [60]	1400	4.665	0.3533	0.0641	0.1059
SiliconNitride	3300	304	0.3	0	0
Silver	10490	74	0.37	0	0
StainlessSteelAlloy304	8000	193	0.3	0	0
StainlessSteelAlloy304_Ono_2020_Viscoelastic [60]	8000	203.1	0.2875	0.014	0.0062
StainlessSteelAlloy405	7800	200	0.3	0	0
SteelAlloy1020	7850	207	0.3	0	0
SteelAlloy1020_Ono_2020_Viscoelastic [60]	7820	208	0.2908	0.0067	0.0058
SteelAlloy4340_Ono_2020_Viscoelastic [60]	7840	202.8	0.295	0.004	0.0024
Tantalum	1660	185	0.35	0	0
Teflon	2170	0.475	0.46	0	0
Tin	7170	44.3	0.33	0	0
Titanium	4510	103	0.34	0	0

TitaniumAlloyTi6Al4V		4430	114	0.34	0	0
TitaniumAlloyTi6Al4V_Ono_2020_Viscoelastic [60]		4500	114.7	0.3267	0.0271	0.014
TitaniumAlloyTi6Al6V2Sn_Ono_2020_Viscoelastic [60]		4540	111.5	0.3289	0.01	0.011
ToolSteelT8_Ono_2020_Viscoelastic [60]		8430	220.2	0.2757	0.0375	0.0135
Tungsten		19300	400	0.28	0	0
Tungsten_Ono_2020_Viscoelastic [60]		19250	405.2	0.2867	0.008	0.0039
Zinc		7140	104.5	0.25	0	0
Zirconium		6510	99.3	0.35	0	0

C.2 Cubic

$$C_{33} = C_{22} = C_{11}, C_{13} = C_{23} = C_{12}, C_{44} = C_{55} = C_{66}$$

ρ in kg/m³, C_{ij} in GPa

	ρ	C_{11}	C_{12}	C_{66}
GaAs [55]	5310	118.8	53.8	59.4
InAs [55]	5670	83.29	45.26	39.59

C.3 Transversely isotropic

$$C_{13} = C_{12}, C_{33} = C_{22}, C_{44} = 0.5(C_{22} - C_{23}), C_{55} = C_{66}$$

ρ in kg/m³, C_{ij} in GPa

	ρ	C_{11}	C_{12}	C_{22}	C_{23}	C_{66}
AS4M3502 [63]	1550	147.1	4.1	10.6	3.1	6
CarbonEpoxy_Rokhlin_2011 [15]	1610	162	11.8	17	8.2	8
SAERTEX7006919RIMR135 [40]	1454	122.692	4.31945	9.21241	4.20204	6.02
SigrafilCE125023039 [63]	1500	131	3.7	8.1	3.1	6.1
T300M914 [64]	1560	143.8	6.2	13.3	6.5	5.7
T700M21 [65]	1571	129.986	6.06192	11.1918	5.19179	4.135
T700PPS [63]	1600	152.7	4.7	11.7	4.4	4.5
T800M913 [63]	1550	154	3.7	9.5	5.2	4.2
T800M924 [66]	1500	164.708	5.45328	11.2997	4.73939	6
T800_Castaings	1510	184	7.09964	12.9996	6.99943	5.5
TVR380M12R_GFRP [21]	1800	49.7605	6.16767	17.1601	5.68314	5.233

C.4 Orthotropic

ρ in kg/m³, C_{ij} in GPa

CarbonEpoxy2_Rokhlin_2011 [15]

ρ	C_{11}	C_{12}	C_{13}	C_{22}	C_{23}	C_{33}	C_{44}	C_{55}	C_{66}
1610	162	10.6	13	15.3	8.2	18.7	4.4	8.8	7.2

CarbonEpoxy_Castaings

ρ	C_{11}	C_{12}	C_{13}	C_{22}	C_{23}	C_{33}	C_{44}	C_{55}	C_{66}
1500	125	6.3	5.4	14	7.1	14	3.45	5.4	5.4

CarbonEpoxy_Castaings_Viscoelastic

ρ	C_{11}	C_{12}	C_{13}	C_{22}	C_{23}	C_{33}	C_{44}	C_{55}	C_{66}
1500	125	6.3	5.4	14	7.1	14	3.45	5.4	5.4

	+2.5i	+0.126i	+0.108i	+0.28i	+0.1421i	+0.28i	+0.069i	+0.108i	+0.108i
--	-------	---------	---------	--------	----------	--------	---------	---------	---------

CarbonEpoxy_Hernando_2015 [33]

ρ	C_{11}	C_{12}	C_{13}	C_{22}	C_{23}	C_{33}	C_{44}	C_{55}	C_{66}
1500	132	6.9	5.9	12.3	5.5	12.1	3.32	6.21	6.15

CarbonEpoxy_Hernando_2015_Viscoelastic [33]

ρ	C_{11}	C_{12}	C_{13}	C_{22}	C_{23}	C_{33}	C_{44}	C_{55}	C_{66}
1500	132	6.9	5.9	12.3	5.5	12.1	3.32	6.21	6.15

	+0.4i	+0.001i	+0.016i	+0.037i	+0.021i	+0.043i	+0.009i	+0.015i	+0.02i
--	-------	---------	---------	---------	---------	---------	---------	---------	--------

HIO₃ [67]

ρ	C_{11}	C_{12}	C_{13}	C_{22}	C_{23}	C_{33}	C_{44}	C_{55}	C_{66}
4640	30.1	16.1	11.1	58	8	42.9	16.9	20.6	15.8

Oak [2]

ρ	C_{11}	C_{12}	C_{13}	C_{22}	C_{23}	C_{33}	C_{44}	C_{55}	C_{66}
597	8.61313	2.17462	2.77298	1.73528	1.06095	2.40251	0.3	0.89	0.92

References

- [1] B. Pavlakovic, M. Lowe, D. Alleyne, and P. Cawley, *Rev. Prog. QNDE*, ch. Disperse: A General Purpose Program for Creating Dispersion Curves, pp. 185–192. Plenum Press, New York, 1997.
- [2] M. Lowe and B. Pavlakovic, “DISPERSE v2.0.20f.” <http://www.imperial.ac.uk/non-destructive-evaluation/products-and-services/disperse>.
- [3] P. Boccini, A. Marzani, and E. Viola, “Graphical User Interface for Guided Acoustic Waves,” *J. Comput. Civil. Eng.*, vol. 25, pp. 202–210, June 2011.
- [4] A. Marzani and P. Bocchini, “GUIGUW v2.2.” <http://www.guiguw.com/>.
- [5] D. R. Ramasawmy, B. T. Cox, and B. E. Treeby, “ElasticMatrix: A MATLAB toolbox for anisotropic elastic wave propagation in layered media,” *SoftwareX*, vol. 11, no. 100397, pp. 1–8, 2020.
- [6] D. R. Ramasawmy, B. T. Cox, and B. E. Treeby, “Elastic matrix.” <https://github.com/dannyramasawmy/ElasticMatrix>.
- [7] A. H. Orta, M. Kersemans, and K. V. D. Abeele, “A comparative study for calculating dispersion curves in viscoelastic multi-layered plates,” *Compos. Struct.*, vol. 294, no. 115779, 2022.
- [8] A. H. Orta, K. V. D. Abeele, and M. Kersemans, “The dispersion box.” <https://github.com/adilorta/The-Dispersion-Box>.
- [9] A. H. Orta, J. Vandendriessche, M. Kersemans, W. V. Paepelgem, N. B. Roozen, and K. V. D. Abeele, “Modeling lamb wave propagation in visco-elastic composite plates using a fifth-order plate theory,” *Ultrasonics*, vol. 116, no. 106482, 2021.
- [10] X. Wang, M. Liu, and K. Wang, “Development of Dispersion Calculator SAFEDC of Guided Wave with Complex Material and Waveguide,” in *11th European Workshop on Structural Health Monitoring*, pp. 1–8, June 2024.
- [11] M. Liu, “SAFEDC.” <https://sourceforge.net/projects/safedc>.
- [12] D. A. Kiefer, “GEWtool.” <https://zenodo.org/records/10427974>.
- [13] S. I. Rokhlin and L. Wang, “Stable recursive algorithm for elastic wave propagation in layered anisotropic media: Stiffness matrix method,” *J. Acoust. Soc. Am.*, vol. 112, pp. 822–834, Sep 2002.
- [14] L. Wang and S. I. Rokhlin, “Stable reformulation of transfer matrix method for wave propagation in layered anisotropic media,” *Ultrasonics*, vol. 39, pp. 413–424, Sep 2001.

- [15] S. I. Rokhlin, D. E. Chimenti, and P. B. Nagy, *Physical Ultrasonics of Composites*. Oxford University Press, Oxford, 2011.
- [16] V. G. A. Kamal and V. Giurgiutiu, “Stiffness Transfer Matrix Method (STMM) for Stable Dispersion Curves Solution in Anisotropic Composites,” in *Proc. SPIE*, 2014.
- [17] E. L. Tan, “Stiffness matrix method with improved efficiency for elastic wave propagation in layered anisotropic media,” *J. Acoust. Soc. Am.*, vol. 118, p. 3400–3403, Dec 2005.
- [18] E. L. Tan, “Hybrid compliance-stiffness matrix method for stable analysis of elastic wave propagation in multilayered anisotropic media,” *J. Acoust. Soc. Am.*, vol. 119, no. 1, pp. 45–53, 2006.
- [19] M. Barski and P. Pajak, “An application of stiffness matrix method to determining of dispersion curves for arbitrary composite materials,” *Journal of KONES Powertrain and Transport*, vol. 23, no. 1, pp. 47–54, 2016.
- [20] M. Barski and P. Pajak, “Determination of Dispersion Curves for Composite Materials With the Use of Stiffness Matrix Method,” *Acta Mech. et Autom.*, vol. 11, pp. 121–128, May 2017.
- [21] M. Barski and A. Muc, “The impact of the fiber orientation angle on the dispersion characteristic of guided waves for multilayered GLARE composites,” in *J. Phys. Conf. Ser.*, vol. 1603, p. 012001, Sep 2020.
- [22] A. Muc, M. Barski, A. Stawiarski, M. Chwał, and M. Augustyn, “Dispersion curves and identification of elastic wave modes for fiber metal laminate,” *Compos. Struct.*, vol. 255, p. 112930, 2021.
- [23] A. H. Nayfeh, *Wave Propagation in Layered Anisotropic Media with Applications to Composites*. North-Holland, Amsterdam, 1995.
- [24] W. T. Thomson, “Transmission of elastic waves through a stratified solid medium,” *J. Appl. Phys.*, vol. 21, pp. 89–93, 1950.
- [25] N. A. Haskell, “The dispersion of surface waves on multilayered media,” *Bull. Seism. Soc. Am.*, vol. 43, pp. 17–34, Jan 1953.
- [26] A. H. Nayfeh, “The propagation of horizontally polarized shear waves in multilayered anisotropic media,” *J. Acoust. Soc. Am.*, vol. 86, pp. 2007–2012, July 1989.
- [27] A. H. Nayfeh, “The general problem of elastic wave propagation in multilayered anisotropic media,” *J. Acoust. Soc. Am.*, vol. 89, pp. 1521–1531, Oct 1991.
- [28] L. Knopoff, “A matrix method for elastic wave problems,” *Bull. Seism. Soc. Am.*, vol. 54, pp. 431–438, Feb 1964.

- [29] M. J. S. Lowe, “Matrix Techniques for Modeling Ultrasonic Waves in Multilayered Media,” *IEEE Trans. Ultrason. Ferroelec. Freq. Contr.*, vol. 42, pp. 525–542, Jul 1995.
- [30] L. Gavric, “Computation and propagative waves in free rail using a finite element technique,” *J. Sound Vib.*, vol. 185, pp. 531–543, Aug 1995.
- [31] A. T. I. Adamou and R. V. Craster, “Spectral methods for modelling guided waves in elastic media,” *J. Acoust. Soc. Am.*, vol. 116, pp. 1524–1535, June 2004.
- [32] F. H. Quintanilla, M. J. S. Lowe, and R. V. Craster, “Modeling guided elastic waves in generally anisotropic media using a spectral collocation method,” *J. Acoust. Soc. Am.*, vol. 137, pp. 1180–1194, Mar 2015.
- [33] F. H. Quintanilla, Z. Fan, M. J. S. Lowe, and R. V. Craster, “Guided waves’ dispersion curves in anisotropic viscoelastic single- and multi-layered media,” *Proc. Roy. Soc. London A*, vol. 471, p. 20150268, Nov 2015.
- [34] F. H. Quintanilla, M. J. S. Lowe, and R. V. Craster, “Full 3d dispersion curve solutions for guided waves in generally anisotropic media,” *J. Sound Vib.*, vol. 363, pp. 545–559, Feb 2016.
- [35] F. H. Quintanilla, M. J. S. Lowe, and R. V. Craster, “The symmetry and coupling properties of solutions in general anisotropic multilayer waveguides,” *J. Acoust. Soc. Am.*, vol. 141, pp. 406–418, Jan 2017.
- [36] D. Kiefer, M. Ponschab, S. Rupitsch, and M. Mayle, “Calculating the full leaky Lamb wave spectrum with exact fluid interaction,” *J. Acoust. Soc. Am.*, vol. 145, no. 6, pp. 3341–3350, 2019.
- [37] E. Georgiades, M. Lowe, and R. Craster, “Leaky wave characterisation using spectral methods,” *J. Acoust. Soc. Am.*, vol. 152, no. 3, pp. 1487–1497, 2022.
- [38] E. Georgiades, M. Lowe, and R. Craster, “Computing leaky Lamb waves for waveguides between elastic half-spaces using spectral collocation,” *J. Acoust. Soc. Am.*, vol. 155, no. 1, pp. 629–639, 2024.
- [39] A. M. A. Huber and M. G. R. Sause, “Classification of solutions for guided waves in anisotropic composites with large numbers of layers,” *J. Acoust. Soc. Am.*, vol. 144, p. 3236–3251, Dec 2018.
- [40] A. Huber, “Numerical modeling of guided waves in anisotropic composites with application to air-coupled ultrasonic inspection.” <https://elib.dlr.de/139819>, 2020.
- [41] A. M. A. Huber, “Classification of solutions for guided waves in fluid-loaded viscoelastic composites with large numbers of layers,” *J. Acoust. Soc. Am.*, vol. 154, p. 1073–1094, Aug 2023.

- [42] L. Rayleigh, “On Waves Propagated along the Plane Surface of an Elastic Solid,” in *Proc. Lond. Math. Soc.*, pp. 4–11, 1885.
- [43] H. Lamb, “On Waves in an Elastic Plate,” in *Proc. R. Soc. Lond. A*, p. 114–128, 1917.
- [44] J. L. Rose, *Ultrasonic Waves in Solid Media*. Cambridge University Press, Cambridge, 1999.
- [45] V. Giurgiutiu, *Stress, Vibration, And Wave Analysis in Aerospace Composites: SHM and NDE Applications*. Elsevier, 2022.
- [46] T. Meeker and A. Meitzler, *Physical Acoustics*, ch. Guided Wave Propagation in Elongated Cylinders and Plates, pp. 111–167. Academic Press, 1964.
- [47] Y. Pao and R. D. Mindlin, “Dispersion of Flexural Waves in an Elastic, Circular Cylinder,” *J. Appl. Mech.*, vol. 27, pp. 513–520, Sep 1960.
- [48] D. Gazis, “Three-dimensional investigation of the propagation of waves in circular hollow cylinders,” *J. Acoust. Soc. Am.*, vol. 31, p. 568–573, May 1959.
- [49] R. Kumar, “Flexural Vibrations of Fluid-Filled Circular Cylindrical Shells,” *Acta Acust.*, vol. 24, pp. 137–146, Mar 1971.
- [50] R. Kumar, “Dispersion of Axially Symmetric Waves in Empty and Fluid-Filled Cylindrical Shells,” *Acta Acust.*, vol. 27, pp. 317–329, Mar 1972.
- [51] J. Qu, Y. Berthelot, and Z. Li, *Rev. Prog. QNDE*, ch. Dispersion of Guided Circumferential Waves in a Circular Annulus, p. 169–176. Plenum Press, New York, 1996.
- [52] G. Liu and J. Qu, “Guided Circumferential Waves in a Circular Annulus,” *J. Appl. Mech.*, vol. 65, pp. 424–430, Jun 1998.
- [53] X. Zhao and J. Rose, “Guided circumferential shear horizontal waves in an isotropic hollow cylinder,” *J. Acoust. Soc. Am.*, vol. 115, p. 1912–1916, May 2004.
- [54] A. Huber, “Dispersion Calculator (DC), available at.” <https://github.com/ArminHuber/Dispersion-Calculator>.
- [55] B. A. Auld, *Acoustic Fields and Waves in Solids*, vol. 1. Krieger Malabar, FL, 1990.
- [56] M. J. S. Lowe, *Plate waves for the NDT of diffusion bonded titanium*. PhD thesis, University of London, 1992.
- [57] M. Lowe and B. Pavlakovic, *Disperse User’s Manual*. Imperial College London, London, 2013.

- [58] A. Bernard, M. Lowe, and M. Deschamps, “Guided waves energy velocity in absorbing and non-absorbing plates,” *J. Acoust. Soc. Am.*, vol. 110, p. 186–196, July 2001.
- [59] K. Ono, “A Comprehensive Report on Ultrasonic Attenuation of Engineering Materials, Including Metals, Ceramics, Polymers, Fiber-Reinforced Composites, Wood, and Rocks,” *Appl. Sci.*, vol. 10, pp. 1–52, Mar 2020.
- [60] K. Ono, “Dynamic Viscosity and Transverse Ultrasonic Attenuation of Engineering Materials,” *Appl. Sci.*, vol. 10, pp. 1–36, July 2020.
- [61] K. Ono, “Experimental Determination of Lamb-Wave Attenuation Coefficients,” *Appl. Sci.*, vol. 12, pp. 1–44, July 2022.
- [62] W. D. Callister, *Material Science and Engineering. An Introduction*. John Wiley & Sons, Inc., 2002.
- [63] M. Sause and M. Hamstad, *Acoustic Emission Analysis*. Academic, Oxford, 2018.
- [64] C. Simon, H. Kaczmarek, and D. Royer, “Elastic wave propagation along arbitrary direction in free orthotropic plates. Application of composite materials,” in *4th French Congress of Acoustics, Marseille, France*, 1997.
- [65] J. Moll, J. Kathol, C.-P. Fritzen, M. Moix-Bonet, M. Rennoch, M. Koerdt, A. S. Herrmann, M. G. Sause, and M. Bach, “Open guided waves: online platform for ultrasonic guided wave measurements,” *Structural Health Monitoring*, 2018.
- [66] W. J. Percival and E. A. Birt, “A study of Lamb wave propagation in carbon-fibre composites,” *Insight*, vol. 39, pp. 728–735, 1997.
- [67] S. Karous, S. Dahmen, M. S. Bouhdima, M. B. Amor, and C. Glorieux, “Multiple zero group velocity lamb modes in an anisotropic plate: propagation along different crystallographic axes,” *Can. J. Phys.*, vol. 97, no. 10, pp. 1064–1074, 2019.